

**THEORETICAL ANALYSIS OF THE  
OPTIMUM BED THICKNESS OF AN  
ELECTROCHEMICAL REACTOR**

**A Thesis**

**Submitted to the College of Engineering  
of Nahrain University in Partial Fulfillment  
of the Requirements for the Degree of**

**Master of Science**

**In**

**Chemical Engineering**

**by**

**AWS ABDULMAHDI SADEQ**

**B.Sc. 2006**

**Muharam**

**1431**

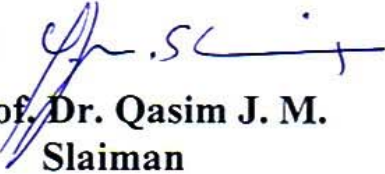
**December**

**2009**

## Certification

We certify that this thesis entitled “**Theoretical Analysis of the Optimum Bed Thickness of an Electrochemical Reactor**” was prepared by **Aws Abdulmahdi Sadeq** under our supervision at Nahrain University/ College of Engineering, in partial fulfillment of the requirements for the degree of Master of Science in Chemical Engineering.

Signature:



Name: **Prof. Dr. Qasim J. M. Slaiman**

( Supervisor )

Date: 10 / 1 / 2010

Signature:



Name: **Dr. Sarmad Talib Najim**

( Supervisor )

Date: 10 / 1 / 2010

Signature: *J. Shanshool*

Name: **Prof. Dr. Jabir Shanshool**

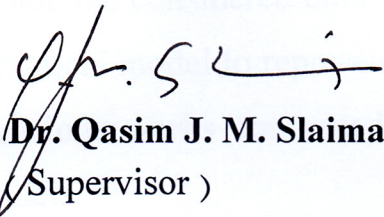
(Head of Department)

Date:

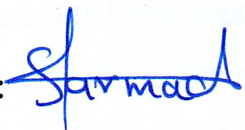
19 / 1 / 2010

# CERTIFICATE

We certify, as an examining committee, that we have read this thesis entitled "Theoretical Analysis of the Optimum Bed Thickness of an Electrochemical Reactor", examined the student Aws Abdulmahdi Sadeq in its content and found it meets the standard of thesis for the degree of Master of Science in Chemical Engineering.

Signature:   
Name: **Prof. Dr. Qasim J. M. Slaiman**  
(Supervisor)

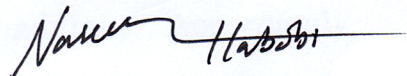
Date: 10 / 1 / 2010

Signature:   
Name: **Dr. Sarmad Talib Najim**  
(Supervisor)

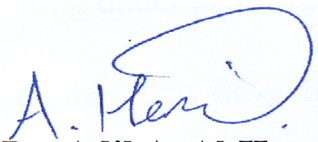
Date: 10 / 1 / 2010

Signature:   
Name: **Ass. Prof. Dr. Cecilia K. Haweel**  
(Member)

Date: 11 / 1 / 2010

Signature:   
Name: **Dr. Naseer About Essa**  
(Member)

Date: 10 / 1 / 2010

Signature:   
Name: **Prof. Dr. Adil A. Al-Hemeri**  
(Chairman)

Date: 11 / 1 / 2010

Approval of the College of Engineering

Signature:   
Name: **Prof. Dr. Muhsin J. Jweeg**  
(Dean)

Date: 25 / 1 / 2010

# Abstract

In this study, a theoretical analysis of optimum bed thickness for realizing a high efficiency and reaction conversion of an electrochemical reactor has been made based on flow-through porous electrode (FTPE) configuration. Another configuration of porous electrode (flow-by) has been reviewed beside the considered one. The method that has been used is to find out a mathematical model to represent the optimum bed thickness by taking a look into previous works concerned and collecting all related information, data, and models.

It has been found that the optimum bed thickness can be classified into two categories depending on reactor operating conditions. Accordingly, models have to be classified into two groups: firstly, electrochemical reactors (ECRs) operating under electron transfer (activation) control, and secondly, (ECRs) operating under mass transfer control.

The models that have been studied and tested are based on FTPE operating under mass transfer control according to the importance of this region in a wide range of applications. Seven models have been selected from literature survey related theoretically to optimum bed thickness of an electrochemical reactor operating under mass transfer control when electrode conductivity is much higher than electrolyte.

The parameters that affect the optimum bed thickness have been visualized and reviewed, and almost all of them have been examined by experimental data from different sources and based on the various models. It has been found that the increase in electrolyte flow rate, concentration,

limiting current density, and specific surface area reduce the optimum bed thickness, and the increase in electrolyte conductivity, void fraction, and overpotential range increases optimum bed thickness.

The most important design parameter that has a great effect on optimum bed thickness is found to be the electrolyte flow rate for any certain operation. The effect of electrolyte entrance (or electrode placement) on optimum bed thickness has been reviewed and the results have shown no significant effects.

It has been concluded that the most appropriate two models to represent the optimum bed thickness of FTPE electrochemical reactor operating under mass transfer control based on the results are those predicted theoretically and stated by **Kreysa [28]** in (1978) and **Doherty et al. [8]** in (1996).

## List of Contents

<b>Contents</b>		<b>Page</b>
Abstract		I
List of contents		III
Nomenclature		VI
List of Tables		IX
List of Figures		XII
<b>Chapter One: Introduction</b>		
1.1	Introduction to Electrochemical Reactors	1
1.2	Electrochemical Technology in Environmental Treatment	2
1.3	The Aim of Work	3
<b>Chapter Two: Electrochemical Concepts and Literature Survey</b>		
2.1	Introduction	4
2.2	Electrochemical Reactor Design (ECR Selection)	4
2.2.1	Factors Affecting the Selection of an Electrochemical Reactor	4
2.2.2	Electrode Configuration	5
2.2.2.1	Flow-through Configuration	6
2.2.2.2	Flow-by Configuration	6
2.3	Effect of Counterelectrode Placement	7
2.4	Flow-through Porous Electrodes Applications & Features	9
2.5	Theoretical Distribution of the Potential in the Electrolyte for Flow- By Electrode.	10
2.6	Application to the Design of Three-Dimensional Flow-By Structure	14
2.7	Polarization Curve	15
2.8	Side Reactions in Electrochemical Reactors	17

2.9	Mass Transfer Coefficient	20
2.10	Types of Packing & Porosity	22
2.11	Specific Surface Area	24
2.12	Literature Review	26

### **Chapter Three: Theory & Models**

3.1	Introduction	33
3.2	Macroscopic Description of Porous Electrodes	33
3.3	Theoretical Analysis of the Flow-through Particulate Bed Electrode	34
3.3.1	Concentration, Potential & Current Density Distribution	36
3.3.2	Analytical Solution	38
3.3.3	Numerical Techniques	40
3.4	Optimum Bed Thickness Models	42

### **Chapter Four: Calculations & Results**

4.1	Introduction	49
4.2	Parameters Affecting on the Optimum Bed Thickness	49
4.3	Models	50
4.4	Calculations Procedure	53
4.5	Results	56

### **Chapter Five: Discussion**

5.1	Parameters Affect on Optimum Bed Thickness	75
5.1.1	Electrolyte Flow Rate & Mass Transfer Coefficient	75
5.1.2	Electrolyte Concentration (Reactant)	78
5.1.3	Electrolyte Conductivity & Temperature	79
5.1.4	Specific surface Area & Porosity	81
5.1.5	Overpotential Difference	83
5.2	Models Results	84

5.2.1	Kreysa's [28] and Doherty's et al. [8], models (1 & 2)	84
5.2.2	Kreysa and Jüttner's [47] & Masliy and Poddubny's [25], Models (3 &4)	88
5.2.3	Newman's et al. [7, 12, and 13], Model 5	91
5.2.4	Masliy's et al. [18, 25], Model 6	92
5.2.5	Nava's et al. [10], Model 7	92
<b>Chapter Six: Conclusions &amp; Recommendations</b>		
6.1	Conclusions	94
6.2	Conclusions & Future Works	95
<b>References</b>		96
<b>Appendix A</b>		A-1

---

## NOMENCLATURES

<u>Symbol</u>	<u>Meaning</u>	<u>Unit</u>
$A_c$	= Cross-sectional area of reactor	$\text{cm}^2$
$a$	= Specific surface area of electrode	$\text{cm}^{-1}$
$a_g$	= Specific surface area of single particle	$\text{cm}^{-1}$
$b, c$	= Coefficients in eq. 2.28	-
$C$	= Electrolyte concentration	$\text{mol}/\text{cm}^3$
$C_b$	= Bulk electrolyte concentration	$\text{mol}/\text{cm}^3$
$C_o$	= Inlet electrolyte concentration	$\text{mol}/\text{cm}^3$
$C_{out}$	= Outlet electrolyte concentration	$\text{mol}/\text{cm}^3$
$D$	= Diffusion coefficient	$\text{cm}^2/\text{s}$
$D_R$	= Reactor diameter	cm
$d_{eq}$	= Equivalent size diameter of non-spherical particles	cm
$d_p$	= Size diameter of spherical particle	cm
$E$	= Electrode potential	Volt
$E^\circ$	= Equilibrium electrode potential at standard condition	Volt
$E_{eq}$	= Equilibrium electrode potential	Volt
$F$	= Faraday's constant (96,487)	C/g.equ.
$h$	= Optimum bed length in eqs. 3.43 and 3.44	cm
$h_e$	= Penetration depth in eq. 3.27	cm
$h_{op}$	= Optimum bed height in eq. 3.39	cm
$I$	= Dimensionless current density ( $i_T / ai_oL$ )	-
$i$	= Current density	$\text{A}/\text{cm}^2$
$i_o$	= Exchange current density	$\text{A}/\text{cm}^2$
$i_L$	= Limiting current density	$\text{A}/\text{cm}^2$
$i_m$	= Current density of solid phase	$\text{A}/\text{cm}^2$
$i_s$	= Current density of electrolyte phase	$\text{A}/\text{cm}^2$
$i_T$	= Total current density based on cross-sectional area of the electrode	$\text{A}/\text{cm}^2$
$K_m$	= Mass transfer coefficient	cm/s
$\overline{K_m}$	= Average mass transfer coefficient	cm/s
$k_m$	= Solid phase conductivity	$(\Omega \text{ cm})^{-1}$
$k_s$	= Effective electrolyte conductivity	$(\Omega \text{ cm})^{-1}$

$k_{so}$	= Initial electrolyte conductivity	$(\Omega \text{ cm})^{-1}$
$l$	= Electrode breadth	cm
$L$	= Electrode length	cm
$L_d$	= Thickness of porous electrode layer operating at the limiting diffusion current.	cm
$L_{max}$	= Maximum channel thickness in eq. 2.17	cm
$L_{op}$	= Optimum bed length	cm
$m$	= constant in eq. 2.27	-
$P$	= Penetration depth	cm
$Q$	= Volumetric electrolyte flow velocity	$\text{cm}^3 \text{ s}^{-1}$
$r_i, r_o$	= Inner and outer diameter of a packed bed electrode in a radial configuration	cm
$Re$	= Reynolds number for bed ( $ud_p/\nu$ )	-
$R$	= Gas constant = 8.314	J/mol. K
$S$	= Surface area of electrode	$\text{cm}^2$
$S_p$	= Surface area of single particle	$\text{cm}^2$
$Sc$	= Schmidt number ( $\nu/D$ )	-
$Sh$	= Sherwood number ( $K_m d_p/D$ )	-
$St$	= Stanton number ( $K_m/u$ )	-
$T$	= Temperature	K
$t$	= time	s
$u$	= Electrolyte flow rate	cm/s
$V_c$	= Applied potential at the cathode current feeder	Volt
$V_p$	= volume of single particle	$\text{cm}^3$
$V_T$	= Volume of reservoir	$\text{cm}^3$
$x, y$	= Normal and longitudinal coordinates	cm
$X$	= Dimensionless length ( $x/L$ )	-
$Y$	= Reduced coordinates ( $y/y_o$ )	-
$y_o$	= Length of the electrode in the electrolyte direction	cm
$z$	= Number of electrons involved in reaction	-

### **Greek Letters**

$\alpha$	= Symmetry factor	-
$\beta$	= $aK_m/u$	$\text{cm}^{-1}$
$\gamma$	= Dimensionless group ( $Lai_o/I$ )	-
$\delta$	= Dimensionless parameter ( $LI \sigma[k_m+k_s]^{-1}$ )	-
$\varepsilon$	= Void fraction	-

$\eta$	= Overpotential	Volt
$\theta$	= Dimensionless exchange current density defined in eq. 3.25	-
$\mu$	= Electrolyte viscosity	g/cm s
$\nu$	= Kinematic viscosity ( $\mu/\rho$ )	cm <sup>2</sup> /s
$\xi$	= Effectiveness factor defined in eq. 3.26	-
$\rho$	= Electrolyte density	g/cm <sup>3</sup>
$\sigma$	= $\alpha (zF/RT)$	-
$\tau$	= Residence time of the electrolyte ( $V_T/Q$ )	s
$v$	= Group parameter defined in eq. 3.19	cm <sup>-1</sup>
$\phi_m$	= Electrode potential	Volt
$\phi_s$	= Electrolyte potential	Volt
$\psi$	= Coulombic efficiency defined in eq. 5.3	-
$\omega$	= Parameter group defined in eqs. 2.5 and 2.6	A $\Omega$ /cm <sup>2</sup>

### **Abbreviations**

CE	= Counterelectrode
ECR	= Electrochemical reactor
Conc.	= Concentration
Conti.	= Continued
FTPE	= Flow-through porous electrode
HER	= Hydrogen evolution rate
M	= Molarity
RVC	= Reticulated vitreous carbon

## List of Tables

Table	Title	page
3.1	Dependence of penetration depth on the electrode electrolyte conductivity.	46
4.1	Operating conditions of <b>Kreysa's</b> data [28].	54
4.2	Values of parameters for models calculations for $L = 1.15$ cm.	54
4.3	Optimum bed thickness according to considered models.	56
4.4	Values of parameters for models calculations for $L = 2.3$ cm.	56
4.5	Optimum bed thickness according to considered models.	57
4.6	Physical properties data and operating conditions for <b>CE</b> placement experiment.	58
4.7	Values of parameters for models calculations, <b>Newman</b> [7].	58
4.8	Effect of flow rate on effluent concentration at limiting current ( <b>experimentally</b> ) for upstream <b>CE</b> .	59
4.9	Optimum bed thickness calculations according to data of table 4.7.	60
4.10	Optimum bed thickness from literature survey [47] for packed bed of specific surface area = $30 \text{ cm}^{-1}$ .	61
4.11	Optimum bed thickness comparison for porosity ( $\varepsilon = 0.4$ ).	62
4.12	Optimum bed thickness comparison for porosity ( $\varepsilon = 0.9$ ).	62
4.13	Optimum bed thickness comparison for porosity ( $\varepsilon = 0.96$ ).	62
4.14	Operating conditions of <b>Saleh's</b> data [29].	63
4.15	Experimental values of parameters for models calculations.	63
4.16	Optimum bed thickness comparison based on experimental data.	63
4.17	Values of parameters for models calculations (theoretically).	64

4.18	Optimum bed thickness comparison based on theoretical data.	65
4.19	Electrolyte physical properties [34].	66
4.20	Electrolyte flow rate and velocity.	66
4.21	Initial electrolyte conductivity for various temperatures and concentrations.	66
4.22	Effective electrolyte conductivity for various temperatures and concentrations according to equation (3.9).	67
4.23	Simulation runs for calculation of the optimum bed thickness for bed of <b>2cm</b> thick, porosity ( $\epsilon = 0.38$ ), and $[\text{Fe}^{3+}] = 2.5 \text{ mM}$ .	67
4.24	Simulation runs for calculation of the optimum bed thickness for bed of <b>2cm</b> thick, porosity ( $\epsilon = 0.38$ ), and $[\text{Fe}^{3+}] = 5.0 \text{ mM}$ .	68
4.25	Simulation runs for calculation of the optimum bed thickness for bed of <b>2cm</b> thick, porosity ( $\epsilon = 0.38$ ), and $[\text{Fe}^{3+}] = 15.0 \text{ mM}$ .	68
4.26	Simulation runs for calculation of the optimum bed thickness for bed of <b>7cm</b> thick, porosity ( $\epsilon = 0.38$ ), and $[\text{Fe}^{3+}] = 15.0 \text{ mM}$ .	68
4.27	Optimum bed thickness comparison for bed of <b>2cm</b> thick, porosity ( $\epsilon = 0.38$ ), and $[\text{Fe}^{3+}] = 2.5 \text{ mM}$ .	69
4.28	Optimum bed thickness comparison for bed of <b>2cm</b> thick, porosity ( $\epsilon = 0.38$ ), and $[\text{Fe}^{3+}] = 5.0 \text{ mM}$ .	69
4.29	Optimum bed thickness comparison for bed of <b>2cm</b> thick, porosity ( $\epsilon = 0.38$ ), and $[\text{Fe}^{3+}] = 15.0 \text{ mM}$ .	69
4.30	Optimum bed thickness comparison bed of <b>7cm</b> thick, porosity ( $\epsilon = 0.38$ ), and $[\text{Fe}^{3+}] = 15.0 \text{ mM}$ .	70

4.31	Operating conditions of Nava's data.	73
4.32	Optimum bed thickness obtained from <b>Nava's</b> model [10].	73
4.33	Optimum bed thickness obtained from <b>Newman's</b> model [7, 12, and 13].	73
5.1	Optimum bed thickness based on experimental data [7].	85
5.2	Calculation of overpotential range error readings for error value = 50 mV.	86
5.3	Calculation of overpotential range error readings for error value = 100 mV.	86

---

## List of Figures

Figure	Title	page
2.1	Decisions during the process of selecting an electrochemical reactor	5
2.2	Porous electrode configurations (a): flow-through electrode, upstream counterelectrode. (b): flow-by electrode	7
2.3	Sketch of the effect of counterelectrode placement on the effective path through the electrolyte. (a) Upstream placement. (b) Downstream placement [7].	8
2.4	Representation of flow-by electrode configuration for mathematical model [14].	11
2.5	A typical current versus overpotential curve for the single electrode process	16
2.6	SEM images of plain RVC (a) and RVC/Pt (b) [39].	23
2.7	Examples of fibre bundle weaving: (a) cloth and (b) serge [40]	24
2.8	Photographs of felt and foam obtained by electron microscopy [37, 41].	24
3.1	Representation of Flow-Through Porous Electrode (FTPE) for mathematical model [8].	34
3.2	Experimental flow circuit and packed bed electrochemical reactor [10].	35
4.1	Potential distribution for bed thickness $L=9.5\text{cm}$ , $a = 81 \text{ cm}^{-1}$ based eq. 3.49 [10].	52
4.2	Potential distribution for bed thickness $L=2.3 \text{ cm}$ based on model (7) eq. 3.49.	57
4.3	Potential distribution for bed thickness $L=12.7\text{cm}$ based on	59

	model (7) eq. 3.49.	
4.4	Potential distribution for bed thickness $L=12.7\text{cm}$ based on model (7) eq. 3.49.	60
4.5	Potential distribution for bed thickness $L=1.7\text{cm}$ based on model (7) eq. 3.49.	64
4.6	Potential distribution for bed thickness $L=2\text{cm}$ , $[\text{Fe}^{3+}] = 15\text{mM}$ based on eq. 3.49.	70
4.7	Potential distribution for bed thickness $L=2\text{cm}$ , $[\text{Fe}^{3+}] = 15\text{mM}$ based on eq. 3.49.	71
4.8	Potential distribution for bed thickness $L=2\text{cm}$ , $[\text{Fe}^{3+}] = 15\text{mM}$ based on eq. 3.49.	71
4.9	Potential distribution for bed thickness $L=7\text{cm}$ , $[\text{Fe}^{3+}] = 15\text{mM}$ based eq. 3.49.	72
4.10	Effective electrode thickness vs. mean linear flow velocity [10].	74
5.1	Effect of flow rate on optimum bed thickness from <b>Najim [34]</b> data based on models (1&2).	76
5.2	Effect of flow rate on optimum bed thickness from data of [10, 28, and 29] based on models (1, 2, and 7).	77
5.3	Effect of electrolyte concentration on optimum bed thickness at various temperatures [34].	79
5.4	Effect of electrolyte conductivity on optimum bed thickness [47].	80
5.5	Effect of electrolyte conductivity on optimum bed thickness [34].	81
5.6	Effect of specific surface area on optimum bed thickness at various flow rates [10].	82

5.7	Effect of void fraction on optimum bed thickness at various conductivities [47].	83
5.8	Polarization curve for a simple electrochemical reaction a) <b>Kreysa and Reynvaan [51]</b> , b) <b>Doherty et al. [8]</b> .	84
5.9	Models comparison based on <b>Kreysa's [28]</b> data.	88
5.10	Models comparison based on <b>Saleh's [29]</b> data.	89
5.11	Models comparison based on <b>Najim's [34]</b> data.	89
5.12	Models comparison based on <b>Newman's [7]</b> data	90
5.16	Comparison between <b>Newman's [7]</b> and <b>Nava's</b> models.	91

---

# Chapter One

## Introduction

### 1.1 Introduction to Electrochemical Reactors

Any device in which chemical reaction occurs directly due to the input of electrical energy can be defined as an "electrochemical reactor" or also, familiarly known as an "electrolyser", "electrolytic cell" or "electrochemical cell" [1].

Electrochemical engineering is a multi-disciplinary subject that concerns the design, characterization and operation of electrochemical reactors and processes. Electrochemical reactors are used for a wide range of applications, ranging from analytical determinations up to full-scale synthesis and environmental treatment [2].

Both in the laboratory and in industry, the electrochemical reactor is a key component of an electrochemical process and special attention must be taken in its design to achieve a high conversion rate of reactant to product as well as a high current efficiency for the desired reaction. In view of the diverse applications of electrochemistry, a wide range of different electrochemical reactor designs is possible, ranging from traditional plate-in-tank configurations up to more sophisticated designs using, for example, modern filter-press cells [3-5], porous three-dimensional [6-8], or rotating electrodes [9-11].

There are increasing economic, social, legal, and environmental pressures to utilize the "best available technology" not entailing excessive cost and to aspire to "performance without pollution", i.e., "zero pollution

processing”. Electrochemical technology has an important role to play as part of an integrated approach to the avoidance of pollution, monitoring of pollution and process efficiency, cleaner processing, and modern techniques for electrical energy storage and conversion.

The early success of major electrochemical activities has brought about a considerable gap between electrochemistry and chemical engineering. However, an electrochemical reactor involves kinetics, heat, mass transfer and fluid flow, all of which basic chemical engineering topics [1].

## **1.2 Electrochemical Technology in Environmental Treatment**

Electrochemical technology continues to make many contributions to environmental treatment, recycling, and monitoring which can play many roles in clean technology and pollution control [3] as shown by the examples below:

- (a) Avoidance of polluting reagents in materials synthesis (clean electro-synthesis), such as zinc powder for organic reductions, by the use of direct electron transfer.
- (b) Avoidance of corrosion (choice of materials/protective coatings).
- (c) Recycling of valuable materials (precious metal deposition).
- (d) Remediation of polluted sites (soil remediation by electro-dialysis).
- (e) Monitoring and sensors of pollutant and reagent levels in process streams, rinse sections, effluents, and gaseous emissions.
- (f) Treatment of water by electrochemically generated species, such as chlorination of swimming pools and sterilization of medical

instruments using a powerful cocktail of oxidizing reagents in “superoxidized” water.

- (g) The removal of environmental contaminants, such as metal ions and organics from industrial process streams.
- (h) Efficient and clean energy conversion of chemical to electrochemical energy using fuel cell and photovoltaic devices.

### **1.3 The aim of work**

This work concerns about finding out the most appropriate mathematical model to represent and simulate the optimum bed thickness of a flow-through porous electrode configuration electrochemical reactor; by:

- (a) Looking for all parameters affecting the optimum bed thickness, and all conditions associating with the process.
- (b) Selection of models from literatures related to or concern about this subject.
- (c) Testing all the available models that have been considered to represent the optimum bed thickness using some experimental data from literatures.
- (d) Analyzing the obtained results from these models to recognize the most appropriate model among them.

# **Chapter Two**

## **Electrochemical Concepts and Literature Survey**

### **2.1 Introduction**

Fixed bed or packed bed porous electrode have become increasingly attractive in the past for use in number of industrially important processes. These electrodes have been suggested for such diverse applications as a removal of dilute metal ions from waste streams, electro-organic synthesis, and off- peak energy [12].

### **2.2 Electrochemical Reactor Design (ECR Selection)**

#### **2.2.1 Factors Affecting the Selection of an Electrochemical Reactor**

It is important to design (or select) an electrochemical reactor for a specific process, and it is clear that reactors for energy conversion and electrochemical synthesis will have different drivers to those used in the destruction of electrolyte-based contaminants. Figure 2.1 shows some decisions during the process of selecting an electrochemical reactor.

Adequate attention must be paid to the form of the electrode, its geometry and electrolyte motion, together with the need for cell division or a thin electrolyte gap [3]. The form of the reactants and products and the mode of operation (batch or continuous) are also important design factors [1]. Desirable factors in reactor design (and their implications) include [3]:

- (a) moderate costs (low-cost components, a low cell voltage, and a small pressure drop over the reactor)

- (b) convenience and reliability in operation (designed for facile installation, maintenance, and monitoring)
- (c) appropriate reaction engineering (uniform and appropriate values of current density, electrode potential, mass transport, and flow)
- (d) simplicity and versatility.

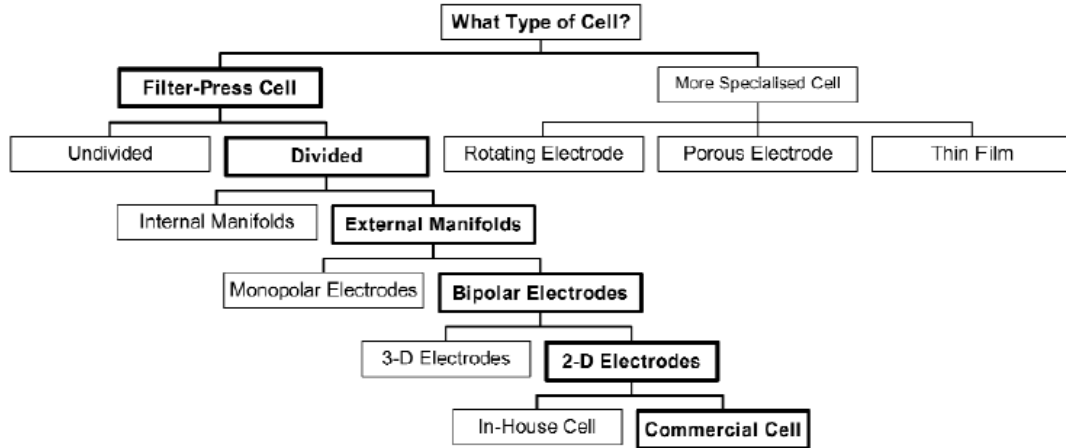


**Figure 2.1** Decisions during the process of selecting an electrochemical reactor [3].

Problem areas for electrode technology and stability may be listed as [3]:

- (a) activity and surface area changes due to catalysis, blockage, and potential-distribution
- (b) adsorption/desorption of reactant, product, intermediates, contaminants
- (c) film formation/removal via, e.g., passivation or polymerization
- (d) phase transformation, e.g., solid–solid, intercalation, dehydration

### 2.2.2 Electrode Configuration

Two principal configurations for packed bed electrode have been developed [12]:

- a- Flow-through configuration.
- b- Flow-by configuration.

### **2.2.2.1 Flow-through Configuration**

For this configuration, the fluid flow and current are parallel. Figure 2.2.a illustrates a flow-through electrode with an upstream counterelectrode (anode), where the porous electrode is represented by rectangle and the separator (diaphragm in case of two compartments) by dashed line. For simplicity, it has been chosen to represent the counterelectrode as a planer electrode; however, in general, the counterelectrode can also be porous electrode. An upstream counterelectrode is favored over a downstream counterelectrode in the flow-through configuration (see fig. 2.3), because it gives a lower ohmic potential drop, particularly at high conversions [13]. The Y direction denotes the direction of fluid flow in fig. 2.2.

For the flow-through configuration, the flow divided as it enters and flows in different directions through the working electrode (cathode) and counter-electrode. Current generated within the porous electrode flows in the same spatial direction as the fluid flow. Because the fluid and current travel in the same direction in this configuration, the analysis remains one-dimensional even in the general case.

### **2.2.2.2 Flow-by Configuration**

For this configuration, the fluid flows perpendicularly to the current. Figure (2.2.b) illustrates a flow-by configuration. In this configuration, the fluid flow is again divided, but here the flow to the working electrode and counterelectrode remains in the same direction. Current generated within the porous electrode travels generally in the X direction, which is perpendicular to the direction of the fluid flow [12]. However, when the directions of the electrical current and electrolyte flow are perpendicular, the general analysis is necessarily two-dimensional [14].

It seems possible to overcome this difficulty using thin electrodes in the current direction and thick in the electrolyte direction [14].

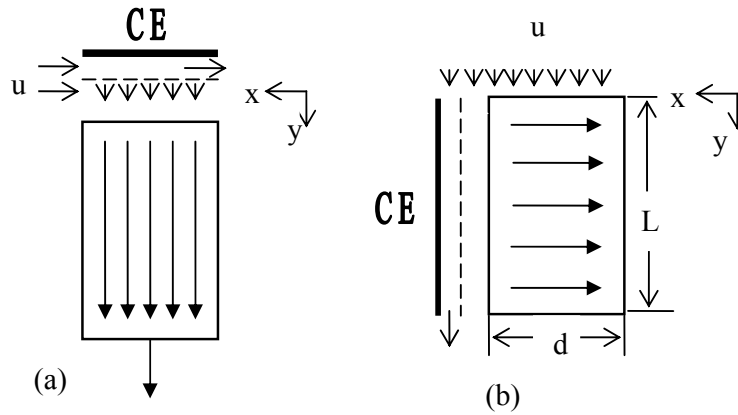


**Figure 2.2** Porous electrode configurations (a): flow-through electrode, upstream counterelectrode. (b): flow-by electrode [12].

### 2.3 Effect of Counterelectrode Placement

Figure 2.3 illustrates the effect of counterelectrode placement on the overall resistance by showing the “effective” current path through the electrolyte for the two cases. In the case of upstream placement, the current must travel only a distance equivalent to approximately  $(u/aK_m) =$  penetration depth  $p$ , whereas in the case of downstream placement, the current path is approximately equivalent to the length of the reactor,  $L$  [7]. If high removal effectiveness is desired, the  $L$  will be much greater than  $(u/aK_m)$ , and consequently, the resistance will be much higher for downstream placement than for upstream placement of the counterelectrode.

(Only the current path through the electrolyte is considered here, since the conductivity of the porous bed is much higher than that of electrolyte. If the conductivity of the electrode matrix is of the same order as that of the

electrolyte, then the placement of the cathode current collector is also important [13]).

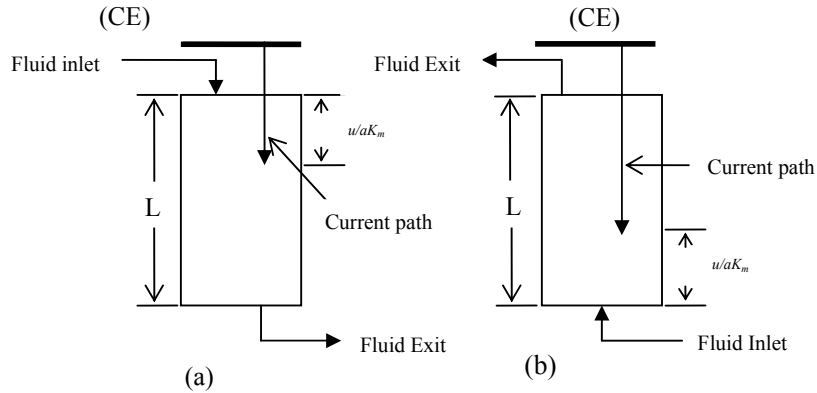


**Figure 2.3** Sketch of the effect of counterelectrode placement on the effective path through the electrolyte. (a) Upstream placement. (b) Downstream placement [7].

In general, the additional cell resistance in the case of the downstream placement causes difficulties in the operation of the reactor, since the possibility of side reaction is increased considerably. Furthermore, this increased likelihood of side reaction has direct effect upon the reactor design [7]. In particular, for high removal efficiency, the current density is directly proportional to the flow rate of catholyte, and ohmic potential drop is directly proportional to the current density. Thus the ohmic potential drop ( $\phi_{Upstream} - \phi_{Downstream}$ ), must be kept below critical value in order to avoid side reactions. The maximum permissible flow rate is higher with upstream placement in the downstream placement. In short, the higher resistance in the downstream counterelectrode configuration limits the throughput of the reactor [15].

## **2.4 Flow-through Porous Electrodes Applications & Features**

The increasing of electrochemical engineering processes for flow-through porous electrodes (FTPE) for diverse applications is come from [7, 12, 14, and 16 - 19]:

- 1- Industrial electrolytic processes including electro-polishing, refining and electro-plating, and machining.
- 2- Electrochemical production of aluminum, chlorine, and other products.
- 3- Off-peak energy, such as electrochemical capacitors (double layer capacitors) which is developed as a back up and pulse power sources for many electronic device.
- 4- Removal of dilute metal ions from waste stream, and electro-organic synthesis.
- 5- Energy conversion in fuel cells and in primary and secondary batteries, recently, they have become of interest in hybrid electric vehicles as an auxiliary power source in combination with a fuel cell or battery.

FTPE posses some attractive features such as [17]:

- 1- They allow for continuous rather than batch operation.
- 2- They provide a high surface area enclosed in a fairly small volume, which enhances the productivity of the cell house.
- 3- They can be operated at fairly high rates, which are maintained by forced convection of the electrolyte within the electrode.
- 4- They separate the reacted from the non-reacted electrolyte when the electrode works with 100% conversion efficiency per pass.
- 5- Removing many polluting metal ions without adding chemicals.

## **2.5 Theoretical Distribution of the Potential in the Electrolyte for Flow- By Electrode.**

It is important to say here that the main concern of this study related with flow-through porous electrode configuration, but for impotency and necessity of this configuration, theories of the flow-by configuration have been reviewed. Comparison can be made between these configurations when the next chapter of this work is presented.

The problem with the flow-through configuration is the difficulty in achieving a uniform potential distribution and high conversion factor simultaneously [14]. However, when the directions of the electrical current and electrolyte flow are perpendicular (i.e. flow-by configuration) as had been mentioned previously, it seems possible to overcome this difficulty using thin electrodes in current direction and long in the electrolyte direction.

Figure 2.4 represents a cathodic fixed electrode, through which the electrolyte flows in the  $y$ -direction at a uniform superficial velocity  $u$ ; the bed void fraction is  $\varepsilon$ , its thickness in the current direction  $x$  is  $L$  and its length in the flow direction is  $y_0$ . The cathodic compartment is separated from the anode with a membrane, which is permeable to the cations and not to the reacting species (anions in this case). Several assumptions are made in order to simplify mathematic treatment [14]:

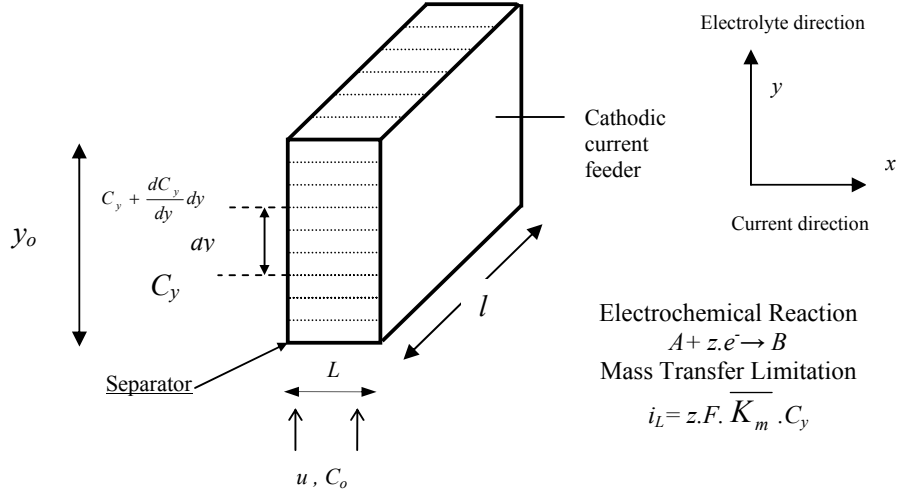


**Figure 2.4** Representation of flow-by electrode configuration for mathematical model [14].

- (a) the porous electrode (metallic phase) is highly conductive, as it is usually the case;
- (b) a single electrode reaction occurs in the cathodic compartment, whose stoichiometry is given by
 
$$A + ze^- \rightarrow B$$
- (c) a supporting electrolyte is present in order to suppress migration of the reacting species;
- (d) axial dispersion is negligible and flow through the cathode is characterized by a plug-flow mode operation in the  $y$ -direction;
- (e) the electrochemical reaction is mass transfer controlled and the local reaction rate is related to the true mass transfer coefficient  $\overline{K}_m$  over the reactor by
 
$$i_L = zF\overline{K}_m C_y \tag{2.1}$$
 $C_y$  denoting the local concentration of the reaction species inside the reactor;
- (f) the structure characterized by an uniform void fraction and specific surface area  $a$ , which do no change during electrolysis.

The equations describing the system in the general tow-dimensional case are:

Mass transfer over a differential element  $dy$  of electrode

$$Q_v C_y = Q_v \left( C_y + \frac{dC_y}{dy} \times dy \right) + \frac{i_L}{zF} a l dy \quad (2.2)$$

Where,  $l$  represents electrode breadth. Conservation of charge equation in the electrolyte phase, which is assimilated to a pseudo-continuous media with the electrical equivalent conductivity  $k_s$  (related to the true electrolyte conductivity  $k_{so}$  by means of the void fraction  $\varepsilon$ )

$$\frac{\partial^2 \phi_s}{\partial x^2} + \frac{\partial^2 \phi_s}{\partial y^2} = \frac{a}{k_s} i_L \quad (2.3)$$

Combining eqs. 2.1 and 2.2 gives the distribution of the concentration  $C_y$  along the electrode

$$C_y = C_o \exp\left(-\frac{a \overline{K}_m}{u} y\right) = C_o e^{-\beta y} \quad (2.4)$$

Which is the well-known equation characterizing a plug-flow type under diffusional conditions. The distribution of  $\phi_s$  in the electrolyte can then be obtained from integration of eq. 2.3, taking into account eq. 2.4.

$$\frac{\partial^2 \phi_s}{\partial x^2} + \frac{\partial^2 \phi_s}{\partial y^2} = \frac{a}{k_s} z F \overline{K}_m C_o e^{-\beta y} \quad (2.5)$$

or

$$\frac{\partial^2 \phi_s}{\partial x^2} + \frac{\partial^2 \phi_s}{\partial y^2} = \omega e^{-\beta y} \quad (2.6)$$

The boundary conditions are chosen to correspond closely to the experimental conditions described in part II of [14].

(a) at the inner boundary of the structure  $x=0$ , the potential is constant:

$\phi_s = 0$  and the membrane is impermeable to the reacting species;

(b) the outer boundary ( $x=L$ ) is an insulator and  $(\partial\phi_s/\partial x)_{x=L} = 0$  for all  $y$  (no current flows through this insulator);

(c) if the electrode is sufficiently long (case of practical interest for industrial applications), no current flows in the  $y$ -direction at the entrance ( $y=0$ ) and outlet ( $y=y_o$ )

$$\left(\frac{\partial\phi_s}{\partial y}\right)_{y=0} = 0 \quad (2.7)$$

and

$$\left(\frac{\partial\phi_s}{\partial y}\right)_{y=y_o} = 0 \quad (2.8)$$

Integration of eq. 2.5 (Poisson's equation) can be achieved by means of the finite Fourier's transformation to obtain

$$\phi_s(x, y) = \frac{\omega}{\beta y_o} \left| 1 - e^{-\beta y_o} \right| \frac{x(x-2L)}{2} + \frac{2\omega\beta}{y_o} \sum_{n=1}^{\infty} \left| \frac{1 - (-1)^n e^{-\beta y_o}}{(\lambda_n^2 + \beta^2)\lambda_n^2} \right| \left| \frac{\cosh \lambda_n(L-x)}{\cosh \lambda_n L} - 1 \right| \cos \lambda_n y \quad (2.9)$$

where  $\lambda_n = n\pi/y_o$ .

The distribution of the local overpotential  $\eta$  inside the structure is of most importance for engineering calculations and for the design of reactors. This overpotential  $\eta$  is defined by  $\eta = E - E_{eq}$  where  $E = \phi_m - \phi_s$  is the local metal-solution potential and  $E_{eq}$  the corresponding equilibrium potential given by the Nernst equation

$$E_{eq} = E^o + \frac{RT}{zF} \ln C_y / C_b \quad (2.10)$$

$C_b$  denotes here the concentration of the reduced species which are present in high concentration and can therefore be considered as a constant. Taking into account eq. 2.4,  $\eta$  is expressed as

$$\eta = \left( \phi_m - E^o - \frac{RT}{zF} \ln \frac{C_o}{C_b} \right) - \phi_s + \frac{RT}{zF} \beta y \quad (2.11)$$

Finally

$$\eta(x, y) = \eta(0, 0) + \frac{RT}{zF} \beta y - \phi_s(x, y) \quad (2.12)$$

## 2.6 Application to the Design of Three-Dimensional Flow-By Structure

The more cathodic point is always located at the cell inlet against the separator but that the less cathodic one is at the level of the current feeder and is characterized by the value  $\eta_{max}(I, Y)$  (i.e. with  $X=1$  and  $Y$  unknown); where  $X = x/L$ , and  $Y = y/y_o$  [14].

In what concerns  $\eta(1, 0) - \eta(0, 0)$ , that this difference is independent of the length  $y_o$  of the working electrode. Taking this result into account, it can be shown from expression (2.8) (by calculating the limit of  $\phi_s$  as  $y \rightarrow 0$ ) that  $\phi_s(X, Y = 0)$  is given by the following expression [14]:

$$\phi_s(X, Y = 0) = \frac{\omega L^2}{2} |X^2 - 2X| \quad (2.13)$$

Consequently

$$\eta(1, 0) - \eta(0, 0) = \omega L^2 / 2 \quad (2.14)$$

which shows that the potential drop at the cell inlet is proportional to  $L^2$  and the overall mass-transfer coefficient (included in  $\omega$ ). This result has been previously observed by different authors [15, 20]. As an example, for a reactor in which the electrolyte flowed in the axial direction and current in the radial direction, Alkire and Ng [20] derived the following expression for the potential drop  $\Delta\eta$  across the width of the electrode

$$\Delta\eta = \omega(r_o - r_i)^2 \exp(-\beta y) \quad (2.15)$$

Which shows that  $\Delta\eta$  is largest at the upstream portion and decreases with axial distance downstream. Expression (2.15) is in good agreement with the one (2.14) obtained in [14] and the conclusion are quite similar. Furthermore

the maximum of  $\eta(X,Y)$  in the porous structure  $\Delta\eta_{\max} = \eta(1,Y) - \eta(0,0)$  is characterized by the relation

$$\Delta\eta_{\max} \geq \eta(1,0) - \eta(0,0)$$

or

$$\Delta\eta_{\max} \geq \omega L^2/2 \text{ [Because } \eta_{\max}(1,Y) \geq \eta(1,0) \text{ ].}$$

This enables one to calculate, for given hydrodynamic conditions the maximum channel thickness  $L_{\max}$  for a maximal allowable range of variation of  $\eta$  (i.e.  $\Delta\eta_{\max}$ )

$$L_{\max} = \sqrt{\left(\frac{2\Delta\eta_{\max}}{\omega}\right)} \quad (2.16)$$

or

$$L_{\max} = \sqrt{\left(\frac{2k_s\Delta\eta_{\max}}{azFK_mC_o}\right)} \quad (2.17)$$

The exact value of the bed thickness  $L_{\max}$  cannot be deduced analytically [14], but expression 2.17 gives as a first approximation, a limiting value of  $L$  useful for a rough engineering design.

## 2.7 Polarization Curve

If the current through an electrode is recorded as a function of electrode potential (with respect to a reference electrode), current vs. electrode potential curves such as those presented in Fig. 2.5 can be achieved. In the general case, three zones can be observed [1, 2, and 21]. The first zone (charge transfer or activation control) is characterized because the use of a larger overpotential leads to an increase in the current; this region is known as

the charge transfer controlled zone because the rate of the process depends on the rate of electron transfer. This zone extends until the overpotential is so large that the reaction rate over the electrodes is very rapid and is only dependent on the rate at which the reactant reaches the electrode, this being known as the mass transport controlled region. If the overpotential ( $\eta$ ) is very high, an increase in the current is observed due to electrolysis of the supporting electrolyte. Three contributions to the mass transport are normally found due to diffusion, convection, and migration.

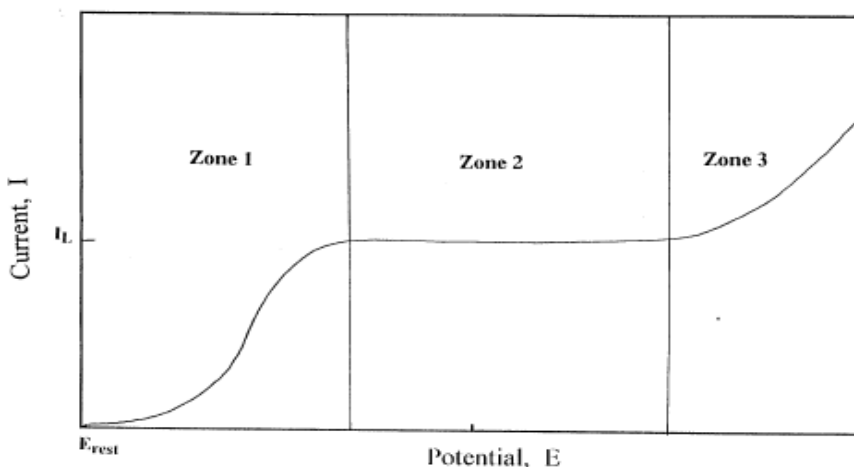


**Figure 2.5** A typical current versus overpotential curve for the single electrode process [2].

Diffusion is the movement of species due to a concentration gradient in the solution and convection is the movement of species due to mechanical forces. Natural convection results if the forces are caused by localized temperature fluctuations and changes of density, whereas forced convection ensues if the solution is moved by external forces, such as electrolyte pumping or electrode movement.

In the case of migration, the movement of electrical charges is due to a potential gradient and this phenomenon is responsible for the passage of ionic current through the electrolyte. In many cases forced convection is the

predominant factor due to the need to achieve high production rates, especially when treating dilute reactants. In practice, it is common to use a large concentration of a conductive background electrolyte and apply forced convection agitation; the conditions are then referred to as “forced-convection”.

According to that mentioned above, two types of operating conditions (charge transfer control, and mass transfer control) classified to calculate the optimum bed thickness for the following reasons:

- (a) The third zone (fig. 2.5) is already charge transfer control [1, 2], it represents a secondary (or side) reaction,
- (b) There are many studies on a flow-through porous electrodes operates under low overpotentials and linear polarization [22-24], which all considers under charge transfer controls regimen,
- (c) There are many studies on a flow-through porous electrodes operates under limiting current conditions [8, 10, 25-28], that means mass transfer control regime, and necessity of classification to reorganization and the accuracy in calculations of such complicated case.

## **2.8 Side Reactions in Electrochemical Reactors**

With the majority of the electrochemical processes only one of the electrode reactions gives a desirable product, so that the reaction that occurs at the counterelectrode has a status comparable with that of a side reaction in a conventional chemical process.

In a number of cases the two electrode reactions proceed more than or less independently except that their reaction rates are coupled. That is to say that the change in the environment which attends either of the reactions has little effect on the progress of the other. If this situation exists, then the most of the reactor design can be accomplished by considering the course of the desired reaction alone [1]. Little more attention need be paid to the second reaction other than to assess its voltage requirement.

In some systems, however, the changes which occur in solution adjacent to an electrode will give rise to an appreciable change in the course of the other electrode process. Not infrequently, this change may be so significant that a side reaction can occur. A relevant example is provided by a metal deposition process with oxygen evolution at the anode. The anodic causes a rise in hydrogen ion transfer to the cathode take place. This result in a decrease in the magnitude of the hydrogen evolution potential and, at some stage, simultaneous hydrogen at the cathode will occur.

A side reaction, however, will occur if the potential of an electrode is greater than the equilibrium potential required for a desired reaction involving any other species present in the system.

The major side reactions associated with the electrolysis of aqueous solutions have already been mentioned previously. These are the cathodic formation of hydrogen and the anodic formation of oxygen according to the respective reactions:



And



Because of the practical importance of cathodic reactions in this case, we shall commence by dealing with hydrogen evolution to determine the

minimum potentials necessary for their occurrence. This negative potential can be realized by knowing the equilibrium potential ( $E_{eq}$ ) of hydrogen through Nernst equation [1]:

$$E_{eq} = E^{\circ} - \frac{2.303RT}{zF} \log \frac{[Reduced]}{[Oxidized]} \quad (2.20)$$

Where the standard equilibrium potential of hydrogen  $E_{H_2}^{\circ}$  is equal to zero by convention  $E_{H_2}^{\circ} = 0$ .

Then eq. 2.20 will be as follows:

$$E_{eq} = 0 - \frac{2.303RT}{1(96487)} \log \frac{[H^+]}{[P_{H_2}]^{1/2}} \quad (2.21)$$

At one atmosphere,  $P_{H_2} = 1$  and as  $pH = -\log[H^+]$ , then eq. 2.21 will become as follows at  $T=298K$ :

$$E_{eq,H_2} = -0.0592 \cdot pH \quad (2.22)$$

or at any temperature

$$E_{H_2} = -\frac{2.303RT}{F} pH \quad (2.23)$$

In this region the current increases above the plateau level and actual hydrogen bubbles are observed on the cathode.

In spite of the evolution of hydrogen consumes power and restricts higher utilization extent of the porous electrode, the gas bubble generated decrease the cross-section available for ionic flow and, consequently, decrease the conductivity of the pore electrode and accentuates the ohmic effects [29].

## 2.9 Mass Transfer Coefficient

The most important kinetic parameter involves in such electrochemical reaction is the mass transfer coefficient. Because of the wide range of reactions controlled by mass transport, the mass transfer coefficient  $K_m$  will justify these limitations of somewhat reaction.

There are many relationships considered to describe the mass transfer coefficient inside the porous electrode over a wide range of conditions. For a packed bed electrochemical reactor of spherical particles that is operated for recovery of heavy metals, the most preferred correlations in many similar works [8, 17, 27, and 30] are the **Wilson and Geankoplis [31]** correlations:

1- for  $10 < R_e < 1500$

$$St = \frac{K_m}{u} = \frac{0.4548}{\varepsilon} R_e^{-0.41} Sc^{-2/3} \quad (2.24)$$

2- for  $0.0016 < R_e < 55, 165 < Sc < 70600$

$$St = \frac{K_m}{u} = \frac{1.09}{\varepsilon} R_e^{-2/3} Sc^{-2/3} \quad (2.25)$$

3- for  $55 < R_e < 1500, 165 < Sc < 10690$

$$St = \frac{K_m}{u} = \frac{0.25}{\varepsilon} R_e^{-0.31} Sc^{-2/3} \quad (2.26)$$

In spite of a wide range of these equations validity over a wide range of operations, these equations, sometimes, don't match the experimental results for various types of packing [7]. Therefore, many studies [7, 10, 25, 32, and 33] predict empirical correlations for a certain situation for a current study. For example: **Al-Habobi and Slaiman (2000) [32]** performed experimental study of flow-through porous electrode of fixed bed of highly conductive

cylindrical copper particles for the reduction of  $Ti^{+4}$  (or  $Fe^{+3}$ ) ions in the presence of sulfuric acid as a supporting electrolyte. They found that mass transfer coefficient, for single particle, is directly proportional to:

$$Sh = \frac{K_m d_p}{D} = m R_e^{0.526(\text{or } 0.5)} \quad (2.27)$$

where  $m$ , is a constant which would be function of the packing geometry. While, **Nava et al. [10]** in a study for determination of effectiveness of FTPE, they used stainless steel fibres as a porous cathode. The mass transfer coefficient calculated from the following expression:

$$K_m a = b u^c \quad (2.28)$$

Where  $a$ , is the specific surface area of the cathode, and the exponent  $c$  is coefficient depend on specific surface area, electrode void fraction, and the shape of the fibre. That's indicates that the flow pattern is a complex function of this coefficient. On the other hand, the values of coefficient  $b$  associated with the electrode geometry, increased with the specific surface area showing the interdependence of this parameter in the mass transport correlation. It is important to mention that the exact form of the mass transport correlation is best evaluated through analysis of experimental data because it depends on the geometry of the electrode, type of fluid flow pattern, and the electrochemical reaction [10].

According to all above mentioned about the importance and complexity of this parameter, it's also important to express the mass transfer coefficient in a general mathematical formula for any process. Therefore and also according to above recommendation [19], the mass transfer coefficient can be estimated from the concentration distribution from experimental results [7] through:

$$\overline{K_m} = \frac{u}{aL} \ln \left[ \frac{C_{out}}{C_o} \right] \quad (2.29)$$

Where  $C_{out}$  and  $C_o$  represent the outlet and inlet electrolyte concentration respectively, and  $\overline{K_m}$  is the average mass transfer coefficient (which is unlike the local coefficient  $K_m$ ) may contain the effects of axial diffusion and dispersion.  $\overline{K_m}$  is more convenient than  $K_m$  for tabulation [7], since its use does not require an independent value of dispersion coefficient ( $D_o$ ), the solution velocity ( $u$ ), the viscosity ( $\mu$ ), and the electrode geometry (pore structure).

Beside expression 2.29 the local mass transfer coefficient  $K_m$  can be obtained from the observed limiting current density  $i_L$  of experimental results through:

$$K_m = \frac{i_L}{zFC_b(x)} \quad (2.30)$$

Comparison can be made between the results of these eqs. (i.e. 2.29 and 2.30), through [7] and [34].

## 2.10 Types of Packing & Void Fraction

A dramatic change in the few years ago for the types of packing have been used in many studies occurred. In order to discover the reasons behind the lifting of many designers of the traditional ways of packing (usually, spherical or cylindrical grains), it should, and first of all classify these types and then showing up the reasons behind this change.

The matrices which have been used in studies concerning fixed bed electrode can be classified into two groups:

(i) On one hand, fixed beds of conducting grains ( $a \approx 1000 - 10\,000 \text{ m}^{-1}$ ), generally spherical and cylindrical (metal, graphite, and metalized glass) with uniform void fraction of about 0.4 [14, 23, 24, 29, 32-34].

(ii) On the other hand, fixed beds consisting of stacks of metallic nets or grid ( $a \approx 500 - 16\,000\text{ m}^{-1}$ ) [27, 35 and 36], or reticulated vitreous carbon (RVC) [7, 39], metallic felts or foams [37, 41], or fibres [10, 18, 25, and 40] with an overall mean void fraction of about 0.8 – 0.96 (see figs. 2.6, 2.7, and 2.8).

Except for small pilot-plant installations, a continuous industrial use of granular fixed bed electrodes would probably be difficult (variation in time of the equipotentiality of the bed, manpower, etc.) [36]. This is the main reason why the earlier works deals with FTPE made of foams, stacks of sheets, etc., indeed, probably this type of electrode matrix could have an easier industrial uses. In addition of their overall mean void fraction of about 0.9, they present indeed a grid of structure and they are relatively easy to construct. Otherwise, their originality is that they have an anisotropic structure and would promote well the turbulence of the electrolyte flowing within their pores. The void fraction  $\varepsilon$  or porosity can be defined as follow [38]:

$$\varepsilon = \frac{\text{Volume of voids in bed}}{\text{Total volume of bed (void + solid)}} \quad (2.31)$$

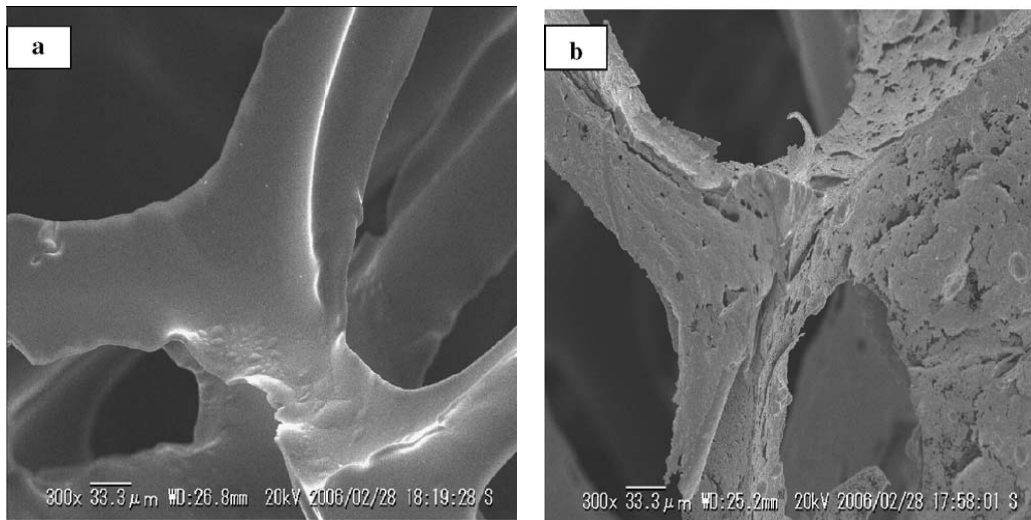


**Figure 2.6** SEM images of plain RVC (a) and RVC/Pt (b) [39].

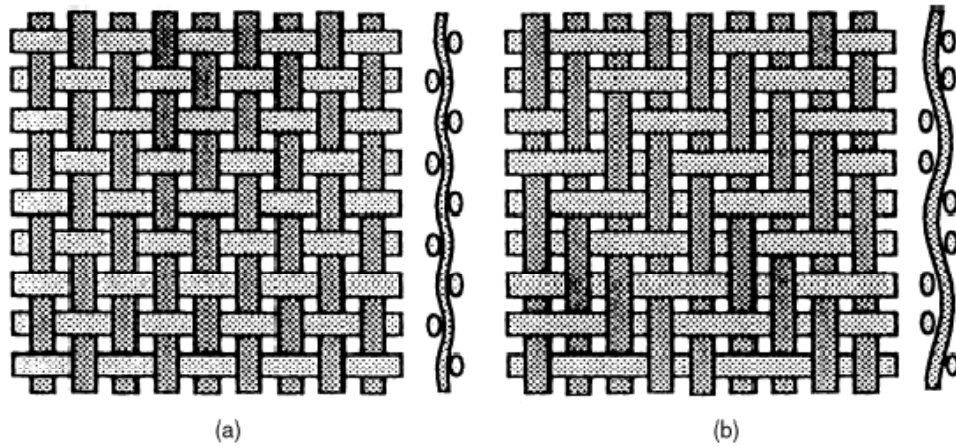


**Figure 2.7** Examples of fibre bundle weaving: (a) cloth and (b) serge [40]

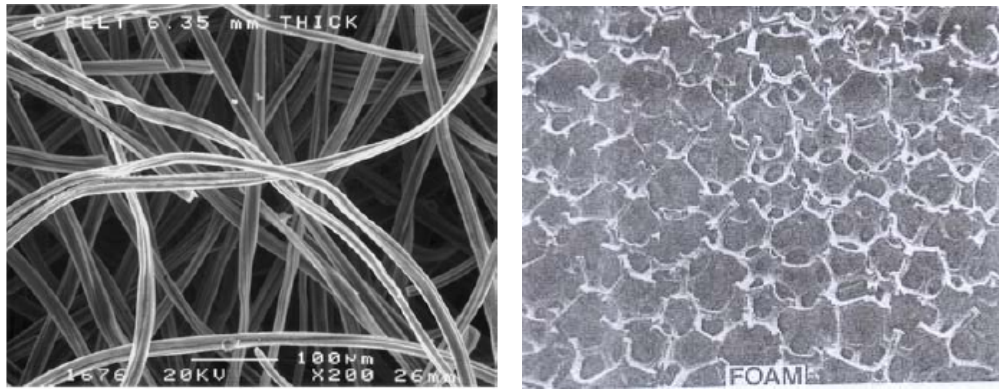


**Figure 2.8** Photographs of felt and foam obtained by electron microscopy [37, 41].

## 2.11 Specific Surface Area

Porous electrode provides a very large electrode surface area in proportional to their size (e.g.  $10^6 \text{ m}^2/\text{m}^3$  volume) and this is several times greater in magnitude than that for non porous structure (typically not greater than  $10^2 \text{ m}^2/\text{m}^3$  for parallel plate system) [42]. The specific surface area of a particle  $a_g$  in  $\text{m}^{-1}$  is defined as:

$$a_g = \frac{S_p}{V_p} \quad (2.32)$$

Where  $S_p$  and  $V_p$  is the surface area of a particle in  $m^2$  and the volume of the particle in  $m^3$  respectively. In case of spherical particle, eq. 2.32 equals:

$$a_g = \frac{\pi d_p^2}{\frac{\pi}{6} d_p^3} = \frac{6}{d_p} \quad (2.33)$$

Therefore, the specific surface area  $a$ , of an electrode of spherical grains equals [5]:

$$a = a_g (1 - \varepsilon) = \frac{6(1 - \varepsilon)}{d_p} \quad (2.34)$$

Where  $d_p$  is the diameter of spherical particle in m. When particles in packed bed are of irregular shape or non-spherical, the equivalent diameter of a particle is defined as the diameter of a sphere having the same volume as this particle. The sphericity shape factor  $\phi_f$  of a particle is the ratio of the surface area of this sphere having the same volume as the particle to the actual surface area of the particle. Therefore,  $\phi_f$  for any particle shape is [38]:

$$\phi_f = \frac{\pi d_p^2}{S_p} \quad (2.35)$$

Consequently, eq. 2.35 leads to changes eq. 2.33 and eq. 2.34 for electrode packed within non-spherical particles as follows:

$$a_g = \frac{6}{d_p \phi_f} \quad (2.36)$$

and

$$a = \frac{6(1 - \varepsilon)}{d_p \phi_f} \quad (2.37)$$

Generally, The specific surface area of the porous electrode,  $a$ , can be defined as the geometric area of the electrode per volume occupied by the electrode).

## 2.12 Literature Review

This section is mainly concerned to previous works for flow-through porous electrodes (FTPE), and (some times) for flow-by porous electrode just in case of similarity or if necessary to point it out. All the mentioned subjects are concerned about optimum bed thickness, penetration depth, effectiveness and any other relevant studies.

**Newman and Teidemann [42]** in (1975) their study for porous electrode theory with battery applications presented macroscopic description for porous electrode and mathematical expression for penetration depth in terms of dimensionless exchange current density of electrode operates under activation control regime. They also presented quantitative design principles for mass transfer control regime, and pointed out that the penetration depth historically, as emphasized by several authors, is similar to the Debye length in diffusion double layer theory.

**Alkire and Gracon [27]** in (1975) investigated experimentally (for a flow-through configuration) the region of operation conditions where mass transfer restrictions affected behavior. They concluded, at low flow rates, that the limiting current is controlled by the rate of reactant supplied to the upstream face of the electrode and the current distribution rather non uniform within the electrode. At high flow rates, the limiting current is controlled by the rate at which reactants are transported to the reactive surface once they have entered the electrode pores, and the current distribution uniform. A theoretical model was developed which includes mass transfer, ohmic, kinetic and geometric parameters.

**Kreysa and Heitz [43]** in (1975) presented the similarity law of effective bed height of packed bed electrodes with a characteristic length derived from electrochemical parameters. The law of similarity derived allows the calculation of the effective bed height on the basis of experimental values.

**Coeuret, Hutin and Gaunand [23]** in (1976) presented a theoretical and experimental study of fixed flow-through electrodes working near equilibrium, i.e. at low local over-potentials. The test reaction used was the cathodic reduction of ferricyanide and the copper deposition. The study establishes the pertinent parameters (effectiveness criterion) of the electrode and outlines the conditions for its 3-dimensional behavior.

**Gaunand, Hutin and Coeuret [26]** in (1977) performed an experimental study of metal-solution potential distribution in flow-through porous electrodes of fixed bed of spherical conducting particles working at limiting diffusion current (the electrolyte flows downward from the cathode to the anode). They also presented a dimensionless parameter characterizing the overall efficiency of the electrode in terms of total current density and limiting diffusion current. They concluded that the metal-solution potential distribution is calculable a priori if the efficiency, the physical and chemical properties of the electrolyte entering the bed, the number of electrons in the electrochemical reaction and the bed height are known.

**Paulin, Hutin and Coeuret [24]** in (1977) studied flow-through porous electrodes consisting of fixed bed of highly conductive spherical grains working under activation control conditions. They re-introduced the effectiveness criterion for electrode operating at high overpotentials by theoretical treatment was similar to that used to solve chemical engineering problems, in which mass transfer between two phases results from competition between diffusion and chemical reaction (gas-solid catalysis, gas-

liquid absorption). They also presented the penetration depth of the reaction in term of the effectiveness criterion, and emphasized that the effectiveness criterion is not a new parameter, but it is a limiting case of the general expression of the dimensionless exchange current density of **Newman and Teidemann [42]**.

**Kreysa [28]** in (1978) studied the kinetic behavior of packed and fluidized bed electrodes. A macro-kinetic model of three-dimensional electrodes was established by introducing overpotential distribution within the electrode into the micro-kinetic rate equation. The developed model was used to derive analytical expression from limiting diffusion current for calculating the optimum bed depth for both packed and fluidized bed electrodes in terms of geometric, hydrodynamics, and kinetic parameters.

The test reaction used was the cathodic quinone reduction to hydroquinone and the experimental parameters studied were electrode potential, flow velocity, bed depth and electrolyte conductivity.

**Trainham and Newman [13]** in (1978) studied a one-dimensional model for flow-through porous electrode (FTPE) approached a prediction of the effluent concentration as a function of electrode placement and matrix conductivity. Two systems were considered for removal of copper from sulfate solutions, and removal of silver from thiosulfate solutions.

**Scott [44]** in (1982) presented the effectiveness of particulate bed electrodes in short communication under activation control for the same definition to that used by **Coeuret et al. [23]**, and **Paulin et al. [24]** and the same way to calculate the penetration depth of the reaction. Comparison had been made between experimental values of effectiveness and theoretical predictions, reasonable agreement was obtained. They also derived the same

expression that had been obtained by **Kreysa and Heitz [43]** for the effective bed height, but by the analogy with the predicted model of effectiveness.

**Storck et al. [14]** in (1982) presented a mathematical model to describe the behavior of flow-by porous electrodes operating under limiting current conditions. Principal results were the effect of electrolyte resistivity, hydrodynamics and cell geometrical parameters on the distribution of the electrolyte potential and overpotential inside the structure. The analytical solution of the predicted model to designing three-dimensional structure (optimum bed thickness) was quite similar to that obtained by **Kreysa [28]** for flow-through porous electrode, but they conclude that the optimum bed thickness  $L_{op}$  cannot be deduced analytically, but it gives a first approximation, a limiting value of  $L$  useful for a rough engineering design.

**Scott [45]** in (1983) presented approximation methods of analysis for the estimation of effectiveness of particulate bed electrodes under activation control. The approximate analysis expression was based on Taylor series. The influence of various parameters such as specific area, exchange current density, electrolyte conductivity, mass-transfer coefficient and charge transfer coefficient were investigated. He concluded that his approximation techniques can quickly give relatively accurate data of performance with reasonable agreement to exact solutions.

**Risch and Newman [12]** in (1984) made a theoretical comparison between flow-through and flow-by configuration at limiting current using the maximum solution-phase potential difference as a basis for comparison. They introduced the penetration depth as a function of the specific surface area, mass transfer coefficient, and electrolyte superficial velocity.

They concluded that at low conversion, a flow-by electrode is favorable, providing it can be constructed with a length-to-width ratio greater

than one. At high conversions, however, a flow-by electrode is favorable if the ratio of the electrode width and penetration depth is less than 2.218 cm.

**Ho and Jorne [22]** in (1986) developed a simple mathematical model and used this model to calculate analytically key parameters (such as overpotential distribution, concentration distribution and local reaction rate distribution) for flow-through porous electrode under linear polarization. They compared the results with numerical solution and concluded that their analytical expressions for key design parameters can be expressed explicitly in terms of the operating conditions, which is easier to design and optimize the electrode.

**Maltosz and Newman [7]** in (1986) performed experimental investigation of a porous electrode made of reticulated vitreous carbon (RVC) to remove mercury from contaminated brine solution. The effect of counterelectrode placement on the cell resistance and the effect of the mass transfer coefficient in the electrode are examined. They concluded that for high removal effectiveness desired, the electrode length will be much greater than penetration depth that has been obtained by **Risch and Newman [12]**, and in case of downstream counterelectrode placement the ohmic resistance would be much greater than for upstream placement of the counterelectrode.

**Kreysa and Jüttner [47]** in (1993) in a study for flow-by three-dimensional electrode of cylindrical geometry operating under limiting current conditions re-introduced the arrangement of electrodes with respect to the direction of the current flow, electrolyte flow, and electrode position. Comparisons have been made among various types of electrode arrangements. Optimum bed thickness also had been investigated for both cylindrical and rectangular arrangements for various electrolyte conductivities. The model used for calculation was similar to that predicted by **Kreysa [28]** with a little difference due to ignoring effects of void fraction.

**Doherty et al. [8]** in (1996) presented a numerical model of flow-through porous electrodes simulates the distribution of potential and current density within a porous electrode. The model includes consideration of the electron transfer control regime of the electrode reaction, mass transport limitations and the finite conductivity of the electrode material. They re-introduced the expression predicted by **Kreysa [28]** for calculation of the optimum bed depth in terms of specific surface area instead of particle size diameter.

They concluded that at high electrode conductivities the optimum length is much less sensitive to electrode depth, whereas, at low conductivities the contrary is true. Therefore, greater accuracy is required when designing porous electrodes with very high porosities and, thus, low electrode conductivities, in order to achieve the optimum electrode depth.

**Masiley and Poudubny [25]** in (1997) presented mathematical simulation of the FTPE operation on the basis of one dimensional model with uniform conducting matrix and the cathode process involving the main and side reaction. They introduced the optimum bed thickness as a part of its total thickness  $L$  proportional to the integral mean value of the ratio of local current of the target reaction to its limiting diffusion value. They also studied the effect of solid and liquid phase conductivity on the effective electrode layer operating under limiting diffusion current. The expression that they obtained in case of solid phase conductivity is much higher than that for electrolyte and was quite similar to that used by **Kreysa and Jüttner [47]**.

**Najim et al. [34]** in (2006) they presented an experimental investigation for production of *P*-aminophenol using a single compartment FTPE electrochemical reactor. The working electrode, (cathode) was of (4.4cm) and a height of (7cm).

They found out experimentally that the intensive polarization took place between 2 and 3 cm at the top of the cathode, little polarization took place between 3-4 cm from the top and almost negligible polarization at the bottom (after 4 cm) of the cathode (near the current collector).

**Nava et al. [10]** in **(2008)** discussed the use of potential distribution analysis during the deposition of metal ions, at limiting current conditions and determine the optimum electrode thickness at which no hydrogen evolution occurs. The potential distribution studies were carried out on stainless-steel fibres of three different surface areas. The fibres were used as cathodic porous electrodes during the deposition of Ag(I) ions contained in  $0.1 \text{ mol dm}^{-3}$   $\text{KNO}_3$  and  $0.6 \text{ mol dm}^{-3}$   $\text{NH}_4\text{OH}$  electrolyte. The comparison of both, experimental and theoretical potential distributions showed that flow rate and specific surface area of the electrode determine the potential drop within the packed bed cathode and therefore the effective thickness of the porous bed electrode at which hydrogen evolution can be avoided.

# **Chapter Three**

## **Theory & Models**

### **3.1 Introduction**

This chapter deals with current, potential and concentration distribution in FTPE from theoretical aspects; and also analytical solution to find out current and potential for both, solid matrix and electrolyte inside the pores. Optimum bed thickness models will be reviewed and classified according to operating conditions.

### **3.2 Macroscopic Description of Porous Electrodes**

Porous electrodes of porous matrices of a single reactive electronic conductor or mixtures of solids which included essentially non-conducting, reactive materials in addition to electronic conductors. An electrolytic solution penetrates the void space of the porous matrix. At a given time, there may be a large range of reaction rates within the pores. The distribution of these rates is depended on physical structure, conductivity of the matrix and of the electrolyte, and on parameters characterizing the electrode processes themselves [42].

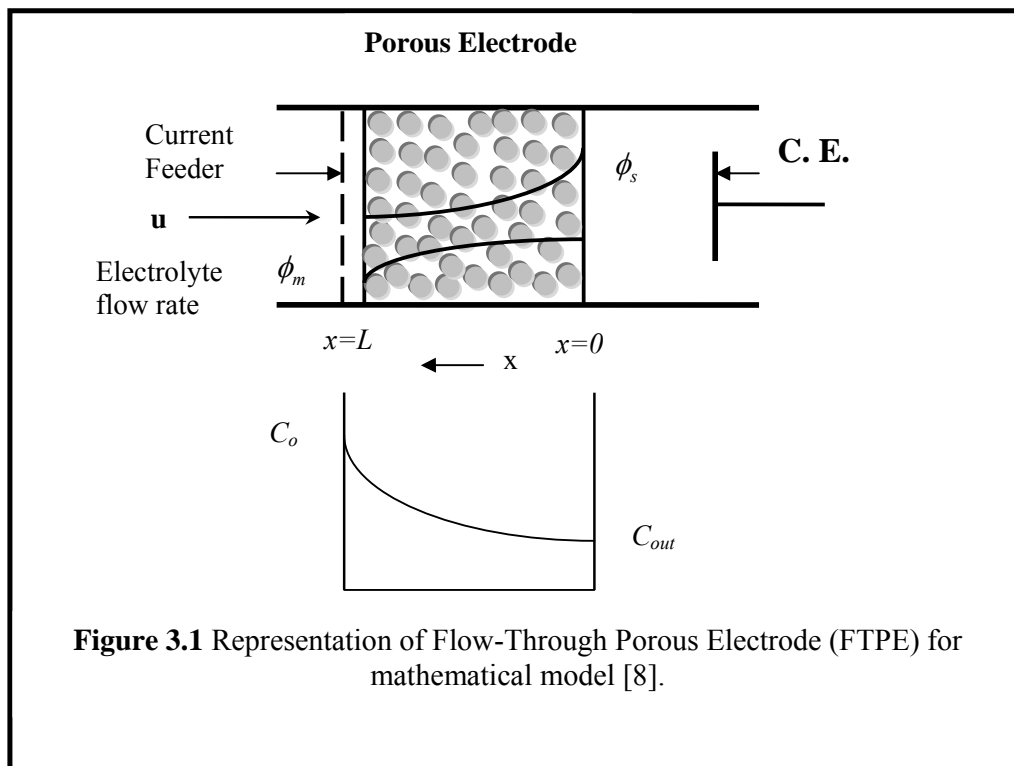
In order to perform a theoretical analysis of such a complex problem, it is necessary to establish a model which accounts for the essential features of an actual electrode without going into exact geometric detail. Furthermore, the model should be described by parameters which can be obtained by suitably simple physical measurements. For example, a porous material of

arbitrary, random structure can be characterized by its void fraction, average surface area per unit volume, volume-average resistivity, etc [42].

### 3.3 Theoretical Analysis of the Flow-through Particulate Bed Electrode

In a part of the previous chapter, theoretical distributions have been made for potential and concentration up to design of three-dimensional flow-by porous electrode.

In this part, the main concern of this study based on finding out an optimum bed thickness for FTPE. First of all, analysis of FTPE is important for such theoretical study.



The analysis considers a one dimensional particulate electrode bounded on one side by a current feeder and on the other by a free solution. Fig. 3.1 shows a particulate electrode of flow-through configuration and fig. 3.2 shows the whole system proposed which includes: flow cycle, pumping, agitating, operation mode, and the main element (packed bed). This type of electrode has been chosen for studying and analysis, in order to select mathematical model to estimate the optimum bed thickness for this kind of electrochemical reactors [10].

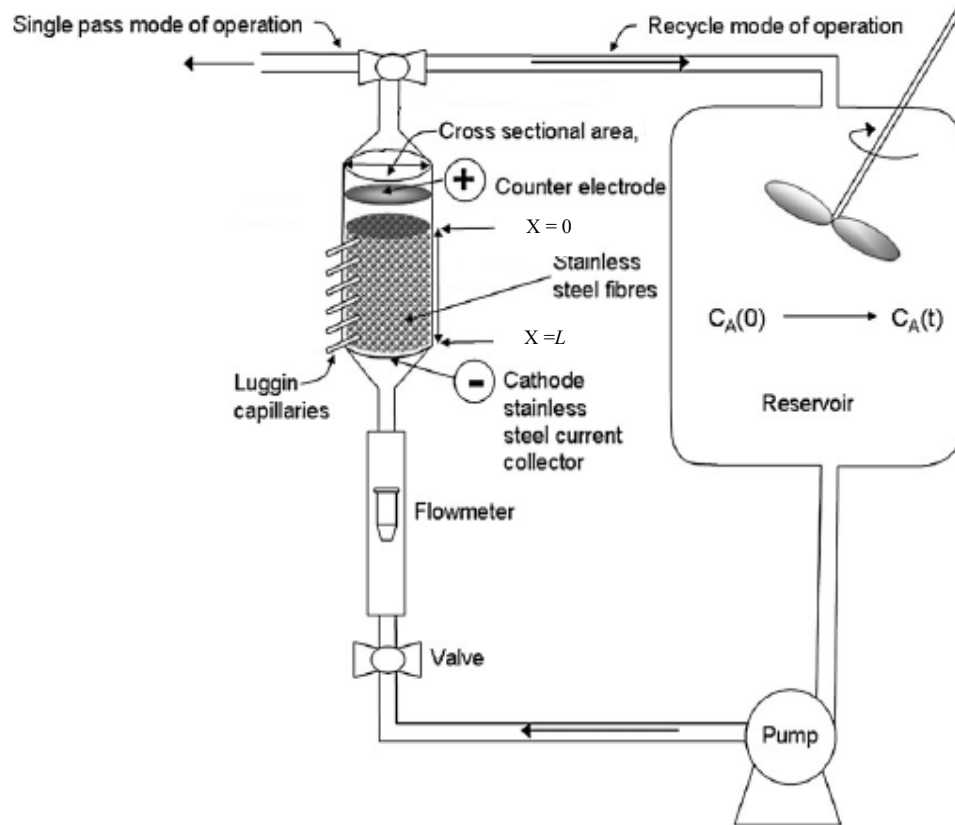


**Figure 3.2** Experimental flow circuit and packed bed electrochemical reactor [10].

### 3.3.1 Concentration, Potential & Current Density Distribution

The considered model simulates the distribution of potential and current density within a porous electrode. The model includes consideration of the electron transfer control regime of the electrode reaction, mass transport limitations and the finite conductivity of the electrode material.

The porous flow through geometry to be studied is shown schematically in Fig. 3.1. Electrolyte flows in the x-direction at the uniform superficial velocity  $u$ ; the bed void fraction is  $\varepsilon$  and its thickness in the x-direction is  $L$ . The treatment is based on a single electrolyte reaction at a cathodic porous electrode:



The conditions at the entrance and exit of the electrode are assumed to be uniform so that the system is one-dimensional (i.e. all variables are a function of position in the x-direction only). The effect of migration of ions in the electrical field is assumed to be negligible. This is acceptable provided there is a sufficient concentration of supporting electrolyte. For the purposes of this simulation axial dispersion is assumed to be negligible. The physical structure of the porous cathode is characterized by uniform void fraction,  $\varepsilon$  and specific surface area,  $a$ . The electrochemical reaction is assumed to be mass transfer controlled for sufficiently high overpotentials. The limiting current per unit of electrode surface area is related to the mass transfer coefficient by [8]:

$$i_L = zFK_m C_o \quad (2.30)$$

Where  $i_L$ , denotes the local limiting current density. The modified Butler-Volmer equation is used to relate the local current density,  $i$  to the local overpotential,  $\eta$ , by means of the kinetic parameters  $i_o$  and  $\alpha$  [8]:

$$i = i_o \left[ \frac{i_L - i}{i_L} \exp\left(\frac{-\alpha zF}{RT} \eta\right) - \frac{i_{LR} - i}{i_{LR}} \exp\left(\frac{(1-\alpha)zF}{RT} \eta\right) \right] \quad (3.2)$$

or equation (3.2) also can be written in an another form [25]

$$i = \frac{i_o \left[ \exp\left(\frac{\alpha z F}{RT} \eta\right) - \exp\left(-\frac{(1-\alpha) z F}{RT} \eta\right) \right]}{\left[ 1 + \frac{i_o}{i_{LR}} \exp\left(-\frac{(1-\alpha) z F}{RT} \eta\right) + \frac{i_o}{i_L} \left(\frac{\alpha z F}{RT} \eta\right) \right]} \quad (3.3)$$

Where  $i_o$ ,  $i_{LR}$ , and  $\alpha$ , are exchange current density, local limiting current for reverse reaction, and symmetry factor respectively. The local overpotential,  $\eta$  can be calculated from the electrolyte potential, electrode potential, reactant concentration and the equilibrium potential calculated from the Nernst equation. Thus [8]:

$$\eta = \phi_m - \phi_s - \left[ E^\circ + \frac{RT}{zF} \ln\left(\frac{C_o}{C_b}\right) \right] \quad (3.4)$$

where  $\phi_s$  and  $\phi_m$  are the electrolyte and electrode potential respectively,  $C_b$  denotes concentration of the reduced species  $B$ , which is present in high concentration and can be considered constant and  $E^\circ$ , is the standard reversible potential of the reaction. The local superficial electrolyte current density (current flow per unit of projected area),  $i_s$ , is given by:

$$\frac{di_s}{dx} = -ai \quad (3.5)$$

Similarly for the electrode phase

$$\frac{di_m}{dx} = ai \quad (3.6)$$

The potential within the electrolyte,  $\phi_s$ , and electrode,  $\phi_m$ , can be related to  $i_s$  and  $i_m$ , using Ohm's law:

$$i_s = -k_s \frac{d\phi_s}{dx} \quad (3.7)$$

$$i_m = -k_m \frac{d\phi_m}{dx} \quad (3.8)$$

Where  $k_s$  and  $k_m$  are the apparent conductivities of the electrolyte and electrode respectively, defined as [8, 10, and 24]:

$$k_s = k_{s_0} \frac{2\varepsilon}{3-\varepsilon} \quad (3.9)$$

$$k_m = k_{m_0} (1-\varepsilon)^{1.5} \quad (3.10)$$

A mass balance for reactant  $A$ , gives a relationship between the concentration,  $C$ , of species  $A$  and the local current density  $i$ :

$$uzF \frac{dC}{dx} = ai \quad (3.11)$$

The boundary conditions for these equations are:

$$C = C_{out} \quad \text{at } x = 0 \quad (3.12)$$

$$i_s = 0 \quad \text{at } x = L \quad (3.13)$$

$$i_m = 0 \quad \text{at } x = 0 \quad (3.14)$$

If the potential applied to the cathode current feeder  $V_c$ , is fixed relative to the electrolyte potential at  $x = 0$ . Thus:

$$\phi_s = 0 \quad \text{at } x = 0 \quad (3.15)$$

$$\phi_m = V_c \quad \text{at } x = L \quad (3.16)$$

### 3.3.2 Analytical Solution

#### \*Concentration distribution

(a) Single Mode of Operation:

Using the assumption that the entire porous electrode is operating under limiting current conditions and the electrode is at a uniform potential (i.e.  $k_m \gg k_s$ ) the above equations can be solved analytically [15]. In this case the local current density,  $i$  is fixed at  $i_L$  and the concentration profile,  $C$ , can be easily obtained by integrating eq. 3.11 with given boundary conditions:

$$C = C_{out} \exp\left(\frac{aK_m}{u} x\right) \quad (3.17)$$

Equation (3.17) represents concentration distribution inside the porous electrode in  $x$ -direction for single-pass or once-through mode of operation. In

case of recycle mode of operation as like fig. 3.2, a mass balance needed in recirculating flow-through reactor with 3-dimensional electrode.

**(b) Recycle Mode of Operation:**

The concentration profile of the electro-active species in a flow-through reactor in batch recycle mode of operation (see fig. 3.2), neglecting phase changes and dispersion effects in the porous electrode, can be described by the following equation [48]:

$$\frac{C(t)}{C(t=0)} = \exp\left[-\frac{t}{\tau_T} \left(1 - \exp^{-[vL]}\right)\right] \quad (3.18)$$

where  $C(t)$  and  $C(t=0)$  are the concentration of the electro-active species during the electrolysis at time  $t$  and  $0$  respectively,  $\tau_T$  is the mean residence time of the electrolyte in the reservoir defined as  $\tau_T = V_T/Q$ , where  $V_T$  and  $Q$  are the volume of the reservoir and the volumetric flow rate.  $L$  is the length of the porous electrode and  $v$  is the following group parameter:

$$v = \frac{K_m a (1 - \varepsilon)}{u} \quad (3.19)$$

Where  $K_m$  is the average mass transport coefficient assuming that it is independent of the axial position ( $x$ ),  $a$  is the specific surface electrode area,  $\varepsilon$  is the electrode void fraction and  $u$  is the mean linear flow velocity of the electrolyte.

**\*\*Potential distribution in a single pass flow-through reactor with 3D electrode**

The potential distribution within the porous electrode is given by [15]:

$$\phi_s = \frac{u^2 z F C_{out}}{a K_m k_s} \left\{ \exp\left(\frac{a K_m}{u} x\right) - \frac{a K_m}{u} \frac{C_o}{C_{out}} x - 1 \right\} \quad (3.20)$$

Where  $C_o$  is the inlet concentration and  $C_{out}$  is the concentration at the front end of the electrode (substitute  $x = 0$  into eq. 3.17). This solution has been

verified experimentally for conditions of low concentration,  $C$  and high electrolyte conductivity by several authors [8, 15].

As an initial approximation the analytical solution of eq. 3.17 and 3.20 are used for the concentration and potential distributions [1]. From these equations the superficial electrolyte and electrode current density  $i_s$  and  $i_m$  can be derived [8]:

$$i_s = uzFC_{out} \left\{ \frac{C_o}{C_{out}} - \exp\left(\frac{aK_m}{u}x\right) \right\} \quad (3.21)$$

$$i_m = uzFC_{out} \left\{ \exp\left(\frac{aK_m}{u}x\right) - 1 \right\} \quad (3.22)$$

The electrode potential distribution can then be derived by integration of equation (3.8) and using equation (3.22):

$$\phi_m = V_c - \frac{u^2 zFC_{out}}{aK_m k_s} \left\{ \exp\left(\frac{aK_m}{u}x\right) + \frac{aK_m}{u}(L-x) - \frac{C_o}{C_{out}} \right\} \quad (3.23)$$

### 3.3.3 Numerical Techniques [8]

The equations are solved using an iterative one dimensional finite difference scheme. The electrode is divided into  $N$  grid points in the  $x$ -direction. Numerical integration is carried out using a scheme based on Simpson's rule. The iterative procedure involves an inner and outer iterative approach [8]. The inner iteration calculates the distribution of current, concentration and overpotential for fixed potential distribution ( $\phi_s$ , and  $\phi_m$ ). The outer iteration calculates  $\phi_s$ , and  $\phi_m$ , from the current distributions calculated from the inner iteration. The iteration steps are as follows:

- (a) The overpotential,  $\eta$  at each grid point is calculated from eq. 3.4.
- (b) The local current density (per unit of electrode surface),  $i$  is calculated at each point from the modified Butler-Volmer eq. 3.3.
- (c) The concentration,  $C$  at each point is calculated by numerically integrating the mass balance eq. 3.9, starting at  $x = 0$  with the boundary condition  $C = C_{out}$  (eq. 3.12).
- (d) Steps (a) to (c) are repeated until convergence in the concentration,  $C$  and current density,  $i$ , is achieved.

The outer iteration involves recalculation of the electrolyte and electrode potential distributions ( $\phi_s$ , and  $\phi_m$ ) from the local current density,  $i$ . The iteration steps are as follows:

- (e) The superficial electrolyte current density,  $i_s$  is calculated using a numerical integration of eq. 3.5, starting at  $x = L$  with the boundary condition  $i_s = 0$  (eq. 3.13).
- (f) Similarly the superficial electrode current density,  $i_m$ , is calculated from a numerical integration of eq. 3.6, but starting at  $x = 0$  with the boundary condition  $i_m = 0$  (equation 3.14).
- (g) The electrolyte potential,  $\phi_s$  is calculated from a numerical integration of eq. 3.7, starting at  $x = 0$  with the boundary condition  $\phi_s = 0$  (eq. 3.15).
- (h) Similarly the electrode potential,  $\phi_m$  is calculated from a numerical integration of eq. 3.8, starting from  $x = L$  with the boundary condition  $\phi_m = V_c$  (eq. 3.16).

Steps (a) to (h) are repeated until convergence is achieved. The convergence criterion is such that the normalized, local change in either, (i) solution potential, (ii) electrode potential, (iii) concentration and (iv) current density. Between adjacent iterations is less than 0.001%. Reducing the convergence criterion to 0.0001% does not change the values observed in distributions (i-iv).

The performance of the porous electrode system can be quantified using the total superficial current obtained (per unit of projected area):

$$i_T = i_m + i_s \quad (\text{at } x = L) \quad (3.24)$$

### 3.4 Optimum Bed Thickness Models

Optimum bed thickness, generally, can be defined as the length of the region where most of the reaction occurs within the electrode [12].

#### (a) FTPE Operate Under Charge Transfer Control (Activation)

(I) Newman & Tiedemann [42] in 1975 defined the penetration depth as “the distance to which the reaction can be penetrating the electrode determines how thick an electrode can be effectively utilized”. This penetration depth is characterized by length in the following equation:

$$\frac{L}{\theta} = \sqrt{\frac{RTk_s k_m}{(k_s + k_m) a i_s z F (\alpha_a + \alpha_c)}} \quad (3.25)$$

(II) K. Scott [44, 45] and Coeuret et al. [24, 26], represented the penetration depth as a function of the effectiveness under activation control. This effectiveness  $\xi$  is defined as follows:

$$\xi = \frac{\text{observed electrolytic current}}{\text{current which would be obtained if } \eta(x) = \eta(L) \text{ at every height } x} \quad (3.26)$$

The penetration depth  $h_e$  given by the following equation:

$$h_e = \xi.L \quad (3.27)$$

And

$$\xi = \frac{I}{Lai_0 \{\exp[-\sigma(\phi_m - \phi_s)]\}_{x=0}} \quad (3.28.a)$$

It is important to say here that the local rate of reaction in the electrode for a Tafel polarization can be written as (cathodic reaction):

$$\frac{dj}{dx} = \frac{Lai_0 \{\exp[-\sigma(\phi_m - \phi_s)]\}}{I} \quad (3.28.b)$$

Where  $\sigma = \alpha (zF/RT)$ ,  $\eta = \phi_m - \phi_s$ . Linear approximation have been used by Newman [49] and result in the following expression for effectiveness

$$\xi = \frac{\tanh \sqrt{\delta}}{\sqrt{\delta}} \quad (3.29)$$

Where  $\delta$  is a dimensionless parameter  $= LI\sigma \left[ \frac{1}{k_m} + \frac{1}{k_s} \right]$ , equation (3.29)

represents the case where the Tafel eq. 3.28.b is linearized at the point of the average reaction rate [44]. At low values of  $\delta$ , i.e. at low current densities or polarization, the electrode kinetic behavior can be represented by a linear polarization equation resulting from the following expression for effectiveness [44, 45]

$$\xi = \frac{\tanh \theta}{\theta} \quad (3.30)$$

Where

$$\theta^2 = \frac{Lai_0 \delta}{I} = \gamma \delta \quad (3.31)$$

The value of the dimensionless group,  $\left(\frac{Lai_0}{I}\right) = (\gamma)$  gives a quantitative criteria for the applicability of the Tafel approximation to particulate electrodes i.e. ( $\gamma < 1$ ) [49]. If  $\gamma = 1$  then the linear approximation to the Tafel analysis, i.e. (3.29) reduced to eq. 3.30. If  $\gamma > 1$  then eq. 3.29 gives value of effectiveness greater than those from 3.30 and hence overestimates the performance.

Therefore, Scott [44] gives a general guide of effectiveness value should be calculated by aid of either following eqs. (3.31 or 3.32) for  $\delta > 1$ , and by aid of eq. 3.30 for  $\delta < 1$ .

$$\xi = 2/\delta \quad (3.31)$$

$$\xi = 0.739 - 0.2445 \log \delta \quad (3.32)$$

(III) **Kreysa [43]** found out the effective bed height  $h_{eff}$  on the basis of experimental values derived from law of similarity as follows:

$$h_{eff} = \varepsilon k_{s_0} \frac{\Delta \eta}{\Delta i} \quad (3.33)$$

### (b) FTPE Operate Under Mass Transfer Control

(I) **Kreysa [28] in 1978** gave expression for optimum bed depth of packed bed electrode derived from diffusion limiting current density as follows:

$$i_L(x) = aK_m zF \int_x^{L_{op}} [C(x)] dx \quad (3.34)$$

$$i_L(x) = aK_m zFC(L_{op} - x) \quad (3.35)$$

For the electrolyte potential  $\phi_s$ , one obtains the expression

$$\phi_s(x) = \int_0^x \frac{i_L(x)}{k_s \varepsilon} dx \quad (3.36)$$

Substitute eq. 3.35 into eq. 3.36 and integrate with boundary condition  $\phi_s(0) = 0$  one obtains

$$\phi_s(x) = \frac{aK_m zFC}{k_s \varepsilon} \left( L_{op} x - \frac{x^2}{2} \right) \quad (3.37)$$

An electrode should be considered as an optimum in the sense explained above if at each point of it  $\geq 99\%$  of limiting current density are realized. Then for packed bed electrode the condition

$$\phi_s(L_{op}) = \eta_{B-F} - \eta_{0.99} \quad (3.38)$$

Substitute for  $a = \frac{6(1-\varepsilon)}{d_p}$  into eq. 3.37 and rearranging to  $L_{op}$  gives the expression:

$$L_{op} = \left[ \frac{\varepsilon k_s d_p (\eta_{B-F} - \eta_{0.99})}{3(1-\varepsilon) K_m zFC} \right]^{0.5} \quad (3.39)$$

Where  $L_{op}$ : the optimum bed depth for which limiting current conditions prevail.

$\eta_{0.99}$ : the over voltage holding the condition:  $i(\eta_{0.99}) = 0.99i_L$

$\eta_{B-F}$ : potential difference between solution potential at the electrode boundary plane nearest the counter electrode and feeder metal potential relative to the equilibrium potential of the electrode reaction.

(II) **Doherty et al. [8]** showed similar expression as above (eq. 3.39) for penetration depth,  $p$  of the limiting current density for metal deposition (assuming that the electrode is fully conducting) is given by:

$$p = \sqrt{\frac{2\varepsilon k_s \Delta \eta}{aK_m zFC_o}} \quad (3.40)$$

Where  $\Delta\eta$  is the range of overpotential where the metal deposition proceeds under limiting current conditions.

(III) **Kreysa et al. [47]** in more recent study than [28] showed the optimum bed depth,  $L_{op}$  in the following expression:

$$L_{op} = \left( \frac{2k_s \Delta\eta}{a.i_L} \right)^{0.5} \quad (3.41)$$

The three models given above are all the same if some rearrangements are made, except a little difference in eq. 3.41 where the void fraction is not in account. Furthermore, these models based on electrode conductivity much higher than electrolyte ( $k_m \gg k_s$ ).

Because of the effects of electrolyte-electrode conductivity on designing of an electrochemical reactor, it has been tabulated. The importance of these parameters is shown in table 3.1.

**Table 3.1** Dependence of penetration depth or optimum bed thickness on the electrode electrolyte conductivity for packed bed **FTPE**.

<i>Case</i>	<i>Penetration depth</i>	<i>[Ref.]</i>	<i>(Eq.)</i>
$k_m \gg k_s$	$h_{op} = \left[ \frac{\varepsilon k_s d_p (\eta_{B-F} - \eta_{0.99})}{3(1 - \varepsilon) z F K_m C_o} \right]^{0.5}$	[28]	(3.39)
$k_m \gg k_s$	$p = \sqrt{\frac{2\varepsilon k_s \Delta\eta}{azFK_m C_o}}$	[8]	(3.40)
$k_m \gg k_s$	$L_{op} = \left( \frac{2k_s \Delta\eta}{a.i_L} \right)^{0.5}$	[25, 47]	(3.41)
$k_m \gg k_s$	$L_d = \sqrt{\frac{2k_s \Delta\eta}{aZFK_m C_o}}$	[25]	(3.42)
$k_m \geq k_s$	$h = \left[ \frac{2\Delta\eta}{ai_L \left( (k_s)^{-1} - (k_m + k_s) \right)^{-1}} \right]^{0.5}$	[50]	(3.43)

**Conti.**

---


$$k_m \leq k_s \quad h = \left[ \frac{2\Delta\eta}{ai_L \left( (k_m)^{-1} - (k_m + k_s) \right)^{-1}} \right]^{0.5} \quad [50] \quad (3.44)$$

$$k_m = k_s \quad L_d = \sqrt{\frac{4k_s \Delta\eta}{azFK_m C_o}} \quad [25, 47] \quad (3.45)$$

$$k_m \ll k_s \quad L_d = \sqrt{\frac{2k_m \Delta\eta}{azFK_m C_o}} \quad [25] \quad (3.46)$$


---

(III) **Newman et al. [7, 12, and 42]** introduced the penetration depth,  $p$  as a function of velocity, specific area, and mass transfer coefficient

$$p = \frac{u}{aK_m} \quad (3.47)$$

(IV) **Masliy et al. [18, 25]** understood the effectively operating thickness  $L_{eff}$  of porous electrode as a part of its total thickness,  $L$  proportional to the integral mean value of the ratio of local current of the target reaction  $i(x)$ , to its limiting diffusion value  $i_L(x)$ .

$$L_{eff} = \int_0^L \frac{i(x)}{i_L(x)} dx \quad (3.48)$$

(V) The more recent study by **Nava et al. [10] (2008)** concerned about determination of the effective thickness of porous electrode in a flow-through porous electrode shows the usefulness type of analysis to estimate the optimum bed thickness from potential distribution which allows efficient recovery of metals by avoiding hydrogen evolution.

$$\phi_s(x) - \phi_s(x=0) = -\frac{zFuC(x=0)}{\nu k_s} [\nu x + \exp^{-\nu x} - 1] \quad (3.49)$$

Where

$$v = \frac{K_m a(1 - \varepsilon)}{u} \quad (3.19)$$

The effective bed thickness obtained can be achieved by plotting the potential distribution (eq. 3.49) vs. electrode thickness  $L$  before hydrogen evolution start.

# Chapter Four

## Calculations & Results

### 4.1 Introduction

An experimental data have been used to simulate the models. Six main different sources have been used in this study for four types of packing material (spherical [28, 29] and cylindrical particles [34], reticulated vitreous carbon (RVC) [7], and stainless steel fibre [10]) as a packed bed cathode. All the experimental data have been used in this study are based on solid matrix conductivity much higher than electrolyte (i.e.  $k_m \gg k_s$ ). All the selected experimental data are performed for FTPE with downstream electrolyte flow, except [7]; which has been performed for both types (upstream and downstream electrolyte flow).

### 4.2 Parameters Affecting the Optimum Bed Thickness

Since the main goal of this study is to find out a mathematical model to represent more suitably the optimum bed thickness for a FTPE, there are several parameters affecting the optimum bed thickness which can be summarized as follows:

- 1- electrolyte flow rate,
- 2- mass transfer coefficient or limiting current density,
- 3- electrolyte concentration,

- 4- electrolyte conductivity (and electrode in case ( $k_s = k_m$ )),
- 5- specific surface area or particle size diameter,
- 6- electrode void fraction,
- 7- temperature, and
- 8- overpotential

### 4.3 Models

Consider the following review for the selected models:

**(1) Kreysa [28]**

$$L_{op} = \left[ \frac{\varepsilon k_s d_p (\eta_{B-F} - \eta_{0.99})}{3(1-\varepsilon)K_m zFC} \right]^{0.5} \quad (3.39)$$

**(2) Doherty et al. [8]**

$$p = \sqrt{\frac{2\varepsilon k_s \Delta \eta}{aK_m zFC_o}} \quad (3.40)$$

Equation 3.39 represents the optimum bed depth ( $L_{op}$ ) of backed bed electrode of spherical particles as a cathode according to [28]. While eq. 3.40 represents the penetration depth ( $p$ ) of the limiting current density for a bed whatever type of packing (i.e., based on specific surface area ( $a$ ) in general) according to [8]. It's important to say here that eq. 3.39 is quite similar to eq. 3.40 by substituting  $a = \frac{6(1-\varepsilon)}{d_p}$  into (3.40) to obtained (3.39).

**(3) Kreysa and Jüttner [47]**

$$L_{op} = \left( \frac{2k_s \Delta \eta}{a i_L} \right)^{0.5} \quad (3.41)$$

**(4) Masliy and Poddubny [25]**

$$L_d = \sqrt{\frac{2k_s \Delta \eta}{azFK_m C_o}} \quad (3.42)$$

Also eq. 3.41 is quite similar to eq. 3.42 since  $i_L = zFK_m C_o$ . Equation 3.41 represents the optimum bed thickness ( $L_{op}$ ) according to [47], while eq. 3.42 represents thickness of porous electrode layer ( $L_d$ ) operating at the limiting diffusion current according to [25].

**(5) Newman et al. [7, 12, and 13]**

Newman presented the penetration length ( $P$ ) in eq. 3.47 below as the length of the region where most of the reaction occurs within the electrode. It is important to refer that the operating conditions of this model are justified by high specific surface area ( $a > 25\text{cm}^{-1}$ ) [13], and low velocities ( $u < 0.09\text{cm/s}$ ) [7].

$$P = \frac{u}{aK_m} \quad (3.47)$$

**(6) Masliy et al. [18, 25]**

They understood the effectively operating thickness of porous electrode ( $L_{eff}$ ) as a part of its total thickness  $L$ , proportional to the integral mean value of the ratio of local current of the target reaction  $i(x)$  to its limiting diffusion value  $i_L(x)$  [25].

$$L_{eff} = \int_0^L \frac{i(x)}{i_L(x)} dx \quad (3.48)$$

(7) Nava et al. [10]

They showed the potential distribution (as in figure bellow) as usefulness type of analysis to estimate the optimum thickness of a packed bed electrode reactor, which allows efficient recovery of metals by avoiding hydrogen evolution [10].

$$\phi_s(x) - \phi_s(x=0) = -\frac{zFuC(x=0)}{\nu k_s} [\nu x + \exp^{-\nu x} - 1] \quad (3.49)$$

$$\nu = \frac{K_m a(1-\varepsilon)}{u} \quad (3.50)$$

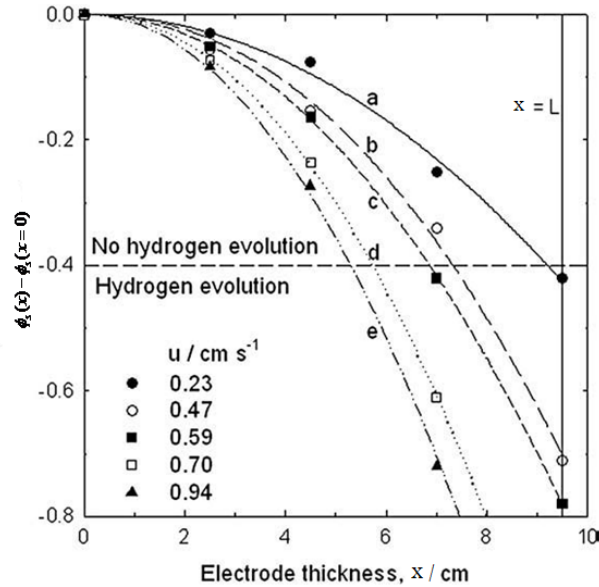


**Figure 4.1** Potential distribution based on eq. 3.49 [10].

Figure 4.1 shows potential distribution for bed of 9.4 cm thick in presence of different flow rates of electrolyte solution. The intercepts of electrolyte potentials for different flow rates within the horizontal line (hydrogen evolution line) represents the optimum bed thickness according to [10]. In order to calculate the start point of hydrogen evolution, the following equation can be used:

$$E_{H_2} = \frac{-2.303RT}{F} pH \quad (2.23)$$

#### 4.4 Calculations Procedure

Considering all models listed above to represent the optimum bed thickness in order to examine, compare, and analyze. The calculations are carried out by using experimental data in order to get best realistic results by avoiding any deviations might occur, in case, if the calculations based on theoretical data (which can be obtained from the related mathematical formulas).

All the calculations carried out are based on the experimental data available in [7, 10, 28, 29, 34, and 47] that have been chosen for this study. These data are almost divided into two categories (e.g., table 4.1 and 4.2). The first category includes the operating conditions, such as reactor dimensions, void fraction, specific surface area, etc. The second category includes the values of the variable parameters that are involved in the calculations and have direct effects or characterize the optimum bed thickness ( $u$ ,  $K_m$ ,  $i_L$ ,  $\Delta\eta$ , etc.).

The limiting current density has been obtained either from polarization curve of experimental data by averaging three points of the limiting current plateau as that way adopted by **Gabe** [46] or from experimental data of concentration distribution based on eq. (2.29) as that adopted by **Newman** [7].

With the aid of the data available in both tables (4.1 and 4.2), the calculations are achieved by using the models previously mentioned

(equations 3.39 – 3.42 and 3.47), while eq. 3.48 needs a special kind of data to perform calculations. These data represented by dimensionless current distribution  $\left(\frac{i(x)}{i_L(x)}\right)$ . The last model eq. 3.49 depends on graphical method to solve the problem as shown in fig. 4.1.

### Sample of calculations

Taking for example **Kreysa's** [28] data as a sample of calculations to show how these calculations are carried out. The study was for quinone reduction at packed and fluidized bed electrodes. The quinone concentration  $C_6H_4O_2$  or [Q], supporting electrolyte concentration  $[Na_2SO_4]$ , and other information are given in tables (4.1 and 4.2).

**Table 4.1** Operating conditions, **Kreysa's data** [28].

$A_c = 7.69 \text{ cm}^2$	$d_p = 0.1 \text{ cm}$	$T = 20 \text{ }^\circ\text{C}$	$[Q] = 10^{-7} \text{ mol/cm}^3$
$a = 36 \text{ cm}^{-1}$	$\varepsilon = 0.4$	$L = 1.15, \text{ and}$ $2.3 \text{ cm}$	$[Na_2SO_4] = 0.5 \text{ mol/l}$
$pH = 5$	$z = 1$		$k_s = 0.053 \text{ (}\Omega \cdot \text{cm)}^{-1}$

The cathodic reduction of quinone to hydroquinone reaction is given by:



**Table 4.2** Values of parameters for models calculations for  $L = 1.15 \text{ cm}$ , **Kreysa** [28].

Run	$u \text{ (cm/s)}$	$K_m \text{ (cm/s)}$	$i_L \text{ (}\mu\text{A/cm}^2\text{)}$	$\Delta\eta \text{ (mV)}$
1	0.57	2.6843E-3	25.9	200
2	4.0	6.6226E-3	63.9	100

It is important to define the term “Run” in the first column of table 4.2, and so on in others, it represents a calculation point; not a programming or

experimental run as it seems at first. Thus, considering the relevant models according to available data in both tables (4.1 and 4.2).

### Run1

$$(1) L_{op} = \left[ \frac{\varepsilon k_s d_p (\eta_{B-F} - \eta_{0.99})}{3(1-\varepsilon)K_m zFC} \right]^{0.5} \quad (3.39)$$

$$= \left[ \frac{0.4 * 0.053 * 0.1(0.2)}{3(1-.04)2.6843 * 10^{-3} * 1 * 96487 * 10^{-7}} \right]^{0.5} = 3.01 \text{ cm}$$

$$(2) p = \sqrt{\frac{2\varepsilon k_s \Delta \eta}{aK_m zFC_o}} \quad (3.40)$$

$$= \sqrt{\frac{2 * 0.4 * 0.053 * 0.2}{36 * 2.6843 * 10^{-3} * 96487 * 10^{-7}}} = 3.01 \text{ cm}$$

$$(3) L_{op} = \left( \frac{2k_s \Delta \eta}{a.i_L} \right)^{0.5} \quad (3.41)$$

$$= \left( \frac{2 * 0.053 * 0.2}{36 * 25.9 * 10^{-6}} \right)^{0.5} = 4.76 \text{ cm}$$

$$(4) L_d = \sqrt{\frac{2k_s \Delta \eta}{azFK_m C_o}} \quad (3.42)$$

$$= \sqrt{\frac{2 * 0.053 * 0.2}{36 * 1 * 2.6843 * 10^{-3} * 96487 * 10^{-7}}} = 4.76 \text{ cm}$$

$$(5) P = \frac{u}{aK_m} \quad (3.47)$$

$$= \frac{0.57}{36 * 2.6843 * 10^{-3}} = 5.89 \text{ cm}$$

As mentioned before, the sixth model (eq. 3.48) needs a special kind of data to do calculations, which is unfortunately not available in this reference (i.e. Kreysa [28]). The remaining model depends on graphical

method summarized by plotting the electrolyte potential difference,  $\phi_s(x) - \phi_s(x=0)$  vs. electrode length; then the optimum bed thickness is characterized by the start point of hydrogen evolution, which can be calculated by eq. 3.49.

## 4.5 Results

### 1- Kreysa's Data [28] (effect of flow rate)

**Table 4.3** Optimum bed thickness according to considered models, (model (5)\* out of its conditions range).

Run	$L_{op}$ (cm) (1) & (2)	$L_{op}$ (cm) (3) & (4)	$L_{op}$ (cm) (5)*
1	3.01	4.76	5.89
2	1.35	2.14	16.77

The numbers between the brackets represent the models according to the sample of calculation that have been made. The “\*” denotes to the results of model 5 is inapplicable out of its conditions range in any position of this chapter and the results are unreasonable.

**Table 4.4** Values of parameters for models calculations for  $L = 2.3$  cm, Kreysa [28].

Run	$u$ (cm/s)	$K_m$ (cm/s)* $10^3$	$i_L$ ( $\mu\text{A}/\text{cm}^2$ )	$\Delta\eta$ (mV)
3	0.57	2.2531	21.74	250
4	1.3	3.3786	32.60	200
5	2.2	4.0046	38.64	200
6	3.0	4.7560	45.89	150
7	3.6	5.0670	48.31	150
8	4.0	5.1312	49.51	100

**Table 4.5** Optimum bed thickness according to considered models, (model (5)<sup>\*</sup> out of its conditions range).

Run	$L_{op}$ (cm) (1) & (2)	$L_{op}$ (cm) (3) & (4)	$L_{op}$ (cm) (5) <sup>*</sup>
3	3.68	5.81	7.02
4	2.68	4.23	10.6
5	2.46	3.88	15.2
6	1.96	3.09	17.5
7	1.91	3.01	19.7
8	1.54	2.43	21.6

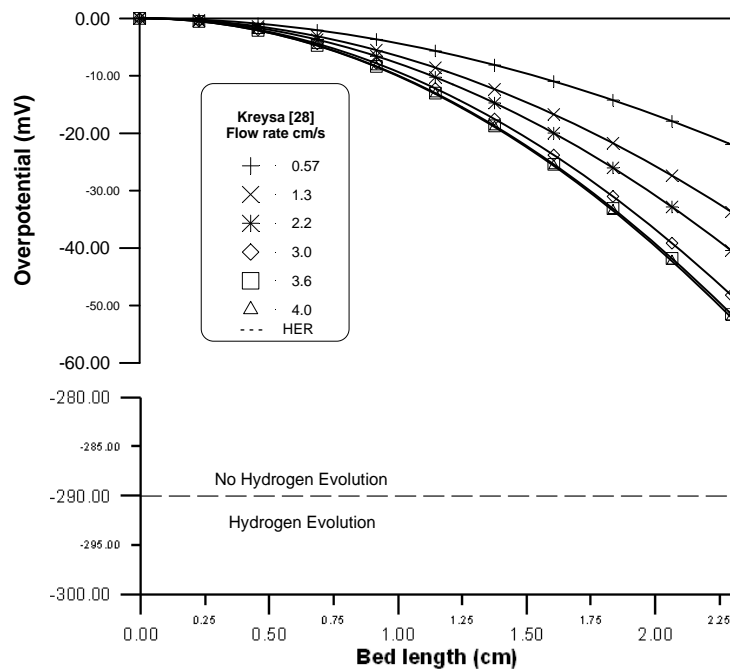


**Figure 4.2** Potential distribution for bed length  $L=2.3$  cm based on model (7) eq. 3.49.

The results of table 4.5 generally show decreasing in the optimum bed thickness for models (1 – 4) as the electrolyte flow rate increase, while the last model appears un-reasonable, and has variant behavior in results. While the result in fig. 4.2 shows no change occurs or the whole bed considered optimum unless the hydrogen evolution line (dashed) intercepts the overpotential curves.

## 2- Newman's Data [7] (effect of flow rate and concentration)

They presented in (1986) experimental study for removal of mercury from contaminated brine in flow-through porous electrode (FTPE) made of reticulated vitreous carbon (RVC). They also investigated the counter electrode placement as a part of the investigation for further study [13]. That study provided some experimental data that could be helpful in the present work for optimum thickness of FTPE calculations. The process is mass-transfer limited at the cathode electrode:



the catholyte was composed of 4.3M NaCl solution containing mercury concentrations between 26 and 110 ppm. The solution was slightly acidic ( $pH=4$ ), but hydrogen gas was not generated under typical conditions because the operating potential for the mercury deposition reaction is not sufficiently negative [7]. The cathode compartment is Plexiglas tube 2 in. (5.08cm) in diameter and 5 in. (12.7cm) in length, other important data obtained in tables below.

**Table 4.6** Physical properties and operating conditions, Newman [7].

$a = 66 \text{ cm}^2/\text{cm}^3$	$k_m = 1.73 (\Omega \cdot \text{cm})^{-1}$	$k_s^o = 0.199 (\Omega \cdot \text{cm})^{-1}$
$\varepsilon = 0.97$	$T = 298.15\text{K}$	$\rho = 1.14 * 10^{-3} \text{Kg}/\text{cm}^3$
$L = 12.7 \text{ cm}$	$pH = 4$	$\mu = 1.52 * 10^{-2} \text{g}/\text{cm} \cdot \text{s}$
$A_c = 20.26 \text{ cm}^2$	$z = 2$	$u = 0.0255 \text{ cm}/\text{s}$

**Table 4.7** Values of parameters for models calculations, Newman [7].

Run	$u \text{ (cm/s)}$	$C_o \text{ (mol/cm}^3 \text{)*}10^7$	$K_m \text{ (cm/s)*}10^4$	$i_L \text{ (}\mu\text{A/cm}^2 \text{)}$	$\Delta\eta \text{ (mV)}$
1	0.0255	2.273	2.102	9.222	300
2	0.0214	3.1253	2.1278	12.833	350

Conti.

3	0.0128	3.1253	1.3811	8.333	350
4	0.00576	3.1253	1.1974	3.563	400

**Table 4.8** Effect of flow rate on effluent concentration at limiting current (experimentally) for upstream CE [7].

Run	$Q$ (cm <sup>3</sup> /min)	$u$ (cm/s)	$C_o$ (mol/cm <sup>3</sup> )*10 <sup>7</sup>	$C_{out}$ (mol/cm <sup>3</sup> )*10 <sup>8</sup>	$\bar{K}_m$ (cm/s)*10 <sup>4</sup>	$L_{op}$ (5) (cm)
1	98	0.0806	1.47745	0.34435	3.615	3.37
2	65	0.0534	3.69362	0.14888	3.513	2.30
3	45	0.0370	6.25075	9.54660	2.862	1.95
4	31	0.0255	3.35267	3.34130	2.102	1.83
5	22	0.0181	2.38665	1.72179	1.562	1.75
6	15	0.0123	3.18220	1.48881	1.125	1.65
7	10	0.00822	3.12537	1.02285	0.787	1.58

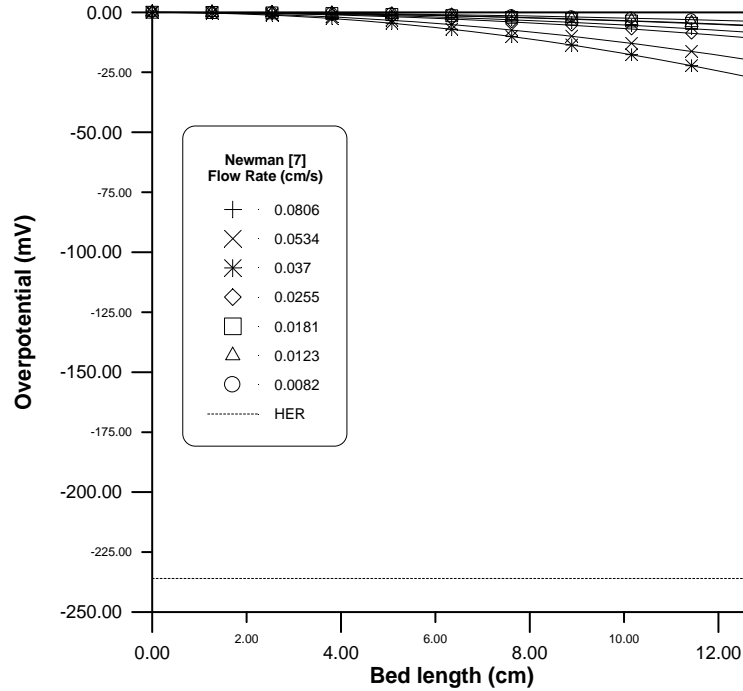


**Figure 4.3** Potential distribution for bed length  $L=12.7$ cm based on model (7) eq. 3.49.

$$\bar{K}_m = -\frac{u}{aL} \ln \left[ \frac{C_{out}}{C_o} \right] \quad (2.29)$$

$$K_m = \frac{i_L}{zFC_o} \quad (2.30)$$

$$k_s = k_{so} \varepsilon^{1.5} \quad (4.3)$$

The results of table 4.8 show an observed change in optimum bed depth according to model 5 due to change in electrolyte flow rate in spite of fluctuation of the concentration. However, fig. 4.3, which is represented by a graphical method [10] to determine the optimum bed height, shows how the overpotential curves are far away from the hydrogen evolution line.

**Table 4.9** Optimum bed thickness calculations according to data of table 4.7.

Run	$L_{op}$ (cm) (1) & (2)	$L_{op}$ (cm) (3) & (4)	$L_{op}$ (cm) (5)
1	13.48	13.69	1.838
2	12.34	12.53	1.523
3	15.30	15.53	1.404
4	25.20	25.59	0.729

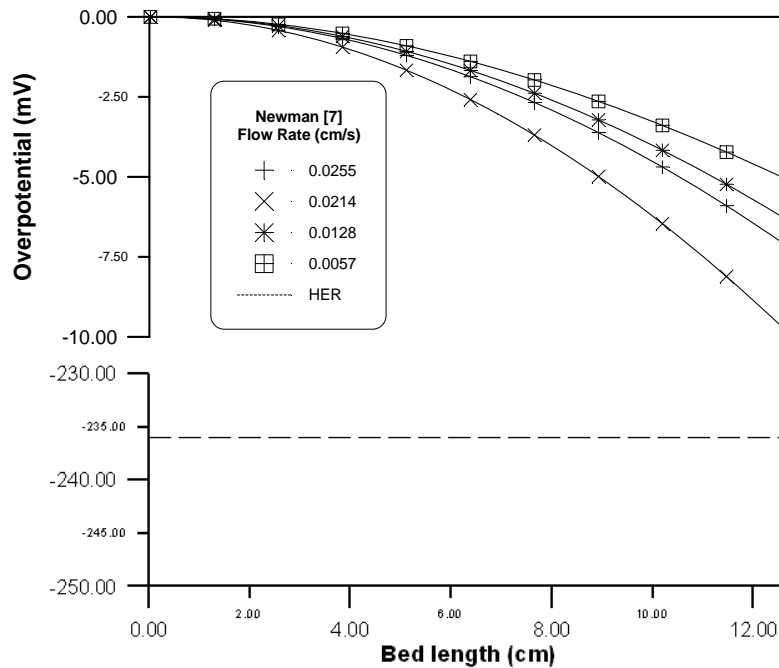


**Figure 4.4** Potential distribution for bed length  $L=12.7$ cm based on model (7) eq. 3.49.

In general, the results in table 4.9 shows a harmony in behavior of the first four models as it was expected, and the differences between the results are slightly small, but the values of the optimum bed thickness in these four models either around or over the actual bed length. While, the results of model 5 shows reasonable values, but the disturbing thing in this results reflect opposite behavior to that appearing in the four other models and that which will discussed in the next chapter. One more thing, figure 4.4 shows how the hydrogen generation is so far to occurs under such typical conditions, and consequently, the whole bed considered here as an optimum or effective according to [10].

### 3- Kreysa and Jüttner's Data [47] (*effect of electrolyte conductivity*)

They presented in study for comparison between cylindrical and rectangular three dimensional electrodes, estimation for optimum bed thickness for different solution conductivities without establishing further details like reaction, type of packing, bed thickness, etc.

**Table 4.10** Optimum bed thickness from literature survey, **Kreysa and Jüttner [47]** for packed bed of specific surface area = 30 cm<sup>-1</sup>.

<i>Run</i>	$i_L$ (mA/cm <sup>2</sup> )	$\Delta\eta$ (mV)	$k_s$ ( $\Omega\cdot\text{cm}$ ) <sup>-1</sup>	$L_{op}$ (cm) (3)
1	5	500	0.5	1.83
2	5	500	0.2	1.15
3	5	500	0.1	0.82
4	5	500	0.05	0.58

Comparison have been made with other models (1, 2 and 4), for void fraction of (0.4, 0.9, and 0.96) with assuming a constant specific surface area ( $a = 30\text{cm}^{-1}$ ), in purpose of testing its effect as a design parameter. This comparison is shown in tables below:

**Table 4.11** Optimum bed thickness comparison for void fraction,  $\varepsilon = 0.4$  and  $a = 30 \text{ cm}^{-1}$ .

<i>Run</i>	$L_{op}$ (cm) (1) & (2)	$L_{op}$ (cm) (3) & (4)
1	1.15	1.83
2	0.72	1.15
3	0.51	0.82
4	0.36	0.58

**Table 4.12** Optimum bed thickness comparison for void fraction,  $\varepsilon = 0.9$  and  $a = 30 \text{ cm}^{-1}$ .

<i>Run</i>	$L_{op}$ (cm) (1) & (2)	$L_{op}$ (cm) (3) & (4)
1	1.73	1.83
2	1.09	1.15
3	0.77	0.82
4	0.54	0.58

**Table 4.13** Optimum bed thickness comparison for void fraction,  $\varepsilon = 0.96$  and  $a = 30 \text{ cm}^{-1}$ .

<i>Run</i>	$L_{op}$ (cm) (1) & (2)	$L_{op}$ (cm) (3) & (4)
1	1.78	1.83
2	1.13	1.15
3	0.80	0.82
4	0.56	0.58

The results in tables above show as the void fraction  $\varepsilon$  approaches to 1.0, as the optimum bed thickness getting a rise and also approaches to both other models. These results show how does void fraction makes differences from mathematical point of view.

#### **4- Saleh's Data [29] (2004) (effect of flow rate)**

Saleh Re-introduced the term of effectiveness factor in his study to investigate the effects of different parameters (effects of ohmic resistance, mass transfer, kinetics, and bubble formation) on the utilization extent of a

flow-through porous electrode operating for simultaneous reactions (zinc deposition with hydrogen evolution).

**Table 4.14** Operating conditions of Saleh's data [29].

$A_c = 1.54 \text{ cm}^2$	$d_p = 0.3 \text{ cm}$	$T = 25 \text{ }^\circ\text{C}$
$a = 12 \text{ cm}^{-1}$	$\varepsilon = 0.5$	$[\text{KOH}] = 3 \text{ M}$
$D_R = 1.4 \text{ cm}$	$L = 1.7 \text{ cm}$	$[\text{Zn}^{2+}] = 8 \cdot 10^{-5} \text{ mol/cm}^3$
$k_{s,o} = 0.4 \text{ (}\Omega \cdot \text{cm)}^{-1}$	$k_s = 0.16 \text{ (}\Omega \cdot \text{cm)}^{-1}$	$\text{pH} = 11.477$
$z = 2$	$D = 1.5 \cdot 10^{-5} \text{ cm}^2 \text{ s}^{-1}$	$\nu = 0.01 \text{ g cm}^2 \text{ s}^{-1}$

**Table 4.15** Experimental values of parameters for models calculations, Saleh [29].

Run	$u \text{ (cm/s)}$	$K_m \text{ (cm/s)} \cdot 10^4$	$i_L \text{ (mA/cm}^2\text{)}$	$\Delta\eta \text{ (mV)}$
1	0.1	6.33500	9.780	400
2	0.3	7.97580	12.31	400
3	1.0	10.0402	15.50	400
4	3.4	15.9088	24.56	400
5	7.3	22.4771	34.70	400

Obviously from table 4.15 there are big effects of electrolyte flow rate on the mass transfer coefficient and consequently on limiting current density.

**Table 4.16** Optimum bed thickness comparison based on experimental data, (model (5)\* out of its conditions range).

$Run$	$L_{op} \text{ (cm)}$ (1) & (2)	$L_{op} \text{ (cm)}$ (3) & (4)	$L_{op} \text{ (cm)}$ (5)*
1	0.73	1.03	13.15
2	0.65	0.91	31.34
3	0.58	0.82	82.99
4	0.46	0.65	178.0
5	0.39	0.55	270.6

The results in table 4.16 show the optimum bed thickness comparison for various models based on experimental data of reference [29]. Figure 4.5 shows the effective bed thickness according to [10] at various flow rates. As shown in figure 4.5 below, the whole bed is optimum for flow rates 0.1 and

0.3 cm/s. The rest flow rates (1.0, 3.4, and 7.3) indicate that optimum bed thickness approximately equal to 1.5, 1.2, and 1.0 cm respectively.

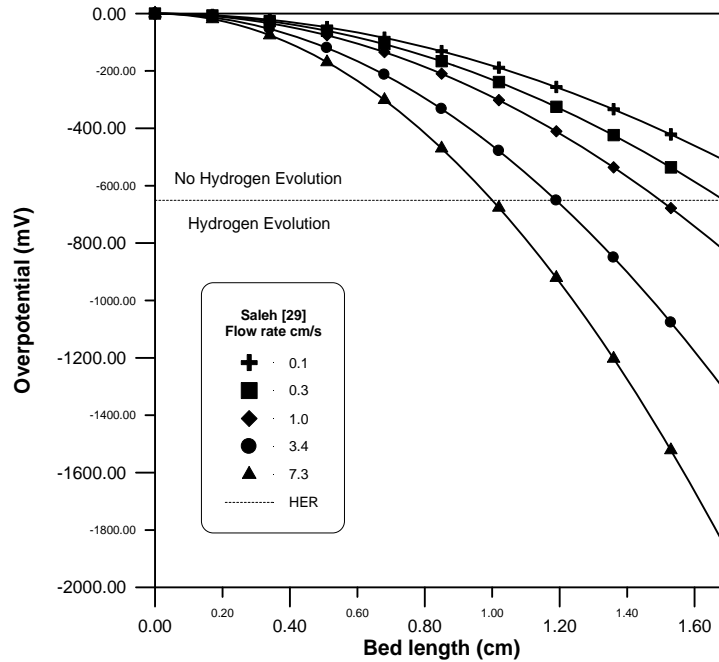


**Figure 4.5** Potential distribution for bed length  $L=1.7\text{cm}$  based on model (7) eq. 3.49.

**Table 4.17** Values of parameters for models calculations (theoretically), Saleh [29].

Run	$u$ (cm/s)	$K_m$ (cm/s)* $10^4$	$i_L$ (mA/cm <sup>2</sup> )	$\Delta\eta$ (mV)
1	0.1	9.4575	14.60	400
2	0.3	17.885	27.61	400
3	1.0	35.956	55.50	400
4	3.4	73.119	112.8	400
5	7.3	113.89	175.8	400

Table 4.17 represents parameters like that in table 4.18 involves in such models to calculate the optimum bed thickness, but these parameters have been calculated from mathematical formulas in order to make comparison with that obtained experimentally as in table 4.15. The mass transfer coefficient  $K_m$ , and the limiting current density  $i_L$ , can be obtained from the equations have been used by [29]:

$$K_m = 1.17u^{0.58} \left[ \frac{d_p}{\nu} \right]^{-0.42} \left[ \frac{\nu}{D} \right]^{-0.67} \quad (4.5)$$

$$i_L = zFK_m C_o \quad (2.30)$$

According to equations above, the data in table 4.20 have been calculated and then used to calculate the optimum bed thickness from the considered models.

**Table 4.18** Optimum bed thickness comparison based on theoretical data, (model (5)\* out of its conditions range).

Run	$L_{op}$ (cm) (1) & (2)	$L_{op}$ (cm) (3) & (4)	$L_{op}$ (cm) (5)*
1	0.60	0.85	8.81
2	0.44	0.62	13.9
3	0.31	0.43	23.1
4	0.21	0.30	38.7
5	0.17	0.24	53.4

The results in tables 4.15, 4.16, and 4.17, 4.18 show the deviation between the experimental and theoretical data and results respectively.

### 5- Najim's Data [34] (Ph.D. thesis)

*(Effects of flow rate, concentration, and temperature)*

They presented experimental investigation for production of *P*-aminophenol using a single and double compartment FTPE electrochemical reactor. Cylindrical particles of copper 0.56cm in diameter and 1.0 cm. long were used as packing. The working electrode, (cathode) has a diameter of 4.4cm and a height of 2 (or 7) cm. For production of *P*-aminophenol, ferric ions had been used as a redox system:



in presence of 0.5M sulfuric acid as a supporting electrolyte;  $[Fe^{3+}] = 2.5, 5$

and 15mM. The void fraction assumed constant vs. time ( $\varepsilon = 0.38$ ). While for this case (i.e. the particles are of cylindrical shape)  $d_p$  in eq. 3.39 would be:

$$a = \frac{6(1-\varepsilon)}{d_p \phi_f} \Rightarrow d_{eq} = d_p \phi_f = \frac{6(1-\varepsilon)}{a} \quad (2.37)$$

Where  $a$ : specific surface area of the electrode ( $m^{-1}$ ),  $\phi_f$  is shape factor (=0.844 for this case).

$$a = (\text{surface area of the particle} / \text{volume of the particle}) (1-\varepsilon)$$

$$= (a_s / V_p) (1-\varepsilon) = 566.85714 m^{-1}$$

$$d_{eq} = 7.77547393 \text{ mm}$$

**Table 4.19** Electrolyte physical properties, Najim [34].

T (C)	$\rho(Kg/m^3)$	$\mu(Kg/m.s)$
30	1038	8.285 E-7
40	1034	7.253 E-7
50	1030	6.602 E-7

**Table 4.20** Electrolyte flow rate and velocity, Najim [34].

Q(l/h)	Q(m <sup>3</sup> /s)	u (m/s)
100	2.777 E-5	0.0182684
200	5.555 E-5	0.0365369
300	8.333 E-5	0.0548054

**Table 4.21** Initial electrolyte conductivity at various temperatures and concentrations, Najim [34].

Concentration (mM)	Conductivity $k_{so} (\Omega.m)^{-1}$		
	T=30 (C)	T=40 (C)	T=50 (C)
0	15.0	18.0	20.0
2.5	35.1	43.1	50.6
5.0	39.0	47.0	55.0
15	41.3	48.6	56.0

The data in table 4.21 above are based on initial values of electrolyte conductivity, and table 4.22 below based on the following relation [10, 23, and 24]:

$$k_s = k_{so} \left( \frac{2\varepsilon}{3-\varepsilon} \right) \quad (3.9)$$

where  $k_s$  and  $k_{so}$ , represents the initial and effective electrolyte conductivity respectively.

**Table 4.22** Effective electrolyte conductivity for various temperatures and concentrations according to eq. 3.9.

Concentration (mM)	Conductivity $k_s$ ( $\Omega.m$ ) <sup>-1</sup>		
	T=30 (C)	T=40 (C)	T=50 (C)
0	4.3511	5.2213	5.8015
2.5	10.1816	12.5023	14.677
5	11.3123	13.6335	15.954
15	11.9801	14.0977	16.244

**Table 4.23** Simulation runs for calculation of the optimum bed thickness for bed of 2cm thick, void fraction ( $\varepsilon= 0.38$ ), and  $[Fe^{3+}] = 2.5$  mM [34].

Run	Q (l/hr)	T (C)	$k_s$ ( $\Omega.m$ ) <sup>-1</sup>	$i_L$ (A/m <sup>2</sup> )	$K_m$ (m/s)*10 <sup>6</sup>	$\Delta\eta$ (mV)
1	100	30	10.1816	2.5	3.45469	200
2	200	30	10.1816	2.5	3.45469	200
3	300	30	10.1816	3.0	4.14563	220
4	100	40	12.5023	2.5	3.45469	200
5	200	40	12.5023	3.5	4.83657	200
6	300	40	12.5023	3.5	4.83657	200
7	100	50	14.677	2.0	2.76375	200
8	200	50	14.677	3.0	4.14563	200
9	300	50	14.677	5.0	6.90939	250

**Table 4.24** Simulation runs for calculation of the optimum bed thickness for bed of **2cm** thick, void fraction ( $\epsilon = 0.38$ ), and  $[\text{Fe}^{3+}] = 5.0 \text{ mM}$  [34].

Run	$Q$ (l/hr)	$T$ (C)	$k_s$ ( $\Omega \cdot \text{m}$ ) <sup>-1</sup>	$i_L$ (A/m <sup>2</sup> )	$K_m$ (m/s)*10 <sup>6</sup>	$\Delta\eta$ (mV)
10	100	30	11.3123	3.0	2.07281	200
11	200	30	11.3123	3.0	2.07281	200
12	300	30	11.3123	4.0	2.76375	225
13	100	40	13.6335	4.5	3.10922	200
14	200	40	13.6335	4.0	2.76375	200
15	300	40	13.6335	4.0	2.76375	200
16	100	50	15.954	2.5	1.72734	200
17	200	50	15.954	4.0	2.76375	200
18	300	50	15.954	5.0	3.45696	175

**Table 4.25** Simulation runs for calculation of the optimum bed thickness for bed of **2cm** thick, void fraction ( $\epsilon = 0.38$ ), and  $[\text{Fe}^{3+}] = 15.0 \text{ mM}$  [34].

Run	$Q$ (l/hr)	$T$ (C)	$k_s$ ( $\Omega \cdot \text{m}$ ) <sup>-1</sup>	$i_L$ (A/m <sup>2</sup> )	$K_m$ (m/s)*10 <sup>6</sup>	$\Delta\eta$ (mV)
19	100	30	11.9801	3.5	0.80609	175
20	200	30	11.9801	4.5	1.03640	200
21	300	30	11.9801	5.0	1.15156	200
22	100	40	14.0977	3.5	0.80609	200
23	200	40	14.0977	5.0	1.15156	175
24	300	40	14.0977	6.0	1.38187	175
25	100	50	16.244	4.0	0.92125	200
26	200	50	16.244	5.5	1.26672	150
27	300	50	16.244	7.0	1.61219	150

**Table 4.26** Simulation runs for calculation of the optimum bed thickness for bed of **7cm** thick, void fraction ( $\epsilon = 0.38$ ), and  $[\text{Fe}^{3+}] = 15.0 \text{ mM}$  [34].

Run	$Q$ (l/hr)	$T$ (C)	$k_s$ ( $\Omega \cdot \text{m}$ ) <sup>-1</sup>	$i_L$ (A/m <sup>2</sup> )	$K_m$ (m/s)*10 <sup>6</sup>	$\Delta\eta$ (mV)
28	100	40	14.0977	4.5	1.03640	250
29	200	40	14.0977	5.0	1.15156	285
30	300	40	14.0977	7.0	1.61219	350

**Table 4.27** Optimum bed thickness comparison for bed of **2cm** thick, void fraction ( $\epsilon = 0.38$ ), and  $[\text{Fe}^{3+}] = 2.5 \text{ mM}$ , (model (5)\* out of its conditions range).

<i>Run</i>	$L_{op}$ (cm) (1) & (2)	$L_{op}$ (cm) (3) & (4)	$L_{op}$ (m) (5)*
1	3.30	5.35	9.33
2	3.30	5.35	18.66
3	3.16	5.12	23.32
4	3.66	5.93	9.33
5	3.09	5.01	13.33
6	3.09	5.01	19.99
7	4.43	7.18	11.66
8	3.62	5.87	15.55
9	3.13	5.07	13.99

**Table 4.28** Optimum bed thickness comparison for bed of **2cm** thick, void fraction ( $\epsilon = 0.38$ ), and  $[\text{Fe}^{3+}] = 5.0 \text{ mM}$ , (model (5)\* out of its conditions range).

<i>Run</i>	$L_{op}$ (cm) (1) & (2)	$L_{op}$ (cm) (3) & (4)	$L_{op}$ (m) (5)*
10	3.17	5.14	15.54
11	3.17	5.14	31.09
12	2.92	4.74	34.98
13	2.85	4.62	10.36
14	3.02	4.90	23.32
15	3.02	4.90	34.98
16	4.13	6.70	18.65
17	3.27	5.30	23.32
18	2.73	4.43	27.96

**Table 4.29** Optimum bed thickness comparison for bed of **2cm** thick, void fraction ( $\epsilon = 0.38$ ), and  $[\text{Fe}^{3+}] = 15.0 \text{ mM}$ , (model (5)\* out of its conditions range).

<i>Run</i>	$L_{op}$ (cm) (1) & (2)	$L_{op}$ (cm) (3) & (4)	$L_{op}$ (m) (5)*
19	2.83	4.59	39.98
20	2.67	4.33	62.19
21	2.53	4.10	83.95
22	3.28	5.32	39.98
23	2.57	4.17	55.97
24	2.34	3.80	69.96

Conti.

25	3.29	5.34	34.98
26	2.43	3.94	50.88
27	2.16	3.50	59.96

**Table 4.30** Optimum bed thickness comparison bed of **7cm** thick, void fraction ( $\epsilon = 0.38$ ), and  $[\text{Fe}^{3+}] = 15.0 \text{ mM}$ , (model (5)<sup>\*</sup> out of its conditions range).

Run	$L_{op}$ (cm) (1) & (2)	$L_{op}$ (cm) (3) & (4)	$L_{op}$ (m) (5) <sup>*</sup>
28	3.23	5.23	31.09
29	3.27	5.30	55.97
30	3.07	4.98	59.96

In general, the results of the current data [34] show overestimated optimum bed thickness for packed bed of 2cm in length for the first four models, while, the results for bed of 7cm, models (1 – 4) show reasonable and acceptable values. The results of model 5 have been carried out by using data which are actually out of its conditions range.

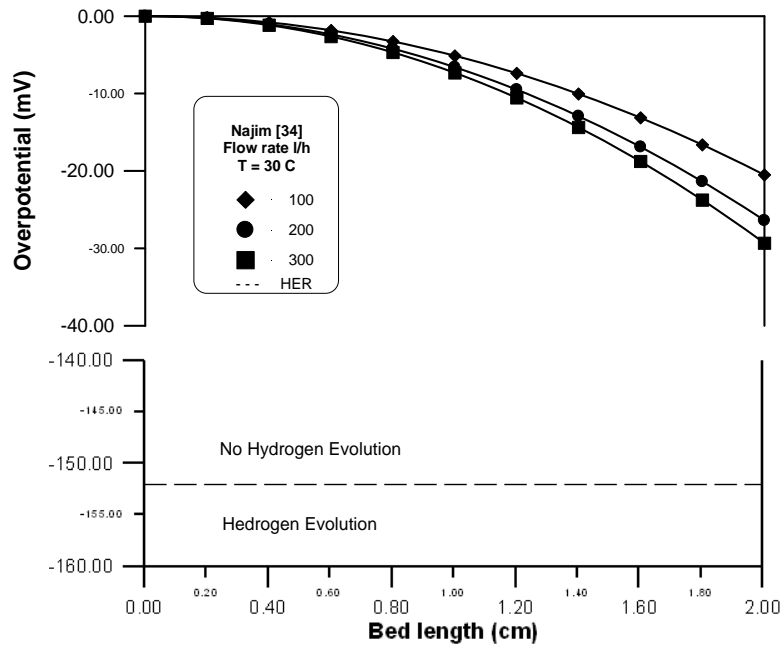


**Figure 4.6** Potential distribution for bed length  $L=2\text{cm}$ ,  $[\text{Fe}^{3+}] = 15\text{mM}$  based on eq. 3.49.

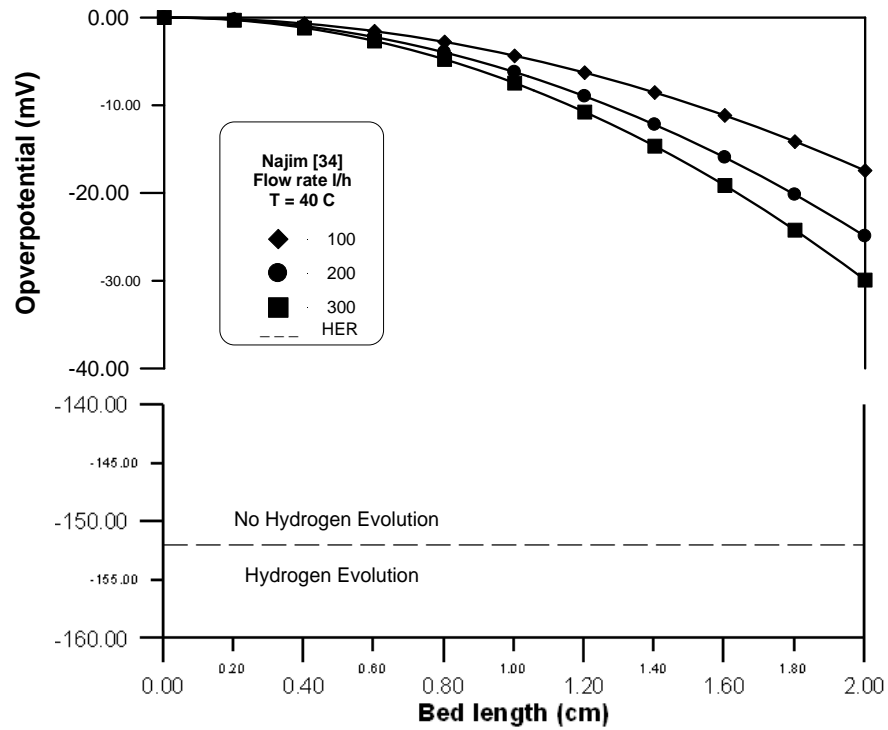


Figure 4.7 Potential distribution for bed length  $L=2\text{cm}$ ,  $[\text{Fe}^{3+}]=15\text{mM}$  based on eq. 3.49.

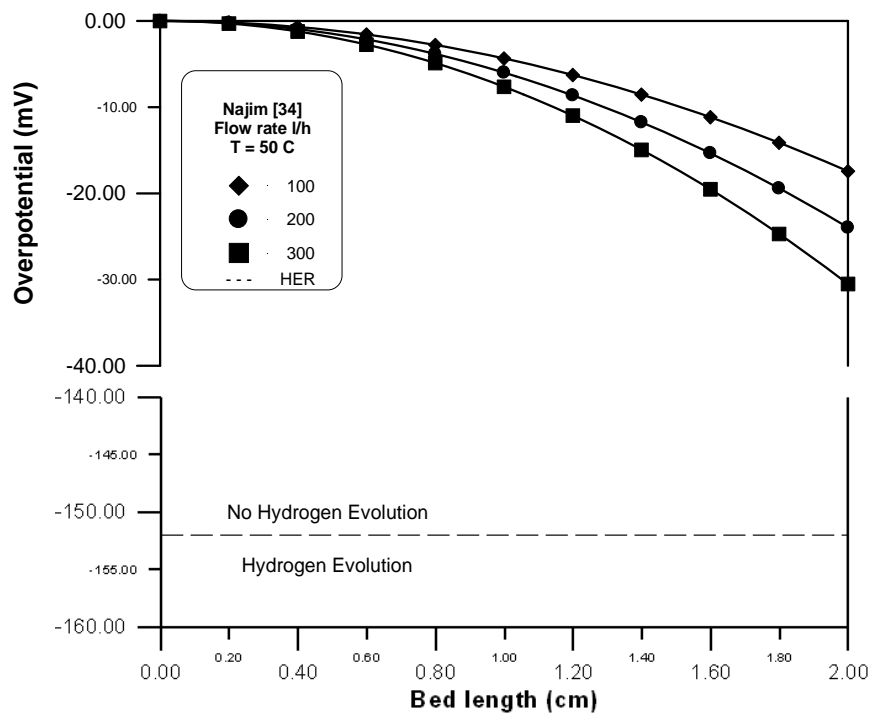
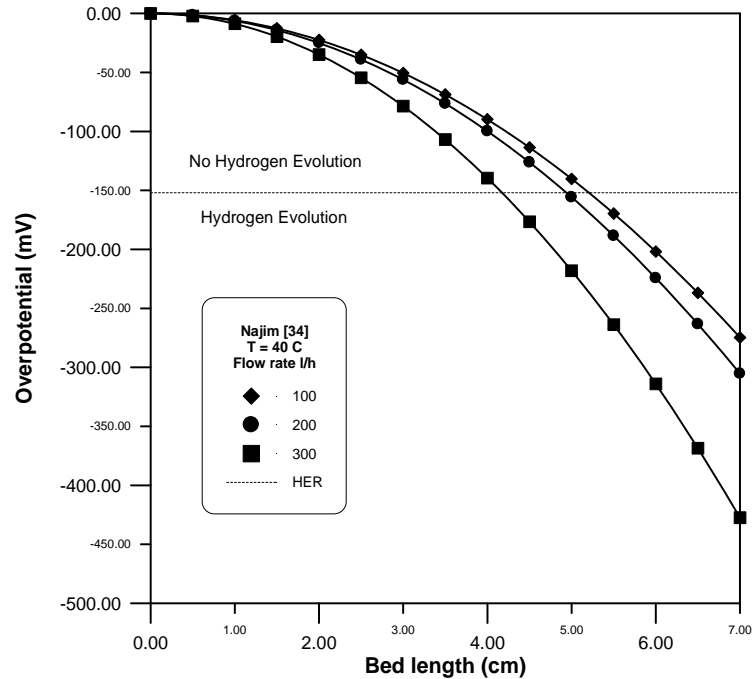


Figure 4.8 Potential distribution for bed length  $L=2\text{cm}$ ,  $[\text{Fe}^{3+}]=15\text{mM}$  based eq. 3.49.

Figures 4.6 – 4.8 show that there is no intersecting between the hydrogen evolution line and the potential distribution lines, which means that all the bed considered optimum according to Nava's [10] model.



**Figure 4.9** Potential distribution for bed length  $L=7\text{cm}$ ,  $[\text{Fe}^{3+}] = 15\text{mM}$  based eq. 3.49.

Figure 4.9 illustrates the optimum bed thickness according to eq. 3.49 at (5.4, 5, and 4.2 cm) for electrolyte flow rate (100, 200, and 300 l/h) respectively.

**(6) Nava's Data [10] (effects of flow rate and surface area)**

They discussed the use of potential distribution analysis during the deposition of metal ions, at limiting current conditions and determined the optimum electrode thickness at which no hydrogen evolution occurs. The potential distribution studies were carried out on stainless-steel fibres of three different surface areas. The fibres were used as cathodic porous electrodes during the deposition of  $\text{Ag(I)}$  ions contained in  $0.1 \text{ mol dm}^{-3} \text{ KNO}_3$  and  $0.6 \text{ mol dm}^{-3} \text{ NH}_4\text{OH}$  electrolyte.

**Table 4.31** Operating conditions, Nava [10].

$\varepsilon = 0.907, 0.91, 0.967$	$z = 1$	$T = 25\text{ }^\circ\text{C}$
$a = 81, 107, \text{and } 193\text{ cm}^{-1}$	$D_R = 9.5\text{ cm}$	$k_s = 0.1\text{ }(\Omega.\text{m})^{-1}$
$[\text{Ag}^+] = 4.6 \cdot 10^{-6}\text{ mol/cm}^3$	$L = 9.5\text{ cm}$	$A_c = 70.88\text{ cm}^2$

**Table 4.32** Optimum bed thickness obtained from Nava's [10] model, (7).

u (cm/s)	optimum bed thickness $L_{op}$ (cm)		
	$a = 81\text{ cm}^{-1}$	$a = 107\text{ cm}^{-1}$	$a = 193\text{ cm}^{-1}$
0.23	9.4	7.5	6.9
0.47	7.2	6.0	5.9
0.59	6.8	5.2	5.4
0.70	6.0	4.5	5.2
0.94	5.5	3.9	4.1

The mass transfer coefficient,  $K_m$  can be found from the following correlations [10]:

$$K_m a = 0.07u^{0.55} \quad (\text{For } a = 81\text{ cm}^{-1}) \quad (4.7)$$

$$K_m a = 0.12u^{0.95} \quad (\text{For } a = 107\text{ cm}^{-1}) \quad (4.8)$$

$$K_m a = 0.32u^{0.69} \quad (\text{For } a = 193\text{ cm}^{-1}) \quad (4.9)$$

**Table 4.33** Optimum bed thickness obtained from Newman's [7, 12, and 13] model, (5).

u (cm/s)	optimum bed thickness $L_{op}$ (cm)		
	$a = 81\text{ cm}^{-1}$	$a = 107\text{ cm}^{-1}$	$a = 193\text{ cm}^{-1}$
0.23	7.37	7.74	1.98
0.47	10.1	8.02	2.47
0.59	11.2	8.11	2.65
0.70	12.1	8.18	2.79
0.94	13.8	8.30	3.06

Figure 4.10 below shows effective electrode thickness vs. mean linear flow velocity based on the data of table 4.32 for the reduction of  $\text{Ag}^+$  ions on three different specific surface areas packed bed electrodes. The lines show the position on the electrode length,  $x$ , before hydrogen evolution starts [10].

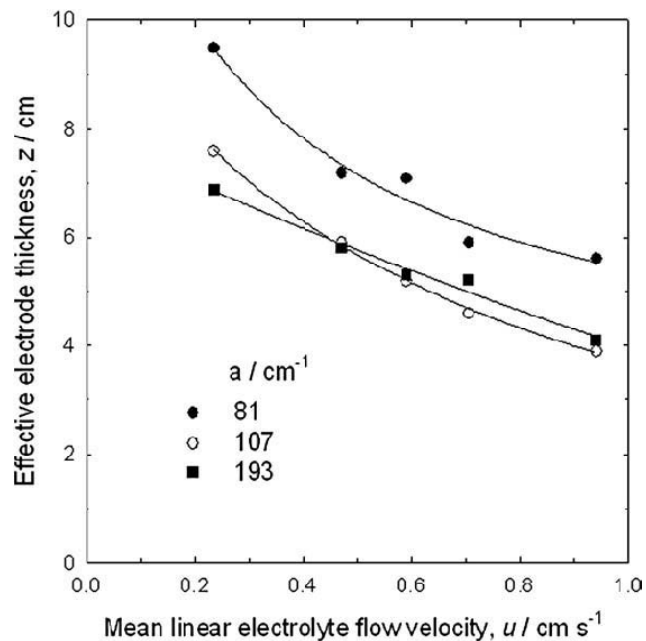


**Figure 4.10** Effective electrode thicknesses vs. mean linear flow velocity [10].

# Chapter Five

## Discussion

In this chapter, the discussion of the results has been made through the following:

- 1- Discussing the parameters that affect the optimum bed thickness through the obtained results supported by figures, and
- 2- Discussing the results of each model.

### 5.1 Parameters Effect on Optimum Bed Thickness

#### 5.1.1 Electrolyte Flow Rate & Mass Transfer Coefficient

Electrolyte flow rate shows a significant effect on the optimum bed thickness through the considered models and results. In spite of the fact that this parameter is not included in some models (1 - 4), but its presence strongly affects the results represented by mass transfer coefficient.

In addition to that mentioned above about the importance of flow rate for such study and for effects on optimum bed thickness, many studies [1 - 5] take it in account as a main parameter in the analysis which enhances its importance. Figures (5.1 and 5.2) represent the effect of this parameter for many different studies [1 – 5] with large range of velocities (0.01 – 7.3 cm/s) based on models (1, 2, and 7). These figs. show that as the flow rate of

electrolyte increases the optimum bed thickness decreases. That is evident by the fact that the mass transfer coefficient is greatly affected by the flow rate.

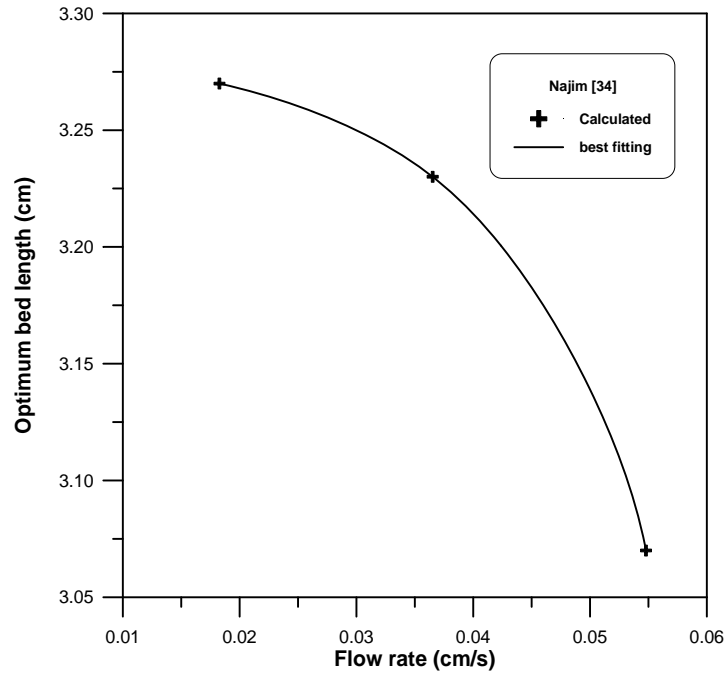


**Figure 5.1** Effect of flow rate on optimum bed thickness from **Najim [34]** data based on models (1&2).

Actually, not only the electrolyte flow rate has an effect on the mass transfer coefficient. The mass transfer coefficient is affected by many factors rather than flow rate like diffusivity, temperature, and physical properties of electrolyte, and that is supported by Wilson and Geankoplis [31] expressions (eqs. 2.24, 2.25, and 2.26). Since each reference considered here has its own specific operating conditions, temperature, and the same physical properties, the flow rate of electrolyte shows up as the domain of these factors.

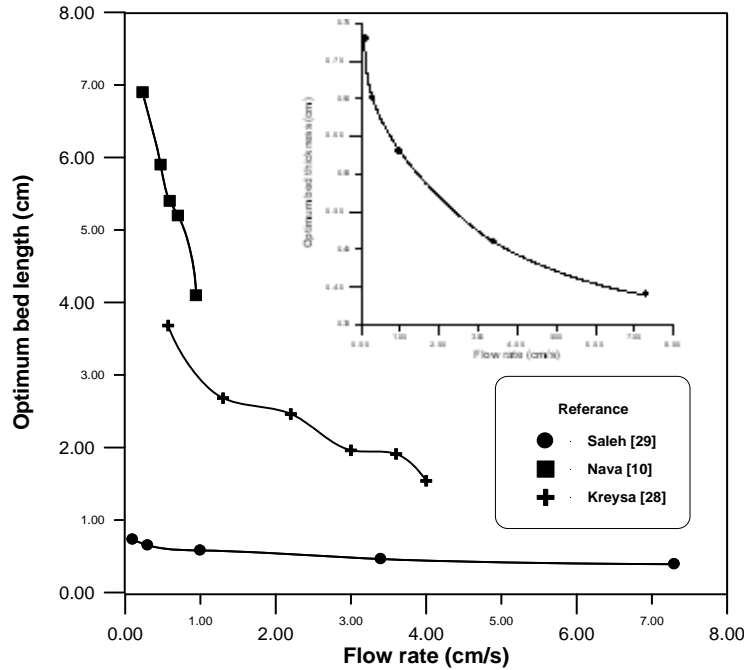


**Figure 5.2** Effect of flow rate on optimum bed thickness from data of [10, 28, and 29] based on models (1, 2, and 7).

Also, at low flow rates ( $u < 1.0 \text{ cm}\cdot\text{s}^{-1}$ ), a new emergence of controlling factor appears, which facilitates the penetration of the process (or maximize the optimum bed thickness) into the porous electrode. This factor is most likely to be the abrupt decrease in the electroactive component concentration over the electrode depth as shown in figs. 5.2 and 5.3 [7, 10, 28], and the corresponding increase in the polarizability of the electrode as concluded by [25].

Figures 5.1 and 5.2 show in general that the increasing in flow rate reduces the optimum bed thickness, but it is also emphasizing in some way that every single case could be a special one for the mass transfer prediction. That can be seen from the style of each curve in the figures of each reference and explain why that is different. The benefits of such study beyond the

selection of broad range of data, that is making possible to examine, analyze and study the phenomenon of these factors and parameters.

Briefly, the increase in electrolyte flow rate increasing the mass transfer coefficient and leading to increase in the limiting current density and consequently decreasing in optimum bed thickness according to models from 1 to 4. While model 5 by Newman [7, 12, and 42] indicates the opposite of that in the four models, which will be discussed in another section of this chapter.

### **5.1.2 Electrolyte Concentration (Reactant)**

The effect of concentration on optimum bed thickness can be seen by fig. 5.3 at various temperatures. The figure shows how the optimum bed thickness decreases as the electrolyte concentration increases at certain temperature and flow rate. This is also true for other temperatures, but the farther increase in temperature in fig 5.3 refers to its effects on optimum bed thickness, not on concentration. It is well known that temperature has no effect on the concentration, but it affects the physical properties of any solution as well as the electrolyte conductivity in this case.

As shown in fig. 5.3 below, the concentration has an observed effect on optimum bed thickness. These effects are calculated from the increasing in limiting current plateau as electrolyte concentration increases as shown in the following equation:

$$i_L = zFK_m C_o \quad (2.30)$$

The increases in limiting current due to increase in concentration leads to that observed decrease in optimum bed thickness [1- 4].

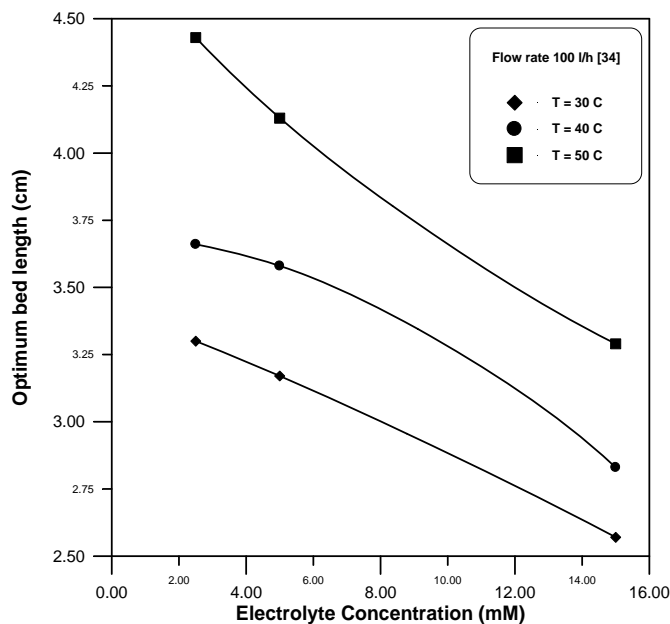


**Figure 5.4** Effect of electrolyte concentration on optimum bed thickness at various temperatures [34].

### 5.1.3 Electrolyte Conductivity & Temperature

Figure 5.4 shows the effect of electrolyte conductivity on optimum bed thickness based on [47] data and model. While figure 5.5 shows the effect of electrolyte conductivity on optimum bed thickness at various temperatures and concentrations based on [34] data and model [28]. These figures show the increase of the optimum bed thickness with increases in electrolyte conductivity. It is also clear that there are some factors which have an effect on the electrolyte conductivity. The figures show that increasing in concentration and temperature leads to increase in the solution conductivity. The reason beyond the optimum bed thickness as increasing in electrolyte conductivity come from the fact that increasing in electrolyte conductivity means decreasing in electrolyte resistivity, which leads to a decrease in ohmic

potential drop in solution, and that decrease leads to increases in electrode polarization which positively reflects in optimum bed thickness.

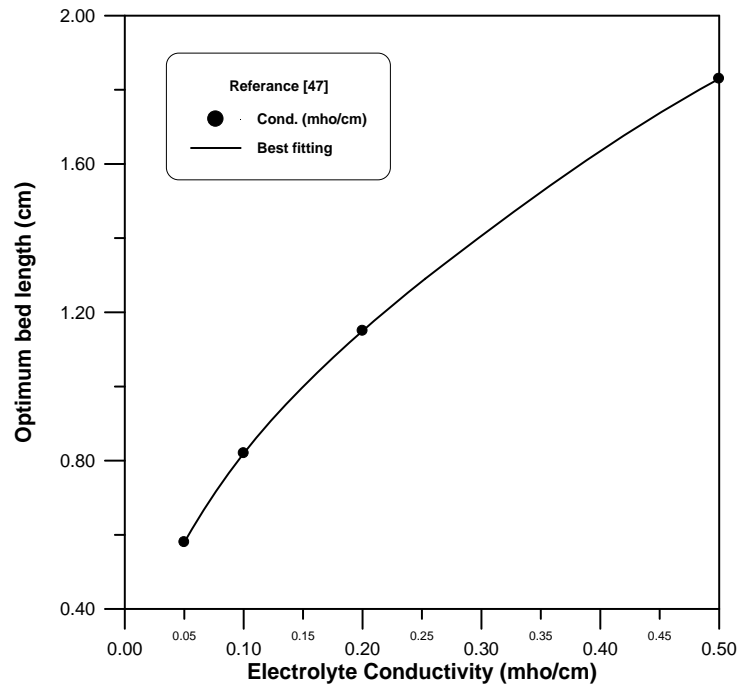


**Figure 5.4** Effect of electrolyte conductivity on optimum bed thickness [47].

It is important to say here that temperature has a considerable effect on electrolyte conductivity bigger than that of concentration. These effects are shown in figs. 5.4 and 5.5. The increase in temperature has been by one magnitude if the concentration doubled, while it is twice if the temperature has increased to 30% of its initial value. However, all these results are directed up to the evidence that increasing in electrolyte conductivity leads to increasing in optimum bed thickness, and this is also true for temperature which enhances the situation of models (1 – 4).

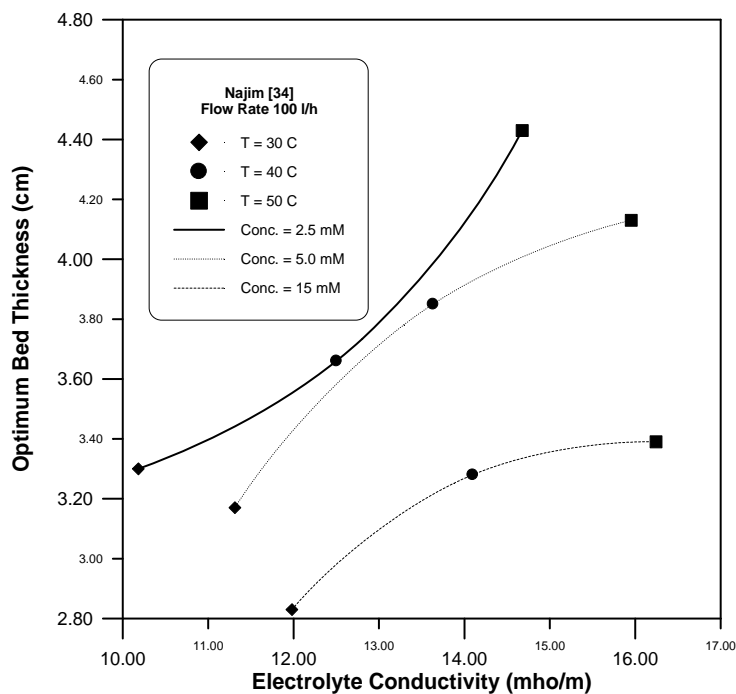


**Figure 5.5** Effect of electrolyte conductivity on optimum bed thickness [34].

### 5.1.4 Specific surface Area & Void fraction

Figure 5.6 shows the effect of the specific surface area on the optimum bed thickness. The data used in this plotting based on Nava's [10] data and model. The results show that the increase in specific surface area of the porous electrode leads to decreases in the optimum bed thickness according to Nava's [10] results and model are considered as a support for what is derived by models (1 – 4). A little increase in the optimum bed thickness at the right side end of fig. 5.6 for  $a = 193 \text{ cm}^{-1}$  have been seen. This has happened because of the increasing in void fraction (see table 4.34) which will be seen in fig. 5.7. This is also true at various flow rates, where fig. 5.6 shows the effect of specific surface area at more than one condition.

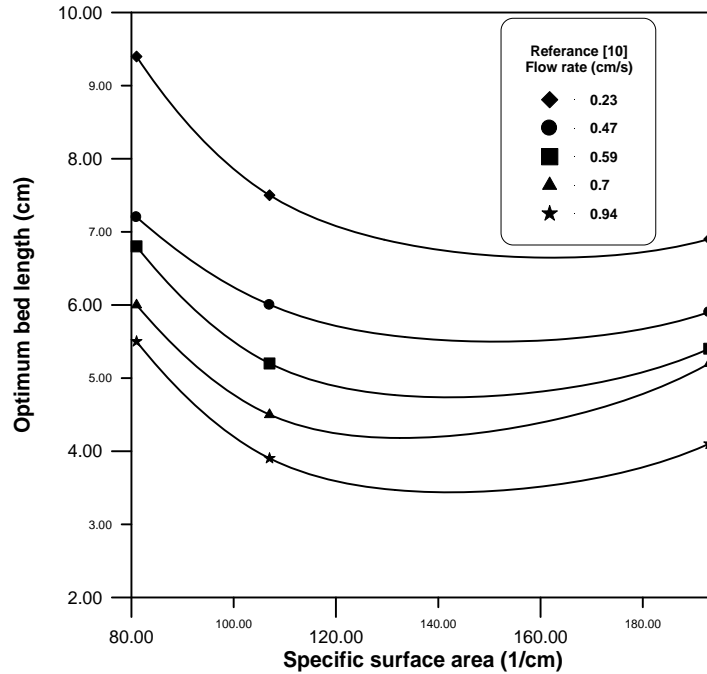


**Figure 5.6** Effect of specific surface area on optimum bed thickness at various flow rates [10]

The reason behind that decrease in optimum bed thickness with the increases in specific surface area belongs to the fact that porous electrode provides a large space (interfacial area) for the electrochemical reaction, and that enables to take a small volume. Therefore, any additional increase in this part leads to decrease in the optimum bed thickness. This also have been proved by several studies [10, 23, 24, and 28], where, for e.g. Coeuret et al. [23 and 24] found out that the increase in size of particle (for the packing of spherical particles) leads to increase in bed effectiveness which consequently means decrease in the interfacial area.

Since the new types of packing (i.e. RVC, fiber, etc.) make possible to control simultaneously void fraction and specific surface area. Figure 5.7 shows how the optimum bed thickness can be strongly affected at certain conditions if the electrode void fraction is made to change.

This figure shows the increase in bed void fraction leads to increase in optimum bed thickness according to [8 and 28].

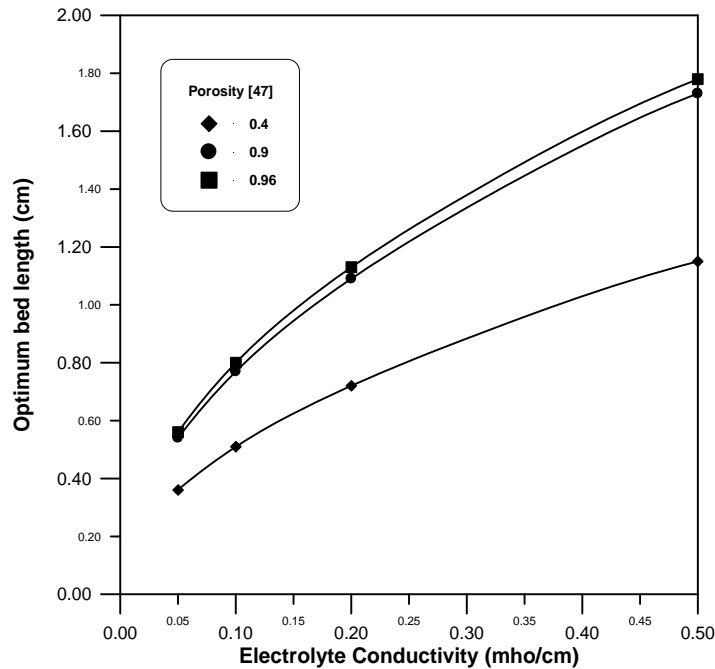


**Figure 5.7** Effect of void fraction on optimum bed thickness at various conductivities [47].

### 5.1.5 Overpotential Difference

The effect of overpotential on optimum bed thickness has been represented in models (1 to 4). Figure 5.8 shows polarization curve for a simple electrochemical reaction displaying region where electrode reaction proceed under mass transport control. Figure 5.8 emphasizes that the effect of the overvoltage determined by the width of the limiting current plateau, or in other word, as the overpotential range increases the effect on optimum bed thickness takes a big effect. This effect is indicated regarding models which

refer to the increase in overpotential range leads to increases in optimum bed thickness.

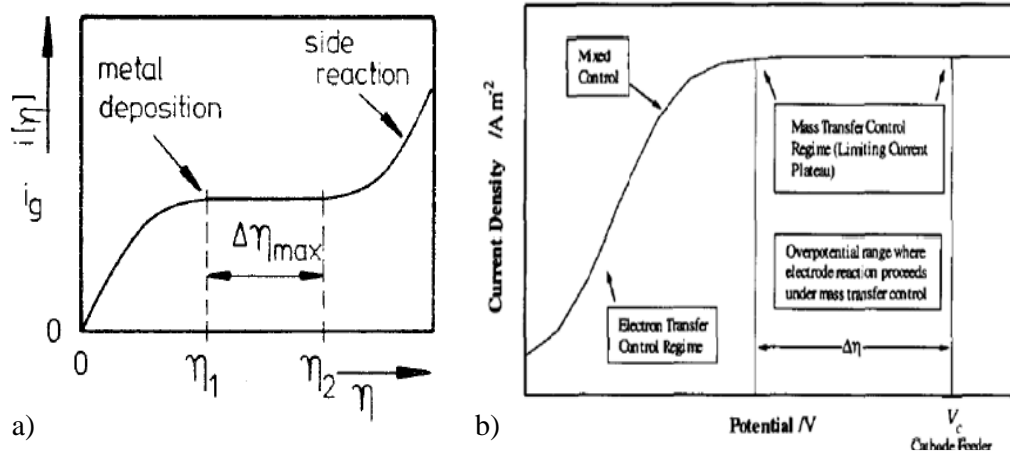


**Figure 5.8** Polarization curve for a simple electrochemical reaction a) **Kreysa and Reynvaan [51]**, b) **Doherty et al. [8]**.

From practical point of view, that's true since the increase in voltages which represent the driving force for any electrochemical reaction leads to increase in reaction areas and consequently reflects on the penetration depth of the reaction inside pores or which here called optimum bed thickness.

## 5.2 Models Results

### 5.2.1 Kreysa's [28] and Doherty's et al. [8], models (1 & 2)

Kreysa's and Doherty's models can be considered as the most appropriate candidates to represent the optimum bed thickness of a FTPE electrochemical reactor to operate under mass transfer control. That's because the most effective parameters are represented in these two models and also the results

show the most acceptable and reasonable results than others. In addition, models 1& 2 show a flexibility to interact with different packing type.

It is also important to mention the disadvantages in these two models and the most important one that is related to the overpotential difference (range)  $\Delta\eta$ . The way that has been suggested to represent this parameter by several studies [8, 28, 47, and 51] based on the polarization curve when reaction proceeds under mass transfer region. This method could be associated with some mistakes and most likely with such theoretical study. These mistakes usually occur when it has to select a start and end point of the mass transfer region. The average approximate error might occur for this case between  $\mp$  (50 – 100) mV in a worst probability based upon experience, but this range of error can cause a noticeable change in optimum bed thickness appreciable to 6 – 13 % for  $\Delta\eta$  equal to 400 mV and that percent candidate to increase as the overpotential range decreases. Consider the following example:

Some results in table 4.9 have been chosen to show up the error might occur in the selection of the overpotential ranges as shown in table below.

**Table 5.1** Optimum bed thickness based on experimental data, Newman [7].

$u$ (cm/s)	$i_L$ ( $\mu A/cm^2$ )	$\Delta\eta$ (mV)	$L_{op}$ (cm) (1) & (2)
0.0214	12.833	350	12.34
0.00576	3.563	400	25.20

The data of table 5.1 are applied to calculate the error by adding the considered error values through the following expression:

$$\text{percentage error} = \left| \frac{\text{final value} - \text{initial value}}{\text{initial value}} \right| \times 100\% \quad (5.1)$$

$$\text{final value} = \text{initial value} + \text{error value} \quad (5.2)$$

Then the results of table 5.1 becomes as listed in tables (5.2 & 5.3):

**Table 5.2** Calculation of overpotential range error readings for error value = 50 mV.

$\Delta\eta_{\text{initial}} (mV)$	$L_{op} (cm)$ (1) & (2)	$\Delta\eta_{\text{final}} (mV)$	$L_{op} (cm)$ (1) & (2)	error %
350	12.34	400	13.19	6.8
400	25.20	450	26.72	6.0

**Table 5.3** Calculation of overpotential range error readings for error value = 100 mV.

$\Delta\eta_{\text{initial}} (mV)$	$L_{op} (cm)$ (1) & (2)	$\Delta\eta_{\text{final}} (mV)$	$L_{op} (cm)$ (1) & (2)	error %
350	12.34	450	13.99	13.3
400	25.20	500	28.17	11.8

These error percents are also true if the error values are negative and also for other reference data. Therefore, if someone has to choose the range of overpotential, he must have some knowledge and experience particularly when most polarization curves are not clear or smooth as appeared in fig. 5.8. Then any error in overpotential range leads either to overestimate or underestimate the optimum bed thickness.

The results of these two models (i.e., 1 & 2) are completely matched because they are already matched as mentioned before. The results of these models over the considered experimental data that have been used in the study show a good agreement for all data [7, 28, 29, 34, and 47] at high flow rates, while for low flow rates, the results are overestimate for [28] and short bed length (2 cm) for [34]. That's probably because the limiting current plateau is

so low due to the very low reactant concentration in [28] which makes the optimum bed thickness represented in these models high even up to or over its actual length. This especially occurs at low flow rates; while the results in short bed length (2 cm) of [34] which overestimating the optimum bed thickness and also the actual bed length probably because of the low specific surface area and flow rates, but even that, the optimum bed thickness has been found experimentally by [34] between 2 and 3 cm, which are showed up in the results.

The most unfavorable situation occurs for the profile  $\eta(x)$  and  $C(x)$  with the opposite character of behavior, that is, the minimum solution concentration corresponds to the most loaded point of the porous electrode and vice versa [18]. This makes the attainment of the limiting diffusion current over the entire porous electrode surface difficult, but in this case the reason is the depletion of the solution in the depth of the porous electrode also cause an increase in the polarization resistance at these points and current redistribution towards the less loaded layers. Eventually, this leads to the efficient function of the entire porous electrode (maximum optimum bed achieved) and that which appears in [7, 28, and 34] at so low flow rates, but it is more costly because of the lower flow rate, high current overload and decrease in the current efficiency [18].

However, the average optimum bed thickness over the total results at six different flow rates of [28] about 2.37 cm, which is approximately the actual bed length (2.3 cm) for that case. In addition, a comparison of specific surface area  $a = 5.66 \text{ cm}^{-1}$  of [34] within that used for example by **Kreysa** [28]  $a = 36 \text{ cm}^{-1}$  or **Newman** [7]  $a = 66 \text{ cm}^{-1}$ , shows how it is small for such application justified by high interfacial area. From practical point of view and according

to reasons mentioned above, it can be concluded that results reflect the whole bed are considered as an optimum more than its value.

### 5.2.2 Kreysa and Jüttner's [47] & Masliy and Poddubny's [25], Models (3 &4)

These two models are so close to that predicted by Kreysa [28] and Doherty et al. [7], the differences only by ignoring the void fraction  $\varepsilon$  as mentioned before. But this neglected parameter causes a dramatic change in the results compared with the previous models (1 & 2). These changes or effects of this parameter can be seen through figs. 5.9 – 5.12. Figures 5.9 – 5.12 show the variation or difference between models 1 and 2, and models 3 and 4 are proportional to or justified by  $(1 - \varepsilon)^{0.5}$ . As the void fraction decreases the differences between the models curves increases and that would vindicate the variation of the shifting ratio among the referred figures.

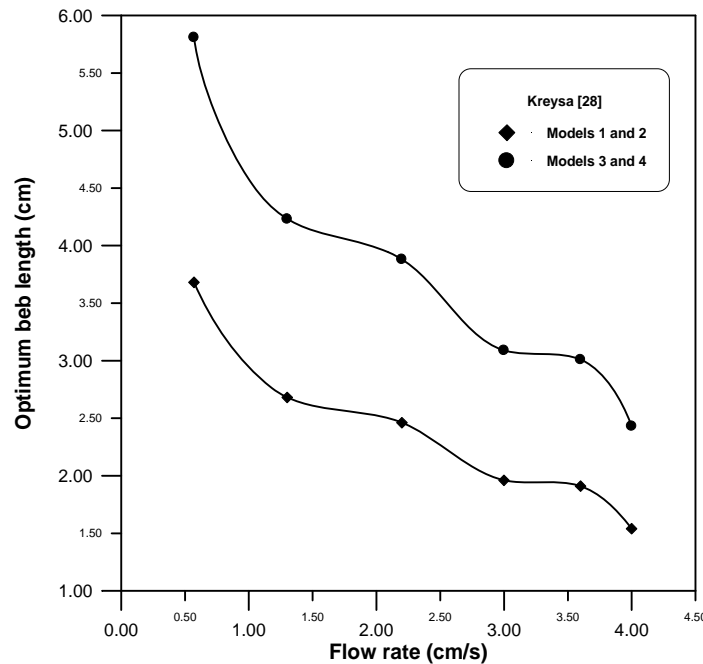
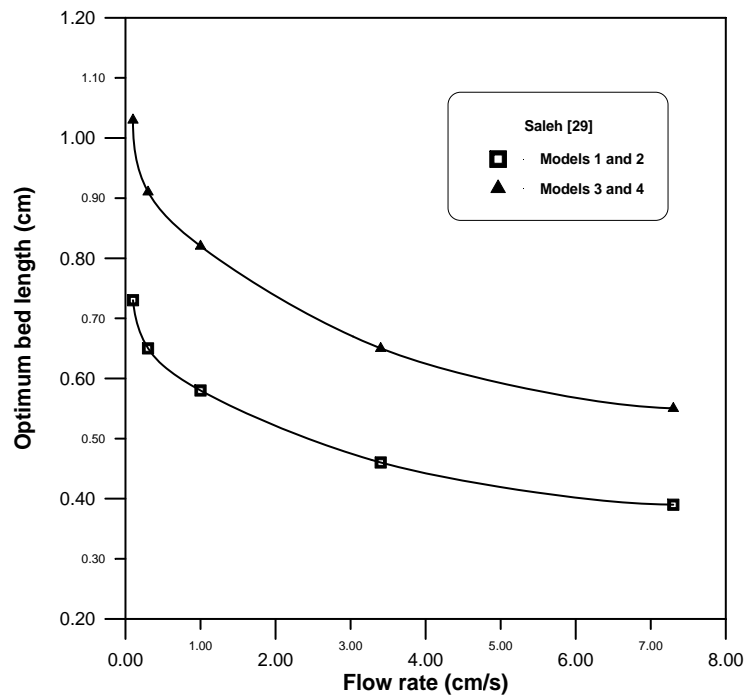
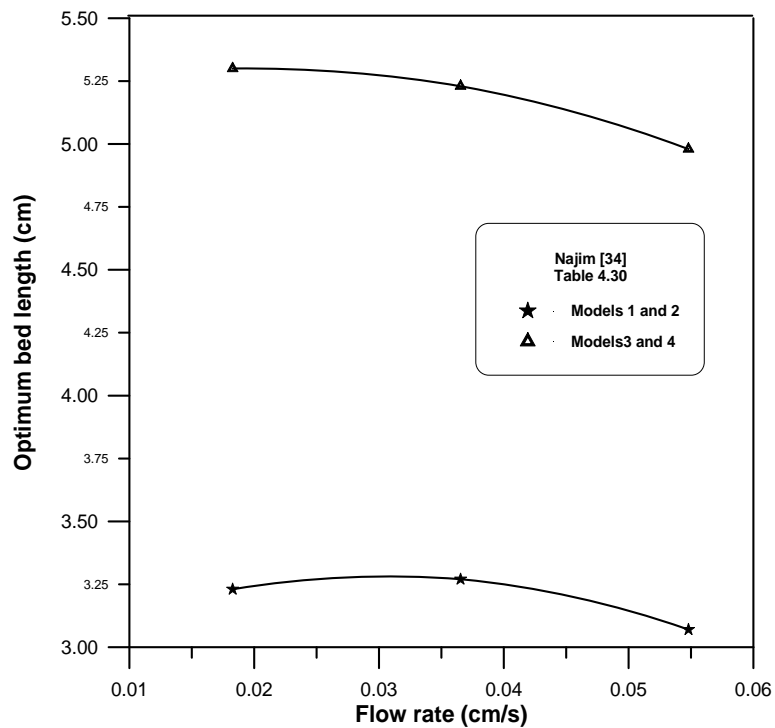


Figure 5.9 Models comparison based on Kreysa's [28] data.



**Figure 5.10** Models comparison based on Saleh's [29] data.



**Figure 5.11** Models comparison based on Najim's [34] data.

Furthermore, these figs. emphasize the importance of that parameter and its effect on the optimum bed thickness. Fig. 5.12 shows how much close could be between models 1 and 2, and 3 and 4 if the void fraction is high, which reflects perhaps the reason beyond the neglecting of this parameter especially before the most recent studies concentrated to use new types of packing that provides simultaneously high specific surface area and void fraction.

One more thing, in spite of these two models sometimes overestimate the optimum bed thickness when the void fraction is small and even overestimate the actual bed length. The surprising thing about these models is even that overestimating results, but it never overtakes the rules of model 7 (i.e. exceeding the side reaction value or hydrogen evolution start) that predicted by Nava et al. [10] (2008), as shown in figs. 4.5 and 4.9. Everything else mentioned about these models is all that is mentioned in discussion about models 1 and 2.

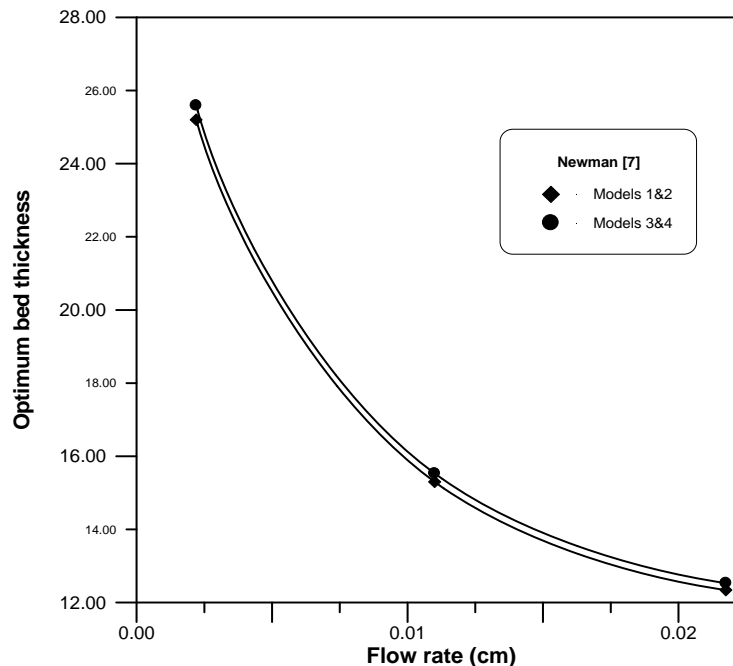


Figure 5.12 Models comparison based on Newman's [7] data.

### 5.2.3 Newman's et al. [7, 12, and 13], Model 5

The behavior of this model is so clear through the results of the considered experimental data. The results show variant behavior compared to other models that have been accomplished by [8, 10, 25, 28, and 47] rather than unreasonable results in many parts. Even that, this variant does not represent the evident scientific mechanisms. But from another point of view, one can notice that the results obtained from the same data source of [7] or from data have the same conditions is quite reasonable values and that obviously seen in fig. 5.13 and that's most likely for low velocities and high specific surface area.

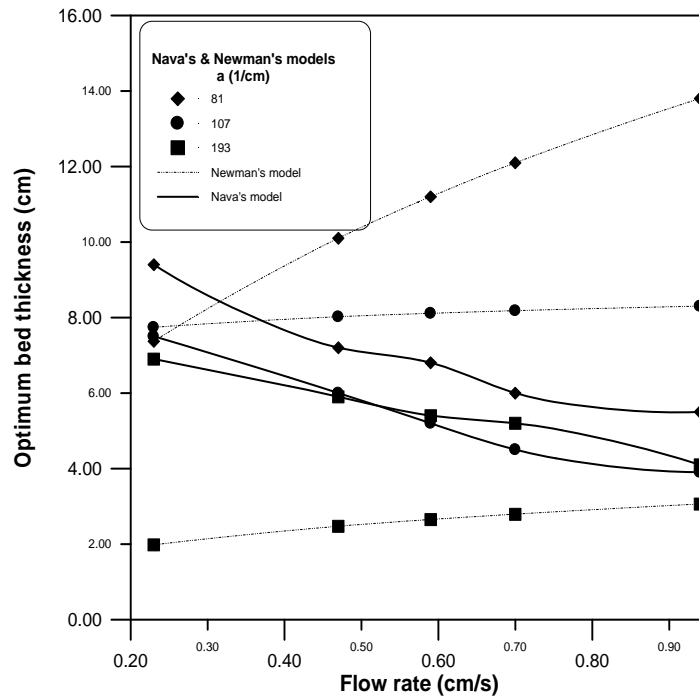


Figure 5.13 Comparison between Newman's [7] and Nava's models.

However, fig. 5.11 also shows variant behavior in model 5 to that shows in model 7 and the other four models (i.e. the optimum bed thickness increases as the velocity). That's could happened at typical conditions of so low flow rates. The poor representation of the parameters and the variant

behavior does not giving the possibility for considering this model to express the optimum bed thickness of a FTPE under wide range of conditions.

However, from other point of view, the reason which makes **Newman [7, 12, and 13]** to consider that represent the penetration depth at first, perhaps because it is a simple model that might give a quick estimation with percent of error for a certain situation, and that's most likely with high specific surface areas and low flow velocities [7, 13] as mentioned before.

#### **5.2.4 Masliy's et al. [18, 25], Model 6**

Unfortunately, there are no experimental data to meet this theoretical model which requires to be executed as a fair action in the present study, in order to make sure to show the method of solution and to cover all the models. The test of this model has been made from a theoretical data based on a simulation study in appendix A just for richness.

#### **5.2.5 Nava's et al. [10], Model 7**

The result of this model which is completely graphical shows a good way to estimate the optimum bed thickness through the entire results. The behavior indicated in this model is agreed with that of the models 1–4 which are supported by figs. 4.5 and 4.9.

The major idea of this model based on Coulombic efficiency calculations. As the Coulombic efficiency of the reaction is 100%, the bed is considered optimum at that efficiency. The Coulombic efficiency  $\psi$  can be

defined as the percentage of the measured current supported by the main deposition reaction [17], i.e.

$$\psi = \frac{i_{main}}{i_{main} + i_{side}} \times 100\% \quad (5.3)$$

Since model 7 is already adopted, then all the optimum bed thickness obtained from this model operates with 100% Coulombic efficiency according to eq. 5.3.

One more thing, the results of optimum bed thickness obtained from model 7 is always greater than that for models 1– 4, that are evident between figs. 4.5 and 4.9, and figs 5.13 and 5.14. This reflects two facts, the first is that model 7 represents a range wider than mass transfer region, and the second is the validity of models 1 – 4 to represent the optimum bed thickness under the mass transfer region (especially model 1 and 2), and avoiding the side reaction.

# Chapter Six

## Conclusions & Recommendations

### 6.1 Conclusions

- 1- The increase in electrolyte flow rate, mass transfer coefficient, concentration, limiting current density, and specific surface area reduces the optimum bed thickness.
- 2- The increase in electrolyte conductivity, porosity, and overpotential range increases optimum bed thickness.
- 3- The first four models (1 – 4) can be use with relatively high flow rates and specific surface area ( $u \geq 0.1$  cm/s,  $a \geq 12$  cm<sup>-1</sup>).
- 4- The best models among the first four that have been tested are models 1 and 2 predicted by **Kreysa [28]** and **Doherty et al. [8]** to represent the optimum bed thickness for reactor operating under mass transfer control.
- 5- Models 3 and 4 predicted by **Kreysa and Jüttner [47]** and **Masliy and Poddubny [25]** are used to estimate the optimum bed thickness when bed porosity is high ( $\varepsilon \geq 0.9$ ).
- 6- Model 5 predicted by **Newman et al. [7, 12, and 13]** can be used for low flow rates and high specific surface area ( $u < 0.09$  cm/s,  $a \geq 25$  cm<sup>-1</sup>).
- 7- The graphical model presented by **Nava et al. [10]** can be a useful way to use in processes when high degrees of conversion are required per pass.

- 8- The exact value of the optimum bed thickness cannot be deduced analytically, but model 1 gives a first approximation value which can be useful for a rough engineering design.
- 9- The bed of a FTPE can be whatever size in diameter, but the thickness of the reactor is very important to take into account for this configuration.

## **6.2 Recommendations & Future Work**

- 1- Trying to make similar study, that including experimental part in order to overcome all difficulties associated with any theoretical work and trying to predict a new model covers a wide ranges of conditions.
- 2- Trying to make extensive study taking into account the effect of time on the optimum bed thickness, and also related with current efficiency (cell efficiency), and collection efficiency.
- 3- Using an electrode of large cross-sectional area (large diameter), and short in length ( $L \leq 2$  cm).
- 4- Using the more recent types of packing materials like RVC and fibre instead of the traditional types in case of experimental study.
- 5- Finding out a method for modifying and improving the best model if possible.

## References

- [1] Pickett, D. J., "Electrochemical reactor design" 2<sup>nd</sup> edition, Elsevier scientific publishing company, Amsterdam (1979).
- [2] Trinidad, P., Walsh, F., Gilroy, D., "Conversion expressions for electrochemical reactors which operate under mass transport controlled reaction conditions, part I: Batch Reactor, PFR and CSTR" *Int. J. Engng. Ed.* **14** (6), 431(1998).
- [3] Walsh, F. C., "Electrochemical technology for environmental treatment and clean energy conversion" *Pure Appl. Chem.* **73** (12), 1819 (2001).
- [4] Gonzalez-Garcia, J., Montiel, V., and Aldaz, A., "Hydrodynamic behavior of a filter-press electrochemical reactor with carbon felt as a three-dimensional electrode" *Ind. Eng. Chem. Res.* **37**, 4501(1998).
- [5] Gonzalez-Garcia, J., Frias, A., Exposito, E., Montiel, V., and Aldaz, A., "Characterization of an electrochemical pilot-plant filter-press reactor by hydrodynamic and mass transport studies" *Ind. Eng. Chem. Res.* **39**, 1132 (2000).
- [6] Stankovica, V. D., Grujic, R., Wragg, A. A., "Water electrolysis and pressure drop behavior in a three-dimensional electrode" *J. Appl. Electrochem.* **28**, 321, (1998).
- [7] Matloz, M.J., Newman, J., "Experimental investigation of a porous carbon electrode for the removal of mercury from contaminated brine" *J. Electrochem. Soc.* **133** (9), 1850 (1986).
- [8] Doherty, T., Sunderland, J.G., Roberts, E.P.L., Pickett, D.J., "An improved model of potential and current distribution within a flow-through porous electrode" *Electrochim. Acta.* **41** (4), 519 (1996).
- [9] Blaedel, W. J., Wang, J., "Characteristics of a Rotated Porous Flow-

- Through Electrode” *Anal. Chem.* **52**, 1697 (1980).
- [10] Nava, J.L., Oropeza, M.T., Ponce de León, C., González-García, J., Frías-Ferrer, A. J., “Determination of the effective thickness of a porous electrode in a flow-through reactor; effect of the specific surface area of stainless steel fibres, used as a porous cathode, during the deposition of Ag(I) ions” *Hydrometallurgy.* **91**, 98 (2008).
- [11] Lanza, M.R.V., Bertazzoli, R., “Removal of Zn(II) from chloride medium using a porous electrode: current penetration within the cathode” *J. Appl. Electrochem.* **30**, 61 (2000).
- [12] Newman, J., Risch, T., “A theoretical comparison of flow-through and flow-by porous electrode at the limiting current” *J. Electrochem. Soc.* **131** (11), 2551 (1984).
- [13] Trainham, J. A. and Newman, J., “The effect of placement and finite matrix conductivity on the performance of flow-through porous electrodes” *J. Electrochem. Soc.* **125** (1), 58 (1978).
- [14] Storck, A., Enriquez-Granados, M. A., Roger, M., Coeuret, F., “The behavior of porous electrodes in flow-by regime-I theoretical study” *Electrochim. Acta.* **27** (2), 293 (1982).
- [15] Bennion, D. N., Newman, J., “Electrochemical removal of copper ions from very dilute solutions” *J. Appl. Electrochem.* **2**, 133, (1972).
- [16] Reddy, R., Reddy, R. G., “Analytical solution for the voltage distribution in one-dimensional porous electrode subjected to cyclic voltametric (VC) conditions” *Electrochim. Acta.* **53**, 575 (2007).
- [17] El-Deab, M. S., Saleh, M. M., El-Anadouli, B., E., Ateya, B. G., “Electrochemical removal of lead ions from flowing electrolytes using packed bed electrodes” *J. Electrochem. Soc.* **146** (1), 208 (1999).

- [18] Masliy, A. I., Poddubny, N. P., Medvedev, A. Zh., Zherebilov, A. F., “Modeling of the dynamics of metal deposition inside a flow-through porous electrode with low initial conductivity” *J. Electroanalytical Chemistry*. **600**, 180 (2007).
- [19] Newman, J., “Engineering design of electrochemical system” *Industrial and engineering chemistry*. **60** (4), 12 (1968).
- [20] Alkire, R., Ng, P. K., *J. Electrochem. Soc.* **124**, 1220 (1977).
- [21] Bard, A.J., Faulkner, L.R., “Electrochemical methods” 2<sup>nd</sup> edition, JOHN WILEY & SONS, INC. New York (2001).
- [22] Ho, K., Jorne, J., “Analytical solution for flow-through porous electrode under linear polarization” *J. Electrochem. Soc.* **133** (7), 1394 (1986).
- [23] Coeuret, F., Hutin, D., Gaunand, A., “Study of the effectiveness of fixed flow-through electrodes” *J. Appl. Electrochem.* **6**, 417 (1976).
- [24] Paulin, M., Hutin, D., Coeuret, F., “Theoretical and experimental study of flow-through porous electrodes” *J. Electrochem. Soc.* **124** (2), 180 (1977).
- [25] Masliy, A.I., Poddubny, N.P., “influence of solid phase conductivity on spatial localization of electrochemical processes in flow-through porous electrodes” *J. Appl. Electrochem.* **27** (9) 1036 (1997).
- [26] Gaunand, A Hutin, D. and Coeuret, F., “Potential distribution in flow-through porous electrodes under limiting current” *Electrochim. Acta.* **22**, 93 (1977).
- [27] Alkir, R. and Gracon, B., “Flow-through porous electrodes” *J. Electrochem. Soc.* **122** (12), 1594 (1975).
- [28] Kreysa, G., “Kinetic behavior of packed bed and fluidized bed electrodes” *Electrochim. Acta.* **23**, 1351 (1978).

- [29] Saleh, M.M., "On the effectiveness factor of flow-through porous electrodes" *J. Phys. Chem.*, **B 108**, 13419 (2004).
- [30] Trainham, J. A. and Newman, J., "A flow-through porous electrode model: Application to metal-ion removal from dilute streams" *J. Electrochem. Soc.* **124** (10), 1528 (1977).
- [31] Wilson, E. J., Geankoplis, C. J., *Ind. Eng. Chem. Fund.* **5**, (1966).
- [32] Al-Habobi, N. A. and Slaiman, Q. J., "Mass transfer measurements in electrochemical packed bed reactors for the reduction of  $Ti^{+4}/Ti^{+3}$  and  $Fe^{+3}/Fe^{+2}$ " Ph.D. Thesis, *Nahrain University* (2000).
- [33] Abdul-Masih, K. S., Sulaymon, A. H., Slaiman, Q. J., Majeed, J. M., "Design of f-through porous electrochemical reactor working under limiting current conditions" Ph.D. Thesis, *University of Baghdad* (2001).
- [34] Najim, S. T., Kashmoula, T. B., Slaiman, Q. J. "Laboratory scale production of *p*-aminophenol using electrochemical reactor" Ph.D. thesis, *Nahrain University* (2006).
- [35] Sioda R. E., "Distribution of potential in a pore electrode under conditions of flow electrolysis" *Electrochim. Acta.* **16**, 1569 (1971).
- [36] Leroux, F. and Coeuret, F., "Mass transfer and potential distribution within axial flow-through electrodes of expanded metal" *Electrochim. Acta.* **28** (12), 1857 (1983).
- [37] Marracino, J. M., Coeuret, F., Langlois, S., "A first investigation of flow-through porous electrodes named of metallic felts or foams" *Electrochim. Acta.* **32** (9), 1303 (1987).
- [38] Geankoplis, C. J., "Transport processes and unit operations" 3<sup>rd</sup> edition, printice hall (1993).

- [39] Saleh, M. M., "Simulation of oxygen evolution reaction at porous anode from flowing electrolytes" *J. Solid State Electrochem.* **11**, 811 (2007).
- [40] Coeuret, F., Vilar, E. O., Cavalcanti, E. B., "Carbon fibre cloth as an electrode material: electrical conductivity and mass transfer" *J. Applied Electrochem.* **32**, 1175 (2002).
- [41] Ateya, B.G., Al-Kharafi, F.M., Abdallah, R.M., Al-Azab, A. S., "Electrochemical removal of hydrogen sulfide from polluted brines using porous flow-through electrodes" *J. Appl. Electrochem.* **35**, 297 (2005).
- [42] Newman, J., Tiedemann, W., "Porous-electrode theory with battery applications" *AIChE Journal.* **21** (1), 25 (1975).
- [43] Kreysa, G., Heitz, E., "The similarity law of effective bed height of packed bed electrodes" *Electrochim. Acta.* **20**, 919 (1975).
- [44] Scott, K., "The effectiveness of particulate bed electrodes under activation control" *Electrochim. Acta.* **27** (3), 477 (1982).
- [45] Scott, K., "The influence of mass transport on the effectiveness of particulate bed electrodes" *Electrochim. Acta.* **28** (9), 1191 (1983).
- [46] Gabe, D. R., Makanjoula, P. A., *AIChE Symposium series.* **15** (98), 309 (1986).
- [47] Kreysa, G., Jüttner, K., "Cylindrical three-dimensional electrodes under limiting current conditions" *J. Appl. Electrochem.* **23**, 707 (1993).
- [48] Walker, A.T.S., Wragg, A.A., "The modeling of concentration-time relationships in recirculating electrochemical reactor systems." *Electrochim. Acta.* **22**, 1129 (1977).
- [49] Newman, J., Tobias, C., W., "Theoretical analysis of current distribution in porous electrodes" *J. Electrochem. Soc.* **109**, 1183 (1962).

- [50] Wendt, H., Kreysa, G., “*Electrochemical Engineering and Science Technology*”. 1<sup>st</sup> edition, Springer scientific publishes company (1999).
- [51] Kreysa, G., Reynvaan, C., “Optimal design of packed bed cells for high conversion” *J. Appl. Electrochem.* **12**, 241 (1982).
- [52] Munji, S.T., Slaiman, Q. J. “Simple model of electrochemical reactor for simulation studies” M.Sc. thesis, *Nahrain University* (2006).
- [53] Furnas, C. C., *Ind. Eng. Chem.* **23**, 1052 (1993).

# Appendix A

## Masliy's et al. [18, 25], Model 6

$$L_{eff} = \int_0^L \frac{i(x)}{i_L(x)} dx \quad (3.48)$$

By using approximate integration formula to solve eq. 3.48 such as Simpson's rule

$$\int_{x_0}^{x_n} f(x) dx = \frac{h}{3} (f_0 + 4f_1 + 2f_2 + 4f_3 + \dots + 2f_{n-2} + 4f_{n-1} + f_n) \quad (A.1)$$

Where  $n$  is even,  $h = \frac{x_n - x_0}{n}$  (interval). In this case, we need current distribution for the target reaction (main reaction) and its diffusional current density to carry out these calculations. In majority of this study to estimate the effective bed thickness, we propose to use data from literatures in order to achieve as much as possible of calculations and to carry out as much as possible of other models. In theoretical study for simulation and studies of flow-through porous electrochemical reactor, **Munji, S.T. [52] (M.Sc. thesis 2006)** presented current, potential, and concentration distribution for copper ions deposition. The studied parameters were:

- 1- Concentration of feed electrolyte was 0.5M H<sub>2</sub>SO<sub>4</sub> and 0.001M CuSO<sub>4</sub>.
- 2- Range of polarization curve studied is mixed control region.
- 3- Electrolyte volumetric flow rates are 5, 10, 50 mL/min.
- 4- Packing particle of spherical shape of diameter 3.5mm.
- 5- Bed of a 4 cm in diameter and of 2 and 3 cm.
- 6- Total current applied to the reactor is 80% of the limiting current corresponding to each of the above conditions.

## Procedure

To calculate effective bed thickness from (22), current distribution for the target reaction (main reaction) and its diffusional current density are wanted as mentioned before. Since the current density distribution obtained from [16] for given concentration distribution  $C(x)$  and flow rate, we need also to know the local mass transfer coefficient  $K_m$  or mean mass transfer coefficient  $\overline{K_m}$  to calculate the local limiting current density  $i_L(x)$ , that's equal to:

$$i_L(x) = zF\overline{K_m}C(x) \quad (2.30)$$

Where  $\overline{K_m}$  can be obtained from concentration distribution as follows

$$\overline{K_m} = \frac{u}{aL} \ln \left[ \frac{C_o}{C_{out}} \right] \quad (2.29)$$

**Table A.1** mean mass transfer coefficient in each runs [52].

Run	Flow rate (mL/min)	$u$ (cm/s)* $10^5$	$L$ (cm)	$C_o$ (mM)	$C_{out}$ (mM)	$\overline{K_m}$ (m/s)* $10^6$
1	5	6.63145	2	1.0	0.470	2.433909
2	10	13.2630	2	1.0	0.609	3.197450
3	50	66.3145	2	1.0	0.836	5.747390
4	5	6.63145	3	1.0	0.320	2.448738
5	10	13.2630	3	1.0	0.461	3.328338
6	50	66.3145	3	1.0	0.748	6.225550

Table A.1 represents the calculation values of eq. 2.29 for each run, while the specific surface area,  $a=1028.5714 \text{ m}^{-1}$  calculated from eq. 2.37 and the porosity  $\varepsilon=0.4$  calculated from the following equation [53].

$$\varepsilon = 0.375 + 0.34 \frac{d_p}{D_R} \quad (A.2)$$

**Table A.2** Effective bed thickness calculations for **Run1**.

Distance (cm)	Reaction rate $i(x)$ (A/m <sup>2</sup> )	Concentration $C(x)$ (mM)	$i_L(x)$ (A/m <sup>2</sup> )	$[i(x)/i_L(x)]$
0	0.4141	1.0	0.469681	0.8816622
0.2	0.3912	0.94	0.441500	0.8860702
0.4	0.3694	0.87	0.408622	0.9040126
0.6	0.3486	0.82	0.385138	0.9051289
0.8	0.3287	0.76	0.356957	0.9208392
1.0	0.3096	0.70	0.328776	0.9416722
1.2	0.2911	0.65	0.305292	0.9535110
1.4	0.2733	0.60	0.281808	0.9698068
1.6	0.2561	0.56	0.263021	0.9736850
1.8	0.2394	0.51	0.239537	0.9994265
2.0	0.2232	0.47	0.220750	1.0110978

$$L_{eff} = \int_0^L \frac{i(x)}{i_L(x)} dx = 1.88 \text{ cm}$$

**Table A.3** Effective bed thickness calculations for **Run2**.

Distance (cm)	Reaction rate $i(x)$ (A/m <sup>2</sup> )	Concentration $C(x)$ (mM)	$i_L(x)$ (A/m <sup>2</sup> )	$[i(x)/i_L(x)]$
0	0.542855	1.0	0.6170247	0.8797952
0.2	0.523864	0.957	0.5904926	0.8871643
0.4	0.505922	0.916	0.5651946	0.8951295
0.6	0.488843	0.875	0.5398966	0.9054381
0.8	0.4724398	0.835	0.5152156	0.9169749
1.0	0.4565342	0.796	0.4911516	0.9295177
1.2	0.4409323	0.757	0.4670877	0.944060
1.4	0.4255802	0.719	0.4436407	0.959290
1.6	0.4102699	0.681	0.4201938	0.9763824
1.8	0.3949434	0.645	0.3979809	0.9923677
2.0	0.3795455	0.609	0.3757680	1.0100526

$$L_{eff} = \int_0^L \frac{i(x)}{i_L(x)} dx = 1.746 \text{ cm}$$

**Table A.4** Effective bed thickness calculations for **Run3**.

Distance (cm)	Reaction rate $i(x)$ (A/m <sup>2</sup> )	Concentration $C(x)$ (mM)	$i_L(x)$ (A/m <sup>2</sup> )	$[i(x)/i_L(x)]$
0	0.967733	1.0	1.109097	0.8725410
0.2	0.958377	0.9846	1.092016	0.8776217
0.4	0.951559	0.9692	1.074936	0.8852238
0.6	0.946887	0.9536	1.057630	0.8952913
0.8	0.943919	0.9378	1.040111	0.9075175
1.0	0.942179	0.9218	1.022365	0.9215681
1.2	0.941181	0.9054	1.004176	0.9372670
1.4	0.940455	0.8886	0.985540	0.9542535
1.6	0.939564	0.8716	0.966668	0.9719614
1.8	0.938127	0.8542	0.947390	0.9902226
2.0	0.933829	0.8367	0.927980	1.0084567

$$L_{eff} = \int_0^L \frac{i(x)}{i_L(x)} dx = 1.856 \text{ cm}$$

**Table A.5** Effective bed thickness calculations for **Run4**.

Distance (cm)	Reaction rate $i(x)$ (A/m <sup>2</sup> )	Concentration $C(x)$ (mM)	$i_L(x)$ (A/m <sup>2</sup> )	$[i(x)/i_L(x)]$
0	0.37441	1.0	0.472543	0.792330
0.3	0.34741	0.91	0.430014	0.807904
0.6	0.32207	0.83	0.392210	0.821166
0.9	0.29810	0.75	0.354407	0.841123
1.2	0.27524	0.68	0.321329	0.856567
1.5	0.25323	0.61	0.288251	0.878505
1.8	0.23193	0.54	0.255173	0.908912
2.1	0.21124	0.48	0.226820	0.931309
2.4	0.19116	0.42	0.198468	0.963177
2.7	0.17176	0.37	0.174841	0.982378
3.0	0.15319	0.32	0.151213	1.013070

$$L_{eff} = \int_0^L \frac{i(x)}{i_L(x)} dx = 2.66 \text{ cm}$$

**Table A.6** Effective bed thickness calculations for **Run5**.

Distance (cm)	Reaction rate $i(x)$ (A/m <sup>2</sup> )	Concentration $C(x)$ (mM)	$i_L(x)$ (A/m <sup>2</sup> )	$[i(x)/i_L(x)]$
0	0.5059599	1.0	0.64228270	0.78775265
0.3	0.4826252	0.941	0.60438801	0.79853535
0.6	0.4611590	0.883	0.56713562	0.81313707
0.9	0.4409531	0.826	0.53052550	0.83116287
1.2	0.4214280	0.770	0.49455760	0.85213127
1.5	0.4020786	0.715	0.45923213	0.87554545
1.8	0.3825147	0.661	0.42454886	0.90099099
2.1	0.3624904	0.608	0.39050788	0.92825374
2.4	0.3419168	0.557	0.35775146	0.95573837
2.7	0.3208555	0.507	0.32563733	0.98531547
3.0	0.2994925	0.461	0.29609232	1.01148350

$$L_{eff} = \int_0^L \frac{i(x)}{i_L(x)} dx = 2.65 \text{ cm}$$

**Table A.7** Effective bed thickness calculations for **Run6**.

Distance (cm)	Reaction rate $i(x)$ (A/m <sup>2</sup> )	Concentration $C(x)$ (mM)	$i_L(x)$ (A/m <sup>2</sup> )	$[i(x)/i_L(x)]$
0	0.9780065	1.0	1.201369286	0.8140760
0.3	0.9653506	0.9766	1.173257244	0.8227953
0.6	0.9575359	0.9531	1.145025066	0.8362575
0.9	0.9531005	0.9291	1.116192203	0.8538856
1.2	0.9504722	0.9044	1.086518382	0.8747870
1.5	0.9481381	0.8791	1.056123740	0.8977528
1.8	0.9447987	0.8532	1.025008275	0.9217473
2.1	0.9394764	0.8269	0.993412262	0.9457064
2.4	0.9315628	0.8005	0.961696113	0.9686665
2.7	0.9208066	0.7743	0.930220237	0.9898802
3.0	0.9072571	0.7485	0.899224910	1.0089323

$$L_{eff} = \int_0^L \frac{i(x)}{i_L(x)} dx = 2.7 \text{ cm}$$

(Flow-through) . وكذلك

(Flow-by)

( )

Flow-)

(through

specific surface area limiting current density

( )

(Flow-through)

**.(1996) Doherty et al. و (1978) Kreysa**

## شكر و تقدير

الحمد لله على اتمامه نعمته و التوفيق لما هدانا اليه. نشكره ونستعين به سبحانه هو الحي القيوم الذي لا اله الا هو. وافضل الصلاة والسلام على نبي الرحمة ابي القاسم محمد وعلى اله وصحبه وسلم.

اتوجه بالشكر الجزيل الى استاذي الفاضل الأستاذ الدكتور قاسم جبار سليمان رئيس قسم الهندسه الكيمياويه المحترم للجهد الذي بذله والنصائح والتوجيهات اللتي قدمها لانجاح هذا المشروع. و الشكر موصول الى استاذي و الأخ الأكبر الدكتور سرمد طالب نجم للمساعدة و المتابعه و الدعم اللذي قدمه لأنجاز هذا المشروع.

شكري و حبي و امتناني لعائلي اللتي وقفت الى جانبي وقدمت كل ما يمكن في مسيرة دراستي و لمساهمتها في انجاز هذا المشروع. كما واشكر جميع اصدقائي اللذين وقفوا معي و ساعدوني في اتمام هذا العمل.

محرم